Newtonian and Non-Newtonian Two-Phase Flow in Complex Pipelines

by

© Faraj Ali Ben Rajeb

A thesis submitted to the School of Graduate Studies in partial fulfillment of the requirements for the degree of

Doctor of Philosophy

Department of Oil and Gas Engineering

Faculty of Engineering and Applied Science

Memorial University of Newfoundland

January 25, 2024

St. John's, Newfoundland and Labrador, Canada

ABSTRACT

Two-phase gas/non-Newtonian fluid flow through pipes commonly occurs in many industrial applications, such as in the chemical industry and oil and gas refineries. Many fluids used in oil and gas industries display non-Newtonian behaviour. Their rheology strongly affects pressure drop, flow structure, interface fluctuation, void fraction, heat transfer, and other flow features. In fact, non-Newtonian systems are not governed by the Newtonian law of viscosity. However, little experimental work has been devoted to studying non-Newtonian flow behaviour.

This present work has conducted an experimental investigation to understand the fundamental physics of non-Newtonian two-phase (gas/ liquid) flow through pipes. In the experiments, several concentrations of Xanthan Gum were used as the non-Newtonian liquid, and both compressed air and carbon dioxide were used as gases. The flow rate and pressure of liquid and gas are changed by using a pump placed ahead of the mixing point. Pressure values are recorded by pressure sensors fixed at specific points along the pipe loop, and more than 10,000 experimental data points have been collected.

The Experimental data analysis went through four categories. The first part is to calibrate all pressure sensors. The second step was applying rheology tests on our non-Newtonian Fluid to define the fluid behaviour and estimate the fluid properties. The third goal is to develop a new model for estimating pressure drop for the gas/non-Newtonian flow. The last part of the experiments is void fraction measurements. Pressure drop is one of the most challenging concerns related to industrial process design. In fact, multiphase flow process design depends on a better understanding of multiphase flow regimes. Numerous research has been done on gas/Newtonian liquid flow in horizontal and vertical pipes in the past few decades. Still, only a few research studies have been carried out to identify gas/non-Newtonian flow regimes. [1].

Creating a new model to estimate void fraction for gas-non-Newtonian flow is another objective done in the present work. The void fraction is considered one of the most important flow parameters used to describe two-phase flows in tubes. Void fraction is an important process variable for the volume and mass calculation required to transport gas-liquid mixture in pipelines, storage in tanks, metering, and custody transfer. Furthermore, it is important to determine other flow parameters such as two-phase density and viscosity or the average velocities of gas and liquid mixture. In addition, it plays a significant role in estimating and modelling two-phase pressure drop and flow pattern transitions. The created void fraction model is used to determine constants of general form posted by Butterworth[2]. Both developed void fraction models give a good estimation for the void fraction with about 5% percent errors compared with our experimental results and other available literature experimental results.

Keywords: Newtonian, Non-Newtonian, Two-Phase Flow, Pressure Drop, Void Fraction, Flow Regime.

Papers Published from this Research

All papers listed below have been presented and published as full papers in conference proceedings. The majority of the results and discussions presented in this thesis have been published in the following papers:

1. **Faraj Ben Rajeb**, Syed Imtiaz, Yan Zhang, Amer Aborig, Mohamed M. Awad, Mohammad Azizur Rahman "Void Fraction, Pressure Drop, and Flow Pattern Behavior For Two-Phase Non-Newtonian Slug Flow", (ASME 2021 40th International Conference on Ocean, Offshore and Arctic Engineering OMAE2021) June 21-30.
2. **Faraj Ben Rajeb**, Mohamed Odan, Amer Aborig, Syed Imtiaz, Yan Zhang, Mohamed M. Awad, Mohammad Azizur Rahman "Experimental comparison of Newtonian and non-Newtonian multiphase flow in horizontal pipes," (ASME 2020 Fluids Engineering Division Summer Meeting FEDSM2020) July 12-16, 2020, Orlando, Florida, USA.
3. **Faraj Ben Rajeb**, Mohamed Odan, Syed Imtiaz, Yan Zhang, Mohamed Awad, and Mohammad Azizur Rahman, "Experimental investigation of pressure drop of gas/non-Newtonian flow in horizontal pipes," OMAE2020 June 28-July 3, Fort Lauderdale, FL, USA.
4. **Faraj Ben Rajeb**, Mohammad Azizur Rahman, Yan Zhang, Syed Imtiaz, Amer Aborig, Mohamed Odan, "Pressure Loss of Water–CO_2 Two-Phase Flow Under Different Operating Conditions," AFM 2018 12th International Conference on Advances in Fluid Mechanics (10 - 12 July 2018) Ljubljana, Slovenia.
5. **Faraj Ben Rajeb**, Mohamed Odan, Yan Zhang, Syed Imtiaz, Amer Aborig, Mohammad Aziz Rahman, "Carbon Dioxide and Water Mixture in Pipeline Flow

Systems," OMAE2018 37th International Conference on Ocean, Offshore and Arctic Engineering, June 17-22, 2018, Madrid, Spain.

6. **Faraj Ben Rajeb**, Mohamed Odan, Syed Hasnain Zaidi, Mohammad Azizur Rahman, Amer Aborig, Syed Imtiaz, Yan Zhang, "Experimental Investigation of Multi-phase Pressure and Temperature Loss Using High-Pressure Flow Loop" (International Conference on Petroleum Engineering ICPE-2016), Dhaka, Bangladesh, December 2016.
7. **Faraj Ben Rajeb**, Mohamed Odan, Syed Hasnain Zaidi, Mohammad Azizur Rahman, Amer Aborig, Syed Imtiaz, Yan Zhang, "Experimental Investigation of Multi-phase Flow Effects on the Hydrate Formation Process in an Offshore Pipeline," The First International Conference on Chemical, Petroleum, and Gas Engineering ICCPGE-2016, Alkhoms, Libya, December 2016.

Co-Authorship Statement

I, Faraj Ben Rajeb, hold principal author status for all the papers listed above. However, each paper is co-authored by my supervisor, Dr. Mohammad Azizur Rahman, my co-supervisor, Dr. Amer Aborig, and the supervisory committee, Dr. Yan Zhang and Dr. Syed Imtiaz. I am the principal author and carried out the experiments. I drafted the papers, and the co-authors assisted me in formulating research goals and experimental techniques and reviewing and revising the articles.

Acknowledgments

I want to express my most profound appreciation to my supervisor, Dr. Mohammad Azizur Rahman, for his continuous support and guidance. He also provides the required equipment in the laboratory to conduct this work. I would also like to express my gratitude to Dr. Amer Aborig, the co-supervisor of this thesis, for his valuable comments, remarks, and engagement. I also wish to acknowledge the care of Dr. Syed Imtiaz and the financial support he provided. Lastly, I want to recognize Dr. Yan Zhang's support and excellent recommendations.

I gratefully acknowledge Memorial University of Newfoundland for the opportunity to complete this research and the Libyan Ministry of Higher Education's financial support.

Finally, I would like to thank my mother, wife, children, brothers and sisters, friends, and relatives for their love, prayers, support, and dedication to the soul of my dear father, who was the reason for my arrival here.

Table of Contents

List of Tables

List of Figures

Nomenclature

A	=	Area, m^2
Bo	=	Bond number, $\equiv gD_h^2(\rho_1 - \rho_2)/\sigma$
Co	=	Laminar Constant
CO_2	=	Carbon Dioxide
c_p	=	Specific heat, $J/kg.K$
D	=	Diameter, m
D_p	=	Pressure Drop, kPa
$D.R.$	=	Dial Reading
f	=	Fanning friction factor
g	=	gravitational constant
H_g	=	Gas Fraction
H_l	=	Head Loss
J	=	Farooqi and Richardson factor
K	=	Consistency Factor
L	=	Length, m
$\dot{m}_l$	=	Liquid mass flow rate, kg/s
$\dot{m}_g$	=	Gas mass flow rate, kg/s
n	=	Flow index

P = Pressure, kPa

$\dot{Q}$ = Volumetric flow rate, m^3/s

q_L = Liquid flow rate, m^3/s

q_g = Gas flow rate, m^3/s

Re = Reynolds number, ≡

T = Temperature, K

u = Velocity, m/s

V_{sg} = Slug Velocity m/s

u_{sl} = The superficial velocity of the liquid, m/s

u_{sg} = The superficial velocity of the gas, m/s

u_m = mixture velocity, m/s

Y_B = Bingham Yield

Y_t = True yield

Greek Symbols

μ = Dynamic viscosity, Ns/m^2

μ_l = Liquid viscosity, Ns/m^2

μ_g = Gas viscosity, Ns/m^2

μ_m = Mixture viscosity, Ns/m^2

ρ = Density, kg/m^3

ρl	=	Liquid density, kg/m^3
ρg	=	Gas density, kg/m^3
ν	=	Kinematic viscosity, m^2/s
x	=	Two-phase quality
δ	=	Film thickness, m
ε		Void Fraction
σ	=	Interfacial tension, N/m
θ	=	Contact angle, ^{o}
τ	=	Shear stress, Pa
τ_0	=	Yield Stress
γ	=	Shear Rate
Δ	=	Difference
Tp	=	Two-phase

CHAPTER 1

Introduction

1.1 Overview

Newtonian fluids follow Newton's law of viscosity. Here, the Newtonian viscosity is independent of shear rate or stress and depends on the fluid flow rate, temperature, and pressure[3]. On the other hand, non-Newtonian fluids have a nonlinear relationship between shear stress and shear rate, which means that their viscosity is not constant at a given pressure and temperature. Therefore, non-Newtonian fluid can be categorized into three major groups:
(a) time-independent, (b) time-dependent, and (c) visco-elastic fluids[4]. However, this grouping of non-Newtonian fluids is sometimes not acceptable because most materials often show a combination of two or all three non-Newtonian types.

Flow can be either shear when fluid components move together or expand when fluid components flow towards or away from each other. The simultaneous fluid flow with different phases (two or more phases) in horizontal or deviated pipes is termed "multiphase flow." This flow has great industrial significance for various fields such as chemical processing, oil refinery, and food industries. Therefore, in the past decades, many researchers have given more attention to flow regime characteristics and multiphase flow assurance monitoring.

Numerous research has been conducted on gas/Newtonian liquid flow in horizontal and vertical pipes in the past few decades. Still, only a little research has been carried out for gas/non-Newtonian flow. Recently, commonly used fluids in the oil and gas industry, like lacquers and polymer solutions, exhibit non-Newtonian characteristics. Their viscosity shows a nonlinear relationship between share stress and share rate. The viscosity of non-Newtonian fluids

significantly affects gas/non-Newtonian flow properties and structures like pressure drop, void fraction, and flow regime[1].

Pressure drop is one of the most challenging concerns related to industrial process design. The design process of multiphase flow equipment depends on a better understanding of the multiphase's pressure drop and flow regimes[5]. The pressure drop for any flow has three elements that manage the flow and energy loss: friction, acceleration, and elevation. The elevation is excluded in the case of horizontal two-phase flow. In fact, the total pressure drop in the system is of concern for any industrial process designation. It depends strongly on the correct understanding of the flow patterns and accurate void fraction prediction[6].

Several correlations were developed to predict gas/Newtonian multiphase flow pressure drop. Most known correlations like Beggs and Brill, Hagedorn and Brown, and Gray have modified both the hydrostatic pressure difference and the friction pressure loss to make them appropriate to multiphase flow conditions[7]. Furthermore, based on theoretical studies, many correlations to predict pressure drop in gas / non-Newtonian flow have been developed or modified from Newtonian correlations. However, only a few pressure loss models have been generated from experimental investigations[8].

Besides pressure drop, the void fraction is considered one of the most important flow parameters describing two-phase flows in tubes. Void fraction is an important process variable for the volume and mass calculation required for transporting gas-liquid mixture in pipelines, storage in tanks, metering, and custody transfer. Moreover, it is a very important parameter required for determining other flow parameters such as two-phase density and viscosity or the average velocities of gas and liquid mixture. In addition, it plays a major role in estimating and modeling two-phase pressure drop and flow pattern transitions.

The void fraction in the multiphase flow of gas and liquid can be defined as the volume fraction of gas that is occupied in the channel flow. In particular, the void fraction of gas-liquid flow is the fraction of the gas flow rate to the total gas and liquid flow rates[9]. The void fraction value varies from zero for a single phase of liquid flow to one for a single phase of gas flow. Therefore, several methods could evaluate void fraction experimentally, such as trapping a section of the flow stream between two quick closing valves and measuring the gas or liquid trapped volume.

In fact, the knowledge of the flow regime is essential since the pressure drop in two-phase flow is sensitive to the gas and liquid phase distribution along the pipe length. Unlike the other correlations, the Beggs and Brill correlation requires that a flow pattern be determined to estimate the pressure drop. In addition, the presence of multiple-phase flow complicates pressure drop calculations because of the interactions between phases. This required using mixture properties and gas and liquid volume fractions throughout the pipe.

1.2 Knowledge and Technological Gaps

1. In the past forty years, several studies have related to pressure drop, flow regime, and volume fraction determination for the multiphase flow of non-Newtonian liquid and gas in pipelines. However, most of the research described comparatively low viscous mixtures, like clay suspensions, kaolin, and CMC, but not high viscous materials like lubricating greases and high concentrations of Xanthan gum (4g/L).
2. In the past few decades, numerous research has been accomplished in gas/Newtonian liquid flow in horizontal and vertical pipes. Still, only a few research have been carried out for gas/non-Newtonian flow.

3. Previous pressure drop models that included the effect of liquid viscosity on void fraction and pressure drop have paid more attention to the flow of non-Newtonian liquids and gas flow, assuming that the gas-liquid interface is smooth.
4. Many void fraction equations for liquid/gas flow have been modified from the Butterworth correlation, but none are suitable for non-Newtonian systems.
5. Most of the void fraction correlations went to the simplest assumption, considering the flow is homogeneous. This assumption means that the gas and liquid phase's velocities are equal, and the two phases behave like a single phase. In fact, the ratio of the velocities of the two phases is required to compute the void fraction, which conflicts with this assumption.
6. The relationship between pressure drop, void fraction, and flow regime for gas/ non-Newtonian flow is not commonly studied.
7. The differences between plug, slug, and elongated bubble flow are unclear. In many research, these three-phase flow regimes are commonly defined and combined as intermittent flow. Studying these three flow patterns is important because the research shows that the pressure drop has been reduced in the slug flow than in other flow patterns.
8. Experimental knowledge of annular flow is limited due to the complexity of experiments, especially with non-Newtonian fluids.

1.3 Scope and Objectives

Flow assurance is an important issue when considering the production of oil and gas (hydrocarbon fluids) from offshore gas systems. In particular, Flow assurance is a major challenge in offshore and deep-water operations in the oil and gas industry. For example, in a survey of 110 oil companies, flow assurance was listed as the major technical problem in offshore energy development[10].

The design and process engineer faces difficulty choosing the proper correlation among the available ones. The fact that there are plenty of correlations available would not be a concern had it not been because most correlations have some form of restrictions attached.

The total pressure drop comprises the hydraulic pressure drop, the friction pressure drop, and the pressure drop through the pipe system's fittings, instruments, and elbows. These pressure effects have an important influence on the output of the oil well. Therefore, they must be determined as accurately as possible to ensure the economic feasibility of oil production. If the pressure drop of a multiphase flow through a pipe is accurately known, the oil extraction can be optimized. Analyzing the different pressure phenomena in oil reservoirs and well- bores is important to forecast the effect of the pressure drop along the length of the pipeline. In particular, a large pressure drop must be overcome if the formation's permeability is poor. Therefore, the pressure drop in the well should be limited, and as a result, the pressure drop and its causes have to be known as accurately as possible [11],[12].

In the oil and gas industries, gas-Newtonian and gas/non-Newtonian liquids multiphase flow through pipelines over long distances is often experienced. Therefore, information about frictional processes is fundamental since it could improve the accuracy of the system design. However, not at all like gas/Newtonian flow; just a little research has been dedicated to

considering the pressure drop of multiphase flow in pipes when the fluid is non-Newtonian liquid. Generally, these studies indicate that the hydrodynamic behavior of gas/non-Newtonian flow in pipes is completely different from the gas/Newtonian flow. This is very important knowledge industrially regarding fluid transportation and related operations. For instance, a gas/non-Newtonian multiphase flow in pipes can result in a huge decrease in the pressure drop compared with a gas/Newtonian flow, which is basically important for the economy because it can reduce the required pumping energy[13]. In fact, maintaining pressure may have critical importance to the system operation, its equipment components, or the output of the process. Therefore, the scope of this work covers both pressure drop and void fraction of gas/Newtonian and gas/Non-Newtonian flow through pipes. The experimental setup was conducted, and more than 10,000 experimental data were collected to fulfill the following objectives:

1- Specify the effect of flow conditions and fluid properties on the non-Newtonian liquid/gas flow pressure drop.
2- Comparison between the experimental pressure drop with the one estimated by well-known empirical correlations to verify which correlation is better for Herschel-Bulkley fluids.
3- Develop an experimental model describing the relationship between void fraction and the flow parameters, such as velocities, gas and liquid densities and viscosities, slip ratio, and flow quality for the gas/non-Newtonian flow.
4- Develop an experimental model to predict the void fraction of gas/non-Newtonian flow, concluding all the above-created models.
5- Estimate the constants of Butterworth's general void fraction equation and use the modified model for gas/non-Newtonian flow estimations.

6- Validate both created void fraction models of gas/non-Newtonian flow with experimental data and other empirical known correlations.

1.4 Organization of The Theses

This thesis has been written in the traditional format. Table 1 shows the main scope of each chapter.

Table (1.1) Organization of the thesis

Chapter Title	Subtitle
Chapter 1: Introduction	Overview, scope, and objectives. Knowledge and technological gaps. Contribution and novelty.
Chapter 2: Literature Review	Literature review of pressure drop and void fraction of Newtonian and non-Newtonian multiphase flow
Chapter 3: Experimental Methods	Pressure drop modeling for Non-Newtonian multiphase flow
Chapter 4: Rheology Tests	Rheology tests and fluid properties
Chapter 5: Pressure Drop Modeling	Comparison of the experimental and estimated pressure drops for non-Newtonian /gas flow.
Chapter 6: Void Fraction Modeling	Create the void fraction model for non-Newtonian /gas flow and the model validation. Estimate the constants of the general form of the void fraction model and the model validation.
Chapter 7: Conclusion	Summary, Conclusion, and Recommendations.

1.5 CONTRIBUTION AND NOVELTY

This section underlines this work's methodological and considerable contributions and their significance against the existing research in the Newtonian and non-Newtonian multiphase flow. One of the essential methodological purposes of this work is a comprehensive experimental investigation of the flow variables' effect on pressure drop and void fraction of non-Newtonian multiphase flow. Following is a brief description of this research's main contributions and novelties:

1. This work provides extensive experimental results in the area of Newtonian and non-Newtonian multiphase flow. The results show the relationship between flow conditions and important parameters in multiphase flow, such as pressure drop and void fraction.

2. Estimate the percentage effect of flow condition and fluids properties on the non-Newtonian liquid/gas flow pressure drop.
3. Select the proper pressure drop for the Herschel-Bulkley fluids from the well-known available correlations. This model has been validated with experimental data and other empirical known correlations. The Xu et al. model provides a better predictive ability than some of the other correlations with an acceptable percentage error.
4. The developed void fraction equation based on the fluids' properties and flow conditions expresses the importance of defining the void fraction and the slip ratio because they also can play an essential role in calculating the pressure drop of the two-phase flow.
5. The other void fraction equation created based on the similarity between the existing models of predicting void fraction for gas-liquid flow (Lockhard & Martinelli [11]; Baroczy [12]; Turner & Wallis [13]) can play an important role in void fraction estimations. This model works for gas /non-Newtonian flow with good estimations compared with the experimental results.
6. Estimate the constants of the general void fraction equation by Butterworth. These constants make the general model work with non-Newtonian flow.

CHAPTER 2

Literature Review

2.1 Multiphase Flow

The simultaneous fluid flow with different phases (two or more phases) in horizontal and deviated pipes is termed "multiphase flow." This flow has great industrial significance for different fields such as chemical processing, oil refinery, and food industries. Newtonian and non-Newtonian multiphase flow has great industrial significance for several fields, such as chemical processes, oil refineries, and food industries. Consequently, in the past decades, numerous researchers have given more attention to flow regime characteristics and multiphase flow assurance monitoring. In the oil and gas industries, gas/Newtonian and gas/non-Newtonian liquids multiphase flow through pipelines over long distances is often experienced. Therefore, information about frictional processes is fundamental since it could improve the accuracy of the system design[14].

The flow behavior in multiphase flow is much more complicated than for single-phase fluid flow. Multiphase flow occurs during hydrocarbon production and transportation due to the variations of fluid phases that flow through the pipe. Due to the different properties and characteristics of gas compared with water and oil for viscosities and other features, the gas tends to flow faster than oil. For instance, the liquid holdup is the in-situ liquid volume in the pipe. The multiphase flow behavior is much more complicated than a single-phase flow. The main reason is the density difference of the phases[15].

2.2 Newtonian/Non-Newtonian Fluid Behavior

Flow can be either shear when fluid components move together or expand when fluid components flow towards or away from each other. Newtonian fluids follow Newton's law of

viscosity. Here, the Newtonian viscosity is independent of shear rate or stress and depends on the fluid flow rate, temperature, and pressure[3]. Non-Newtonian fluids have a nonlinear relationship between shear stress and shear rate, which means that their viscosity is not constant at a given pressure and temperature. Non-Newtonian fluids can be categorized into three major groups, which are time-independent, time-dependent, and visco-elastic fluids. However, this grouping of non-Newtonian fluids can not be acceptable sometimes because most materials, in reality, often show a combination of two or all three non-Newtonian types. As a result, it is necessary to classify the main non-Newtonian features and to take this as the base for the consequent process estimations.

Viscosity is considered to be the most important element for non-Newtonian materials and is defined as the ratio of shear stress to shear rate. Fluids' viscosity also depends on the time when they are subjected to the shear force [3]. If fluids are placed at shear stress for a long, their actual viscosity becomes so much. Those fluids include mud suspension, crude oils, foods, water suspensions, cement paste, etc.

2.3 Rheology

The design and implementation of numerous activities consistent with the oil and gas industry depend on the unusual properties of a group of materials known as non-Newtonian liquids. These unique properties are called rheology, and the process of estimating and representing these properties has fallen a long way behind the field application of these liquids in the industry.

While Rheometry is defined as a technique used for analyzing material rheological behavior, rheology is defined as the matter analysis when it flows or deforms. Accordingly, rheology explains strains and forces over time.

The word rheology, as in most fields of science, has its roots in ancient Greek, with the root rheo meaning "flow." As the area has developed, it is no longer interested only in the flow of fluids but also in the solids' deformation and complex behavior of viscoelastic substances that have both liquid and solid properties, according to the forces/deformations that are applied to them.

2.4 Flow Regimes

In the past decades, numerous researchers have given more attention to flow regime characteristics and multiphase flow assurance monitoring. The most common flow regimes for vertical wells are bubble, slug, annular, churn, and mist flow. The possible flow regimes also dispersed bubble, slug, annular, stratified wavy, and stratified smooth for horizontal wells. In order to increase the gas flow rate from top to bottom, the gas/liquid flow regimes in horizontal pipes are summarised below:

Bubble flow: Small bubbles of gas flow along the top of the tube.

Elongated bubble flow: Collisions between different bubbles happen more frequently as the gas flow increases.

Smooth stratified flow: The gas plugs join to generate continuous gas flow along the top of the pipe and have a smooth gas-liquid interface representing a stratified flow at a relatively low flow rate.

Wavy stratified flow: In most cases, the gas-liquid interface is infrequently smooth, and ripples occur on the liquid interface. The level increases with increasing gas flow rate.

Slug flow: When the waves' amplitude on the liquid surface increases considerably to reach the upper part of the pipe, the flow goes into the slug flow. The gas then flows intermittently in the form of plugs and with small bubbles penetrated by the liquid. The slug flow

was noticed for the superficial gas velocity range of (3-50) m/s and superficial liquid velocity between (0.2-11) m/s. It is simply a continuous liquid flow that contains gas bubbles like a wave travelling along the liquid surface and flows as intermittent slug bubbles entrained in the liquid.

Annular flow: This ensues when the gas flow is large enough to support the liquid film surrounding the pipe's walls. In addition, the fluid is transported like drops flowing in a continuous gas flow through the center of the pipe. Finally, the liquid film is trapped at the bottom of the pipe due to the effect of gravity.

Taitel and Dukler[16] created a horizontal flow regime map for gas-Newtonian flow as shown in Fig (2.1)

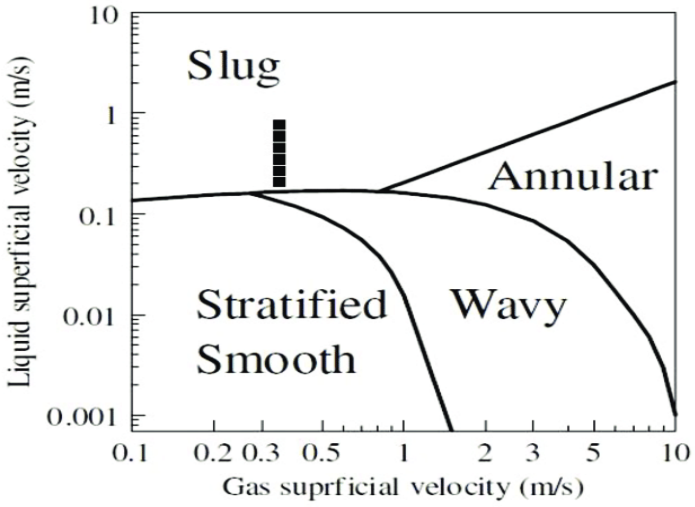

Fig. 2.1 - Flow pattern map for gas Newtonian flow [16]

Slug flow is one of the most common flow patterns in Newtonian and non-Newtonian two-phase flow pipes. It is a widespread occurrence in gas-liquid two-phase flow in the pipe. Usually, it is a negative flow pattern due to its unsteady nature, intermittency, and high-pressure drop. The differences between slug flow and elongated bubble flow are not clear because these two types

of flow are usually combined under one flow category. These two-phase flow regimes are generally defined as intermittent flow[17].

The prediction of slug flow features is very complex due to the unsteady of most of the design variables. These variables include liquid and gas velocity profiles, non-Newtonian liquid concentrations, and pressure drop fluctuations even when the inlet gas and liquid flow rates are constant. Basically, the slug flow breakdown may result in a radical change in pressure gradient, and this can cause damage to equipment in the industrial process. Generally, slug flow occurs in horizontal flow through pipes when the gas velocity increases, causing waves to come to the top of the tube. Whether the flow will be plug or slug depends mainly on the void fraction that causes the accumulation of the bubbles to produce large plugs and slugs. While in plug flow, the dimensions of the bubbles are smaller than the tube diameter, slugs are compared in width to the tube diameter. Also, the slugs travel at a speed that is a significant part of the gas velocity and appears intermittently. Because these large gas slugs are separated from each other by liquid slugs, they cause huge liquid flow rates and pressure drop fluctuations[18].

The flow mechanism of slug flow is that the gas bubble is trapped in the liquid and drives the liquid forward nearly at the same velocity as the gas velocity. However, when the liquid becomes viscous, the gas requires more energy to move the liquid forward. At a constant gas flow rate, it is hard to achieve extra energy, so the process becomes slow, and the slug velocity and the number of slugs decrease, Syed Imtiaz et al. [19].

In fact, the pressure drop of non-Newtonian multi-phase flow is strongly affected by gas-liquid interface roughness. However, most previous models that were created depending on the liquid viscosity to predict void fraction and pressure drop of gas non-Newtonian flow assumed that the gas-liquid interface is smooth [18]. Nevertheless, Parsi et al. 2015 [20] experimentally

investigated the effect of huge gas/non-Newtonian flow waves in pipes for the slug flow regime. The research concluded that the liquid film works as a rough wall when the waves go up and down through the tubes. Therefore, its roughness considerably affects the frictional part of the pressure drop.

Xu Jing et al. [1] investigated two-phase gas/non-Newtonian flow and stated that the features of non-Newtonian fluids had a minimum effect on the flow regime in horizontal flows when the low concentrations of the non-Newtonian fluid were applied. The research also concluded that non-Newtonian properties of liquids considerably affect the void fraction of two-phase flows, and the average void fraction is reduced by using a shear-thinning liquid[21].

The slug flow regime may generate high fluctuations in the flow rate of the two-phase flow of gas and liquid at the pipeline outlet. Therefore, observing slug flow regimes and examining their characteristics, like the gas void fraction, are essential to reduce the disturbance of flow process facilities[22]. The slug initiation mechanism has been experimentally investigated, and many researchers have recently carried out research on the mechanism of slug flow initiation.

Kordyban and Ranov [23] used classical linear stability analysis to describe the transition from stratified to slug flow. Viscous analysis by Kelvin–Helmholtz included effects of interfacial shear stress and wall effects on slug flow initiation, with better predictions concluded.

Taitel and Dukler [24] described various stages for developing pipelines' slug flow, starting with the pipe inlet. Due to the shear stress of the walls and gravitational force, the liquid velocity slows down, and small turbulences make the stratified layer. These would result in growing waves. An increase in gas velocity could lead to a pressure effect and cause the liquid height to cover the cross-section of the pipe, blocking the gas flow rate. This blockage leads to gas

pressure accumulation till the gas velocity accelerates. Along the way, the blocked fluid picks up slow-running liquid and increases the volume of liquid to form a slug.

Gas is trapped due to the differences between the velocities of the slug unit and the liquid film. The distribution of small bubbles can be transported throughout the body of the liquid slug. In the meantime, at the slug back, liquid and previously dragged gases are released from the slug body. As a result, the liquid slows down and becomes a stratified layer.

The shed gas mostly passes into the elongated bubble region above the stratified layer, although the slug continues to grow as long as the volumetric pick-up rate is larger than the shedding rate. However, the slung length stabilized after the slug became fully developed, as described in Fig. (2.2). Nydal et al. [25] experimentally studied the length of the pipe required to reach stable flow conditions and found that it is between 300 and 600 times of pipe diameter. After the stable circumstances are reached, the mean value of slug length goes between 12 and 15 of pipe diameter.

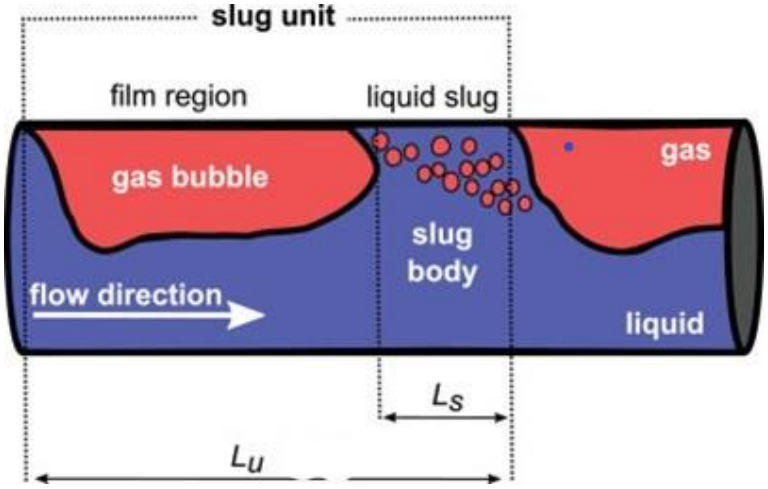

Fig. 2.2 - Slug unit description [25]

Faraj et al.[9] As shown in Fig(2.3), a flow regime map was created for the Xanthangum gas flow for the range of gas and liquid velocities reached during the experimental work. Several experimental investigations of non-Newtonian liquid gas flow have been done in this work. Xanthan gum was

used as a non-Newtonian liquid during the experiments for concentrations of 1,2 and 3 g/L. Both air and carbon dioxide are examined as gases that flow simultaneously with non-Newtonian liquids through tubes. Four multiphase flow patterns have been investigated for non-Newtonian/gas flow in this work. These flow regimes are Stratified, Slug, Bubbles, and Annular. The slug flow was noticed for the superficial gas velocity range of (3-50) m/s and superficial liquid velocity between (0.2-11) m/s. It is simply a continuous liquid flow that contains gas bubbles like a wave travelling along the liquid surface and flows as intermittent slug bubbles entrained in the liquid.

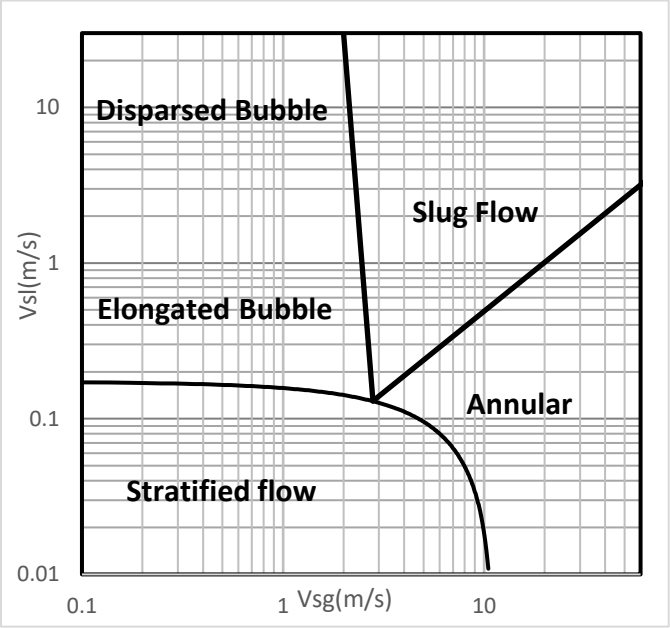

Fig. 2.3 - An experimental flow regime map of non-Newtonian gas flow

2.5 Pressure Drop

Several correlations were developed to obtain liquid holdup in multiphase flow in horizontal pipes. Mandhane et al. [26] published a well-known flow regime map and pressure drop prediction method for gas-liquid flow in horizontal pipes. This correlation was developed using the multiphase pipe flow data bank to capture flow regimes and estimate pressure drop using the

magnitude of the superficial liquid velocity and superficial gas velocity on a logarithmic scale. Most of the Newtonian multiphase flow correlations were developed using experimental data, while Taitel and Dukler [24] established the most common physical model. Numerous authors investigated the performance of the Taitel and Dukler model and found that this model is inclined to underestimate liquid holdup values for stratified smooth flow regimes. Abdul-Majeed [27] investigated the Taitel-Dukler model and also improved the model performance in a horizontal pipe using a mixture of air-kerosene fluids. The original model was claimed to overestimate liquid holdup for stratified wavy, annular flow, and slug patterns. For instance, the author proposed an improved correlation to find flow regimes by experimental data. The model was claimed to have excellent results compared to the existing correlations. Newly, Mohammad Azizur Rahman et al.[19] assessed the predictability of the multiphase flow regimes in the horizontal pipe by coupling machine learning and experimental data such as liquid and gas velocity, liquid and gas density, surface tension, pipe diameter, and absolute roughness.

Commonly used fluids in the oil and gas industry, like lacquers and polymer solutions, exhibit non-Newtonian characteristics. Their viscosity shows a nonlinear relationship between stress and share rate. The viscosity of non-Newtonian fluids has a major effect on gas/non-Newtonian flow properties and structures[17].

However, unlike for gas/Newtonian flow, just a little research has been dedicated considering the pressure drop of multiphase flow in pipes when the fluid is non-Newtonian liquid. Generally, these researches indicate that the hydrodynamic behavior of gas/non-Newtonian flow in pipes is completely different from the gas/Newtonian flow. This is very important knowledge industrially regarding fluid transportation and related operations. For instance, a gas/non-Newtonian multiphase flow in pipes can result in a huge decrease in the pressure drop compared with

gas/Newtonian flow, which is basically important for economics because it can reduce pumping energy[13].

One of the earliest and most reliable correlations for pressure drop arising from the flow of gas-liquid mixtures in a pipe was derived by Lockhard & Martinelli [28]. Ward and Dallavalle [29] improved the fact that the pressure drop due to frictional losses when shear-thinning fluid flowing through a pipeline at a fixed flow rate may be reduced by the injection of gas into the fluid. This fact is defined as drag reduction. Singhal et al. [30] Investigated frictional pressure loss and flow behavior of Newtonian and non-Newtonian fluids depending on Experimental work and simulation studies for concentric annular flow. Water was investigated as Newtonian, and many concentrations of Xanthan gum and guar have been experimented with as Non-Newtonian fluids. Both turbulent and laminar flow regimes were studied for various annular dimensions. The Reynolds number and friction factor were modified using effective diameter for annular geometry.

In fact, the pressure drop of non-Newtonian multiphase flow is strongly affected by gas-liquid interface roughness. However, most of the previous models that were created depended on the liquid viscosity to predict void fraction, and pressure drop of gas non-Newtonian flow assumed that the gas-liquid interface is smooth[31]. Nevertheless, Parsi et al. 2015 [20] experimentally investigated the effect of huge gas/non-Newtonian flow waves in pipes for the slug flow regime. The research concluded that waves going up and down through the pipes could make the liquid film work as a very rough wall. Its roughness considerably affects the fractional part of the pressure drop.

2.5.1 Pressure Drop Models

The pressure drop in two-phase flow is heavily influenced by gas-liquid interface roughness, and the pressure drop calculations generally depend on the fluid properties. The pressure drop for any flow system is a summation of the system's hydrostatic, friction, and acceleration pressure drops. For instance, the hydrostatic term depends on the fluid mixture density, a function of the liquid holdup. For instance, the frictional pressure drop depends on the friction factor for the fluid mixture. Furthermore, the acceleration pressure drop term occurs due to the change in velocity resulting from the change in pressure. The friction factor calculations depend on the flow regime, which depends on the superficial velocity of liquid and gas phases[32].

In the last-few decades, both mechanistic models and empirical correlations were derived to obtain pressure drops in pipes. Based on the literature survey, empirical correlations can be grouped into three categories based on slip ratio (Ansari et al.) [33]. First, some correlations assume that there is no slip and do not consider flow patterns to estimate pressure drops, such as Poettmann and Carpenter [34]. A few numbers of correlations considered only the slip but not the flow patterns, like Hagedorn and Brown[35]. Several authors, like Beggs and Brill (1973), considered both the slip and the flow patterns to estimate the pressure drop.

Dziubinski and Chhabra (1989) [36] modified Lockhart and Martinelli's pressure drop correlation by introducing the Farooqi and Richardson (J) factor into the correlation, as follows:

$$\left(\frac{d_p}{d_l}\right)_{tp} = \left(\frac{d_p}{d_l}\right)_{l} \left(J + \frac{C_0}{x} + \frac{J}{x^2}\right) \tag{2.1}$$

where C_0 = 12 for a liquid-laminar and gas-turbulent flow.

$$x = \sqrt{(dp/dl)_g / (dp/dl)_l} \tag{2.2}$$

$$J = \left(\frac{u_{sl}}{u_{cl}}\right)^{1-n} \tag{2.3}$$

This model has an approximate 40% error and is related to laminar flow. The diameter range used in the model is 2.9 ≤D≤ 207 mm, while the superficial liquid velocity range is $0.17 \leq u_{sl} \leq 2$ m/s, and the superficial gas velocity range is $0.11 \leq u_{sg} \leq 23$ m/s.

Xu et al. modified the Two-Fluid Model for gas/Newtonian fluid slug flow to include power-law fluids. [13] assumed that the film does not contain bubbles and that both fluid and gas are incompressible by ignoring pressure drop across the gas slug.

The pressure drop can be calculated as follows:

$$\left(\frac{dp}{dl}\right)_{tp} = \left(\frac{dp}{dl}\right)_{ls} = 2\frac{f_{ls}}{D}\rho_{ls}u_m^2 k \tag{2.4}$$

Where:

$$\rho_{ls} = (1 - a_s)\rho_g + a_s\rho_l \tag{2.5}$$

$$f_{ls} = \frac{C}{Re_{ls}^{nl}} \tag{2.6}$$

$$a_s = \frac{(1-sin\theta)^{0.05}}{1+3.166\times10^{-5}Re_{tp}^{1.225}} \tag{2.7}$$

The Reynolds number is given by:

$$Re_{tp} = \frac{D^n u_m^{2-n}}{8^{n-1}K}\rho_l \tag{2.8}$$

C = 0.079, n_l = 0.25 for turbulent flow and

C = 16, n_l = 1 for laminar flow.

The Reynolds number for two-phase flow in the liquid slug is:

$$Re_{ls} = \frac{D^n u_m^{2-n}}{8^{n-1}K}\rho_{ls} \tag{2.9}$$

Xu et al. used carboxymethyl cellulose (CMC) solutions in their experiments. The results indicate that the two-fluid model agrees well with drag reduction and pressure drop data.

K. Wang. et al. [31] Created an analytical model to determine pressure drop and void fraction for non-Newtonian mixtures. In addition, the study focused on wave behavior for churn flow. The study concluded that the non-Newtonian flow characteristics like pressure drop, wave behavior, velocity profiles, and void fraction are strongly affected by liquid viscosity.

Jing-yu 2010, Experimented with Gas/Newtonian and Gas/Non-Newtonian flow through two 10 m long pipes and 60 mm diameter connected by a U tube. Tab water has been used as a Newtonian fluid, and carboxymethyl cellulose is a non/Newtonian fluid. The gas used in this work was air, which the compressor injected into the system, and the liquid was circulated through the system by a centrifugal pump.

Hwang et al.[37]. Derive a mathematical model to predict pressure gradient and the film thickness of Non-Newtonian liquid and gas flow. The study focused on annular two-phase flow through horizontal pipes. The model has been created based on many assumptions, such as the flow is laminar at the liquid film, turbulent in the gas core, and has a no-slip condition. Results show that the model predicted the film thickness and pressure drop with a variation of about 10% between analytical and experimental results. is lower than10%. Concluded with a comparison between Newtonian and non-Newtonian flow for the same flow rates, the non-Newtonian two-phase flow comes up with a lower pressure drop.

Pressure Drop Models (stratified flow):

Hwang et al. [38] developed a mathematical model to predict pressure drop and liquid holdup for non-Newtonian stratified two-phase flow. The interface shape is determined by solving the Young–Laplace equation. The study described the interface shape between gas and liquid for different values of Bond number, and the results show that the interface can be explained using

an arc shape when the Bond number is lower than 10. The interfacial tension effect is significant, especially for stratified-gas–liquid flow with low liquid holdup.

2.6 Void Fraction (ε)

The void fraction in the multiphase flow of gas and liquid can be defined as the volume fraction of gas that is occupied in the channel flow. In particular, the void fraction of gas-liquid flow is the fraction of the flow rate of gas to the total gas and liquid flow rates.

The void fraction is restricted to the flow patterns. Regardless of the pipe diameter and fluid properties, the void fraction increases with a slight increase in the gas flow rate for slug and bubbly flow regimes. However, in the case of the annular flow, the void fraction remains nearly constant, even with a significant increase in the gas flow rate because the liquid film separates gas bubbles from the channel wall [6][39].

2.6.1 Void Fraction Modeling

Many void fraction correlations are created based on the liquid holdup of the slug body, Gregory et al.[40].

The liquid holdup can be given as a function of the mixture velocity Vmix as follows:

$$H_L = \frac{1}{1 + \left(\frac{V_{mix}}{8.66}\right)^{1.39}} \tag{2.10}$$

V_{mix} slug mixture velocity in m/s is the total of the superficial liquid and gas velocities.

The most common correlation to estimate void fraction depending on slug mixture velocity is the Hughmark correlation[41]:

$$\boldsymbol{\varepsilon} = \frac{V_{sg}}{1.2V_{mix}} \tag{2.11}$$

V_{sg} is the superficial gas velocity, the gas flow rate divided by the cross-sectional area of the tube.

Ferschneider[8] created another model to estimate slug body holdup $H_{L.}$ by using a 0.15 m diameter for a 120 m tube long in the test section operated at a pressure between 10 and 50 bars. This correlation has been considered both Bond number Bo and surface tension of fluids as follows:

$$B_O = \frac{(\rho_L - \rho_g) \times g \times D^2}{\delta} \tag{2.12}$$

$$H_L = \frac{1}{\left\{1 + \left[\left(\frac{V_{mix}}{\sqrt{(1-\rho_g/\rho_L)gD}}\right) \times \left(\frac{B_O^{0.1}}{25}\right)\right]^2\right\}^2} \tag{2.13}$$

The relationship between void fraction and gas velocity has been presented early by K. Wang et al. [31]. Increasing gas velocity led to the void fraction increasing; in contrast, increasing liquid velocity caused a decrease in the void fraction. The void fraction has been the subject of many investigations, and most of these investigations have focused on larger tube diameters with adiabatic Air/water flows. There are comparatively fewer studies conducted on small channels like Winkler et al.[42], and Marcin Pietrzak[43] presented a comprehensive review of experimental and modeling techniques to obtain void fractions, focusing on small channels.

Most void fraction correlations strongly depend on determining the velocity ratio. Therefore, many experimental studies concluded that the parameters affect the gas/liquid velocity ratio[44]. The physical properties of the fluids, such as the ratio of gas and liquid densities and viscosities, are critical parameters affecting the void fraction[45]. Other parameters like mass velocity, flow

quality, tube diameter, and flow pattern have been studied by numerous researchers[46]. Butterworth combined all the parameters affecting void fraction in one general standard form. However, other essential parameters affect void fraction, like slip ratio, which is not included in the general form. Gun Sim. et al.[47] indicated the difficulty of void fraction determination because it depends on the slip ratio.

Triplett et al. [48] used photographs of flow patterns in 1.1mm diameter pipe and 1.45 mm diameter for horizontal circular channels (although, as noted in the previous section, flow patterns were also recorded for semi-triangular channels) to obtain the volumetric void fraction. They found that the void fraction increases with increasing superficial gas velocity at a constant liquid superficial velocity. They also compared their results with the void fraction correlations of Butterworth [2] and the correlation of Chexal and co-workers Chexal et al.[49] . They found that the homogeneous flow model best predicted the measured void fractions in bubbly and slug flow at low values of superficial gas velocities. However, the homogeneous model and other empirical models significantly overpredicted the experimental values for annular and churn flow. They believe this overprediction by the empirical correlations, typically based on annular flow in large channels, is due to the greater slip in the larger channels than in microchannels.

Yashar et al. [50] recognized the higher vapour phase densities in the evaporating flows compared to Air–water flow. They pointed out that this led to lower gas velocities and more stratified flows and concluded that the void fraction is entirely affected by the mass flux of the gas. This group [51] also used the Froude number to develop a simple model for changing the void fraction from stratified to annular flows. They used the ratio of the gas kinetic energy to the gravitational drag and the Lockhart–Martinelli parameter, which accounts for the ratio of the viscous drag to the gas kinetic energy. The group used Linked shutoff valves, which were also

used by Koyama et al. [52] to measure the volume of gas trapped in the test section, yielding the volumetric void fraction but not the cross-sectional void fraction.

The above discussion has shown that void fraction models for standard tubes have been developed based on an assumption of homogeneous flow or as a function of slip ratio, the Lockhart–Martinelli parameter, and mass flux. In addition, many of these models assume annular flow regardless of the flow conditions. Also, several of these models were developed using data from air–water adiabatic flow or vaporizing flows, although, in practice, they are also routinely used for condensation.

2.6.2 Void Fraction and gas kick early detection

When unusual high-pressure formations occur in deep waters, the gas kick is likely to occur, causing severe blowouts. For example, the Deepwater Horizon oil spill and blowout in 2011[53] caused heavy human deaths, substantial economic losses, and marine natural environment damage. Therefore, as an essential part of well control technology in deep water drilling, the earlier the gas kick is detected, the smaller the volume of influx gas, the lower the bottom hole pressure change, and the higher the probability of successful reasonable control.

The Doppler ultrasonic wave technique has been used widely in flow measurement and medical imaging[54]. This method was developed using the ultrasonic propagation velocity section to measure the void fraction and bubble flow velocity. This method's advantages are low cost, no direct contact with the measured fluids, and simple tool structure. Abbagoni et al. [55]. The gas void fraction increases rapidly when the well depth is less than 500 m. It is too late to control the well if the gas kick is detected at this moment, and the gas kick could lead to an out-of-control blowout.

Fig. 2.4 - DEEP WATER HORIZON **- Macondo Well Blow-Out**[53]

2.7 Supercritical Carbon Dioxide and Hydrate Formation

Global warming is considered the most challenging issue facing humanity today, with many research studies now focusing on investigating the main cause of this problem. Studying the behaviour of carbon dioxide in its different phases can provide the key to resolving this critical issue. A wide range of CCS (CO_2 capture & storage) will transport large quantities of CO_2 from capturing locations to storage sites. Major transportation processes occur through pipeline networks, and CO_2 must be liquid or dense. Usually, this flow will be a mixture of gas and liquid (two-phase flow) and sometimes contain various impurities (three-phase flow). Industrially, CO_2 is transported over supercritical conditions between gas and liquid with a density like a liquid and viscosity like a gas. Transporting CO_2 by pipeline is completely different from natural gas transportation because CO_2 is often delivered in the dense liquid phase, while natural gas is transported in a dense gas state [56][57].

Depending on the fuel source and capture process, CO_2 might contain nitrogen, oxygen, water, sulfur oxides, methane, and other impurities. Erikade Visser et al.[58] concluded that under normal transport conditions (pressures, temperatures, and the presence of other possible components), a water level of 500 ppm is sufficiently low to minimize risks of free water and hydrate formation.

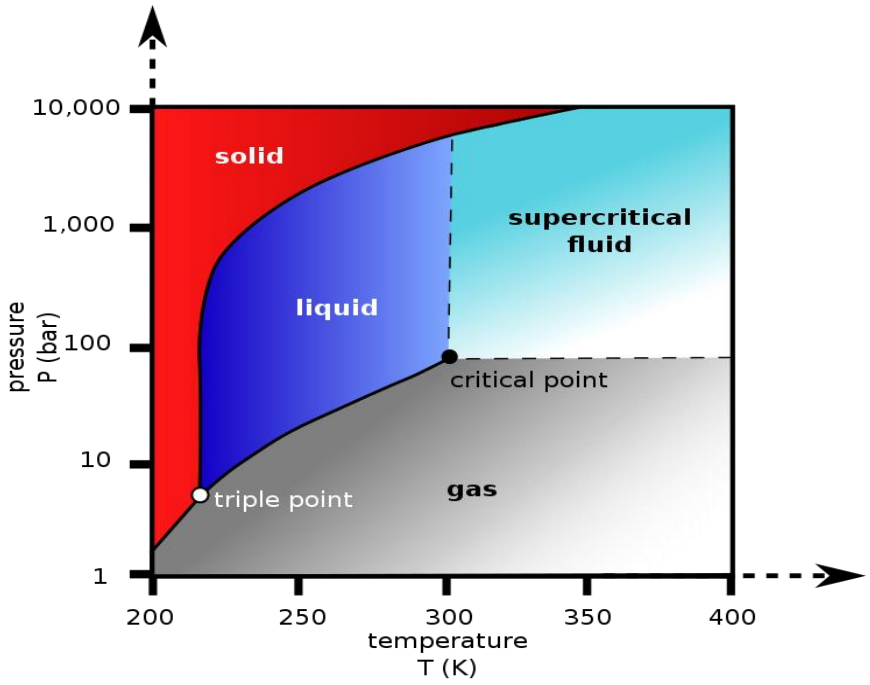

Fig. 2.5 - Critical point of Supercritical Carbon Dioxide[59]

Austegard and Barrio [60] Reported that When transporting CO_2 above its critical pressure of 71.3 bar, the solubility of water is above 1300 ppm for a temperature range of −10 °C to 25 °C. However, for offshore pipelines, the temperature of the seawater at storage depths (North Sea) is about four °C. Therefore, water solubility is above the proposed 500 ppm for pressures above 40 bar at this temperature.

Nordhagen et al.[61] Argue that because the widespread implementation of CCS will, in some cases, require onshore CO_2 transport pipelines running through populated areas., this may need strict safety guidelines due to the pipeline pressure and since CO_2 is toxic at high concentrations. As a result, pipelines should be explicitly designed to avoid significant hazards. Pictures of the pipeline (methane at 122 bar) are shown in Figure (2.6) after the crack arrest. A simulated picture is seen in (a), and a picture after the full-scale experiment is seen in (b).

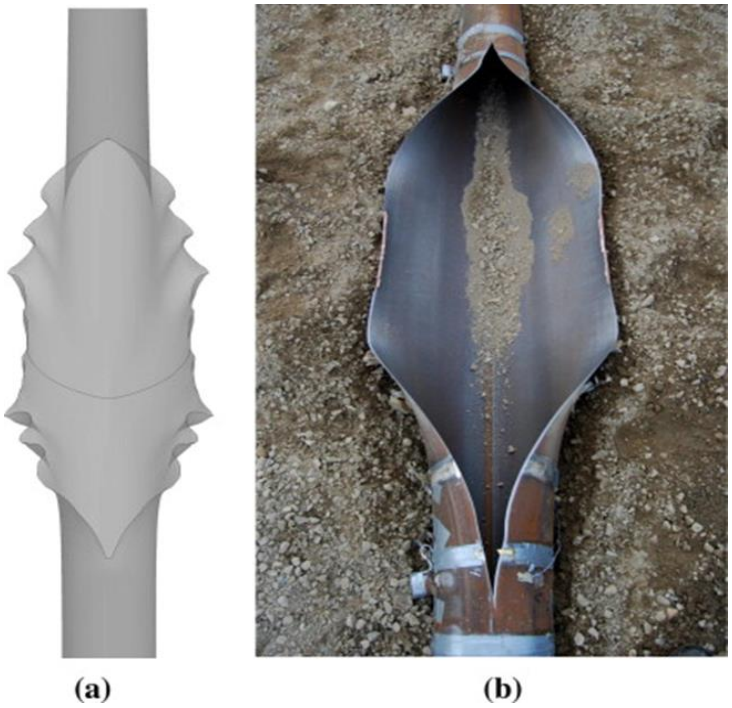

Fig. 2.6 The pipeline cracked after high pressure was applied.[61]

From a modeling point of view, several specific challenges related to CO_2 transport make it different from oil and gas transportation. First, the critical point (7.38 MPa at 31.1 °C) and the triple point (about 518 kPa at −56.6 °C) differ. This highlights that CO_2 is usually transported in a dense liquid state, whereas natural gas is in a dense gaseous state[62]. In conclusion, all previous research recommended minimizing water content to avoid corrosion and hydrate formation when transporting CO_2 in supercritical conditions.

Production facilities, especially offshore wells and transmission lines, may operate under favourable hydrate formation conditions. Gas hydrate formation occurs when water molecules surround neutral gas molecules. These cages are known as “clathrates.” Gas hydrates are similar in appearance to ice. Both materials have crystalline structures with similar characteristics. The important difference between ice and natural gas hydrates is the guest molecule, which is an integral part of their structure[63]. Examples of typical hydrate-forming gases include nitrogen, carbon dioxide (CO_2), hydrogen sulphide (H_2S), and light hydrocarbons (such as methane up to heptane). Depending on the gas composition and the pressure, gas hydrates can form at temperatures of up to 30 °C (86 °F) where gas co-exists with water.

Mahmood Farzaneh-Gord et al. [64] investigated the possibility of gas hydrate formation for the natural gas pipeline process. Results show that natural gas composition affects the hydrate formation conditions. He plotted gas hydrate formation temperature versus pressure for various natural gas compositions. He concludes that hydrate formation temperature is higher for natural gas with higher molar mass (such as Pars) than for natural gas with lower molar mass (such as Khangiran). For all natural gases, hydrate formation temperature increases with increasing pressure. He investigated that the hydrate formed under the range of Temperature between 17 C^O and -12 C^O for different types of gas composition, and the pressure range was (250 – 1000) psi. The pipeline length was about 160 Km.

Experimental and empirical phase equilibrium conditions of carbon dioxide (CO_2) hydrate in a porous medium were investigated by Mingjun Yang et al. [65] examined that carbon dioxide (CO_2) can form hydrate under the range of Temperature between $3C^O$ and -10 C^O and the pressure range between (2 – 4) Mpa in different porous media. First, the researcher distributed water throughout a mineral medium (e.g., packed moist sand, drained sand, moistened silica gel,

and other porous media). Then, the mixture was brought to hydrate-stable conditions (chilled and pressurized with gas), allowing hydrate to form. This method typically produces grain-cementing hydrate from water in the sand.

In the dissolved gas method, Tohidi et al. [66] bring water with necessary dissolved guest molecules to hydrate-stable conditions where hydrate forms. In the laboratory, this can be done by pre-dissolving the gas of interest in water and then introducing it to the sample under the appropriate conditions. This method makes forming hydrate from more soluble gases such as carbon dioxide easier. In addition, this method is thought to more closely simulate how most natural gas hydrate has formed.

Gupta et al.[67] In his method, water-wetting sand is uniformly moistened and packed into a vessel or sleeve. The void space is evacuated, and the hydrate-forming gas is introduced. Hydrate is formed either by pressurizing the system well into the stability zone and cooling or by pressurizing the chilled sample. He concluded that hydrate begins to form in specific locations. The conditions at those locations govern these locations at the time hydrate starts to form and the stochastic nature of nucleation.

Robert W. Henning et al.[68] Investigated the formation of CO_2 clathrate hydrate by using time-of-flight neutron powder diffraction at temperatures ranging from 230 to 290 K with a CO_2 gas pressure of 900 psi. CO_2 clathrate hydrate was prepared in situ from deuterated ice crystals at 230, 243, 253, and 263 K by pressurizing the system with CO_2 gas to produce the hydrate in approximately 70% yield. Nearly complete conversion from the hexagonal ice to the sI type CO_2 hydrate was observed as the sample temperature slowly increased through the melting point of CO_2 ice.

In his study, R. Hegde [60] used the SRC two-layer model to predict friction loss for liquid CO2 slurry. They then used predicted friction loss to calculate specific energy consumption SEC for liquid CO_2 slurry. The researcher mentions that experimental data is necessary to validate the friction loss calculations. In short, R. Hegde didn't experiment with CO_2 slurry in his pipe loop. Instead, he used water slurry at 70 C^0 because he thought water viscosity at 70 C^0 was similar to the viscosity of CO_2 liquid. Therefore, he couldn't use the CO_2 liquid in the laboratory for safety considerations.

In fact, comparing theoretical calculations for flowing fluid with experimental results for another flowing fluid in terms of friction loss estimations is acceptable since the two fluids have similar viscosity. Still, it is not adequate for other flow condition estimations. For example, in his thesis, the writer did not include any values for system pressure or pressure gradient in the loop, either experimentally or theoretically.

In summary, on the one hand, all previous studies recommended that when transporting CO_2 above supercritical conditions, water content should be minimized to avoid corrosion and hydrate formation. On the other hand, CO_2 transportation through pipelines in supercritical conditions needs safer equipment designed especially in populated areas to protect humanity against exposure to high concentrations of carbon dioxide. As a result, and for greenhouse applications, CO_2 must be transported at low pressure with water moisture.

CHAPTER 3

Experimental Methods

3.1 Experimental Setup

Pipe bends (also known as ‘elbows’) are commonly used in industrial pipelines. Pipe bending allows for flexible thermal expansions to happen without causing damage or overloading the piping network.

The experimental setup consists of the fluid supply section, the flow loop section, and the data acquisition system. As shown in Figures (3.1) and (3.2), the fluid supply part consists of the liquid tank, CO_2 cylinder, and compressed Airline.

The flow loop length is about 23 m pipe (test section), as shown in Figure (3.4). The liquid is pumped from the tank through a (3/4) inch 19.05 mm PVC pipe. Transparent PVC pipes are used for good visualization. Fig. (3.5) describes the flow loop pipeline set-up schematic diagram.

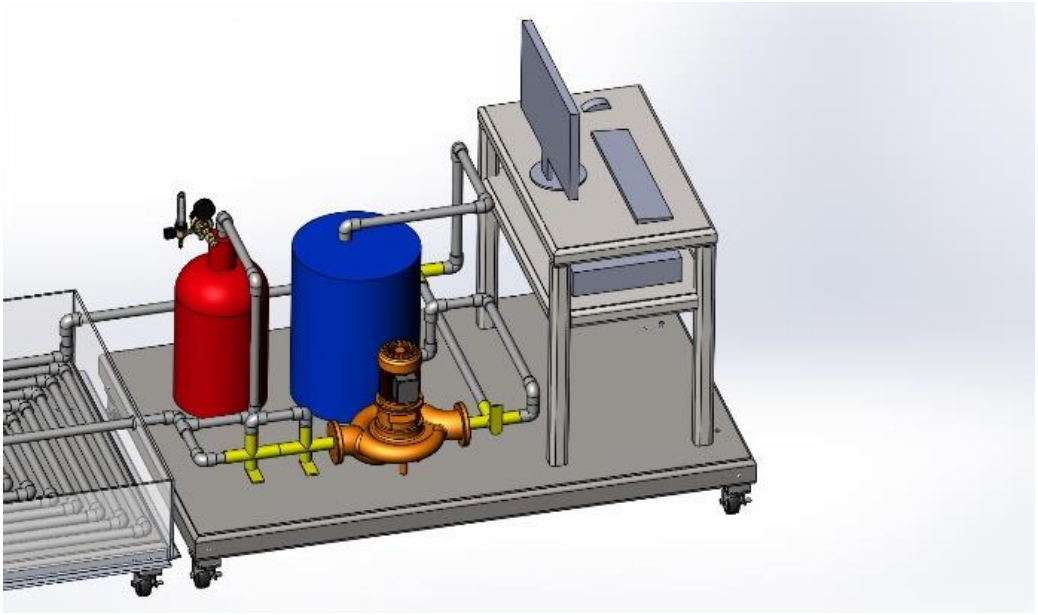

Fig. 3.1 - Fluid Supply Section

Fig. 3.2 - Picture of Fluid Supply Section

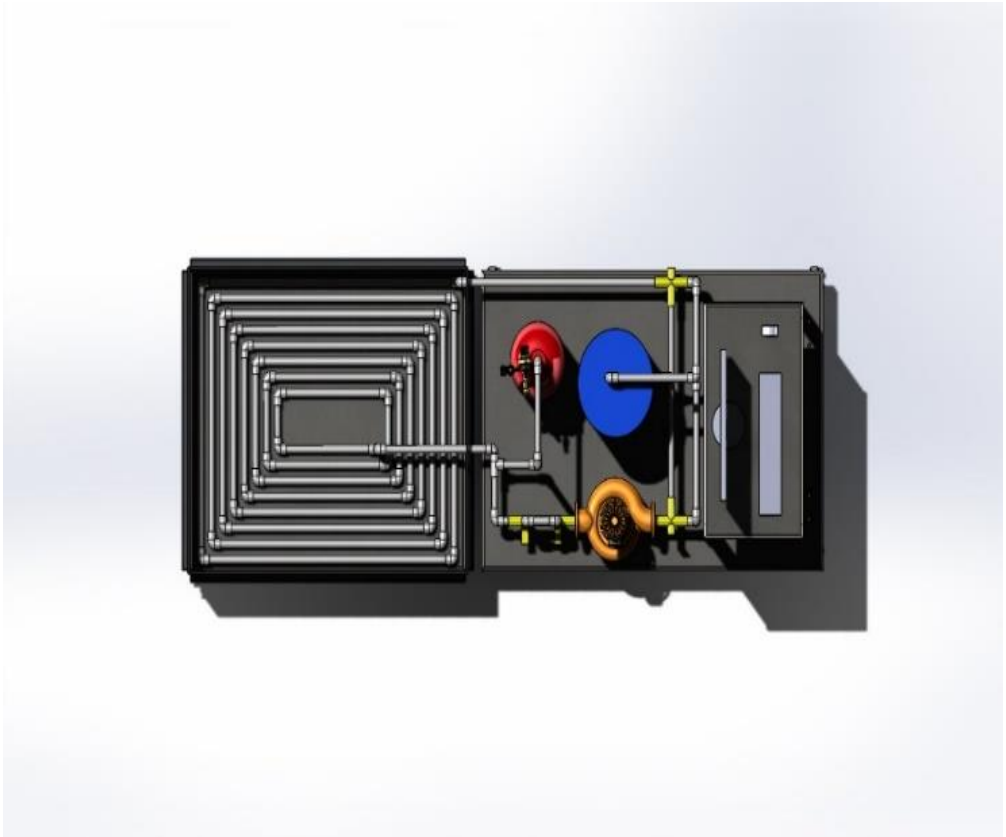

Fig. 3.3 Flow Loop Section

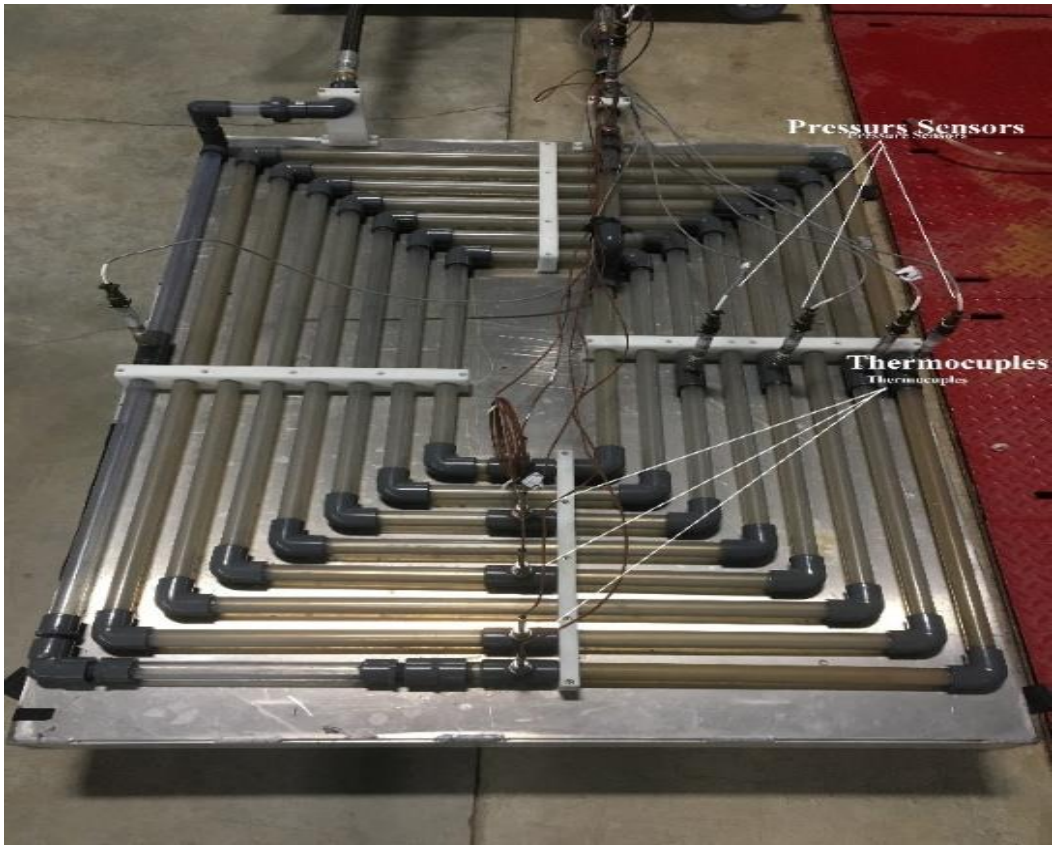

Fig. 3.4 - Picture of Flow Loop Section

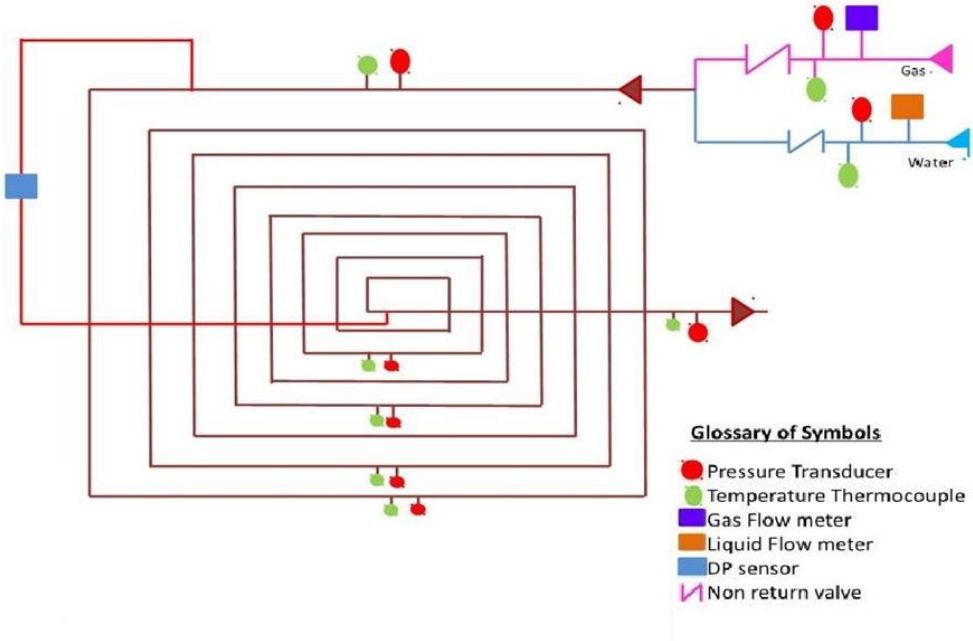

Fig. 3.5 Schematic Diagram of Flow Loop Pipeline Set-up

The two-phase flow can be formed by mixing the gas from the airline and the liquid from the tank. Instrumentation includes seven pressure and temperature sensors and flow meters for the gas and liquid to measure the individual gas and liquid flow rates. The air injection pipe is also provided to run the pump. The pump is a Wilden's H200 25mm (1in) high-pressure pump that is reliable, variable, and able to transfer viscous solid-laden slurries at high discharge pressure up to 300 Psig (2068kPa). Manual control valves are installed on the fluid supply section to facilitate and control the flow conditions and generate different flow regimes. The control of the flow loop is implemented through a fully integrated online computer system, which also operates the data acquisition system.

The liquid tank (Xanthan gum and water) and CO_2 cylinder beside the airline are the sources of liquid and gas, respectively, as shown in Fig (3.2). The liquid tank is connected to a high-pressure pump that drives liquid to the pipeline loop. Mixing Xanthan gum and CO_2 or air occurs at the start of the pipeline loop. Additionally, liquid and gas flowmeters are fixed before the mixing location to record liquid and gas flow rates separately. Finally, all the thermocouples and pressure sensors are connected to a data acquisition system associated with a computer to record the results.

3.2 Flow Loop Apparts

3.2.1 The Tank

The flow loop starts with a 5 Gallon, about (18.92 Liter) steel tank used for the liquid. The tank is connected to the circulation pump via a 0.75 in (19.05mm) pipe. Figure (3.6) shows the tank used.

Fig. 3.6 - Flow Loop Tank

3.2.2 The Lquid Pump

The pump produces the required significant volume flow rates through the flow loop, as shown in Fig (3.7). It is a Wilden's H200 25mm (1in) high-pressure pump that is reliable, variable, and able to transfer viscous liquids at high discharge pressures of up to 300 Psig (2068kPa). The pump's model number is H200/WWWAA/FWS/WF/MWF.

Figure (3.7) Wilden's pump[69]

3.2.3 Liquid Flow Meter

The liquid flow meter is required to record the flow rates of the liquids in the flow loop. The liquid flow meter is placed in the lines just before the point where the streams are joining.

The Wafer Magnetic Flow meter (Flow tube, Rosemount Model 8711; Model # 8711SHAOU1NOG1), as shown in Fig. (3.8), is installed in the liquid line. The accuracy of this meter is Up to 0.15% of volumetric flow rate accuracy over 13:1 flow turndowns, 0.25% over 40:1 flow turndowns, and is feasible with 0.15-8 inch (4-200mm).

Figure (3.8) Liquid Flow Meter[70]

3.2.4 Gas Flow Meter

The Omega brand gas flow meter (model # FLR6725D) covers the range of gas flow in the flow lines of the flow loop. This flow meter can cover flow rates from 5 to 50 SCFM (8.50 to 84.95 m3/h), as shown in Fig. (3.9). The gas flow meter is installed in the PVC pipe before the gas-liquid mixing point. Each flow meter has an attached signal conditioner that interfaces each meter with the DAQ system. Furthermore, the flow rate is shown on the display of each flow meter. A Hall Sensor takes the flow measurements by counting the pulses per minute. The sensor can be screwed open to change the basic settings.

Figure (3.9) Gas Flow Meter[71]

3.2.5 Pressure Sensors

The flow loop contains seven pressure sensors distributed along the pipeline. Figure (3.10) shows the Omega sensors installed on the flow loop.

The pressure sensors are Omega PX603 series cable-style. These sensors are consistent with liquid and gas. The model of the sensors is PX603-300G5V. These sensors produce a 1-5 V output signal and are connected to the data acquisition system. Each sensor is equipped with a DN 8 (1/4 in) male National Pipe Thread Taper (NPT) fitting, which can be installed into the flow loop.

Figure (3.10) Pressure Sensor[72]

3.2.6 Thermocouples

There are seven thermocouples distributed on the flow loop. The temperature thermocouples of T-type thermocouples, the Omega TC-(*)-NPT Series, theses thermocouples are pipe plug probe style. The thermocouple-grade lead wires are stranded 20 American Wire Gauge (AWG), fibreglass insulated, and stainless steel over braided with stripped leads. There is a hex section that is 22 mm (0.56 in) across flats that are 5.8 mm (0.23 in) wide to tight thermocouples on the pipe [3]. Figure (3.11) shows the thermocouples used. They produce a millivolt signal related to the temperature.

Connecting the thermocouples to the DAQ board requires an extra wire made of different metals from Omega. Tees with DN 8 bushings allow thermocouples to be installed in the pipelines. The sensors are mounted to the PVC pipe by using clamp-it saddles that seal around the pipe with an O-ring. [4].

Figure (3.11) Omega Temperature sensor[73]

3.2.7 Data acquisition system

The data acquisition system (DAQ) related to National Instruments (NI) was designed and created using National Instrument Data Acquisition Module NI 9319 DSUB, 4ch, 24-bit, 100S/s/ch, dynamic universal AIC series module. The program translates the incoming signals from the pressure sensors, flow meters, and thermocouples, as in Figure (3.12).

LabVIEW SignalExpress program is used to translate data from DAQ and show the outcome numbers. The screen displays the numeric values of the pressure, temperature, and flow rate for all active sensor inputs. As shown in Figure (3.13), the SignalExpress software monitor displays flow rates, pressure signals, and temperature signals of the

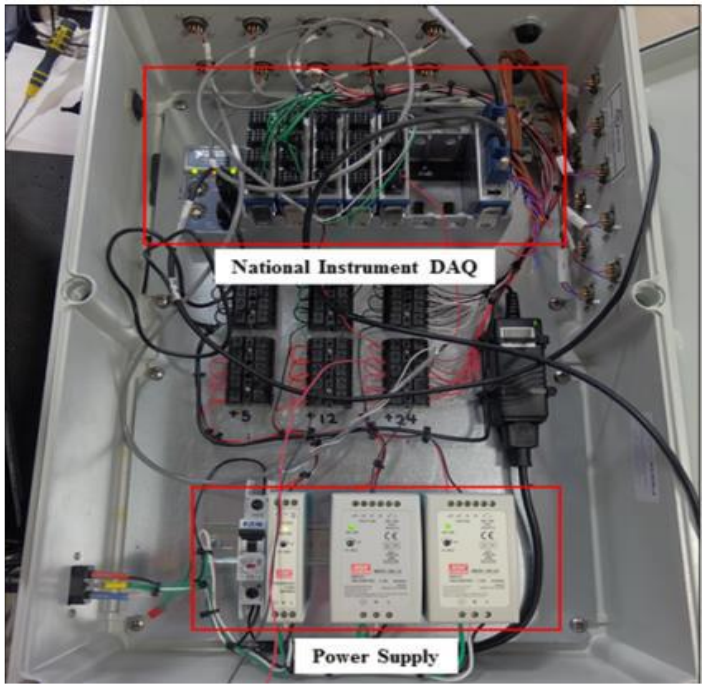

Figure (3.12) Data Acquisition System

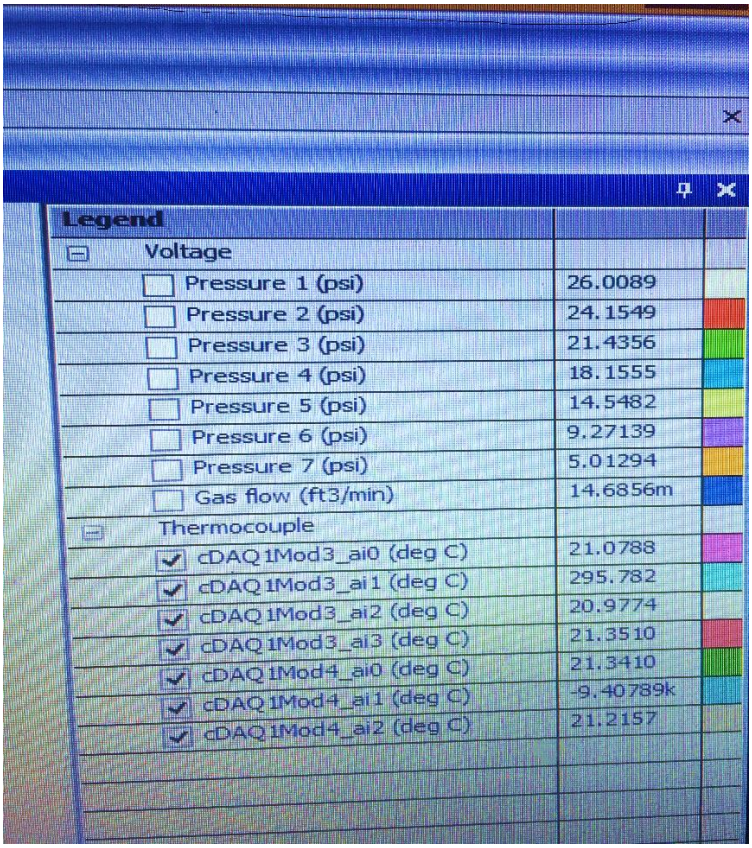

Figure (3.13) SignalExpress Screen Shot

3.2.8 Air Filter

In addition to the air pressure regulator, an Air filter was installed in the system. The model number of the filter is 52.160 TOPRING brand, as indicated in figure (3.14). This filter is designed for high air flow rates and can remove any water from the air using centrifugal force and impurities down to 40 microns in size. This filter is important for filtering any pollutants created during the compression cycle.

Figure (3.14) Air Filter

3.2.9 High-Speed Camera

The model of the high-speed digital camera used for recording is Mega Speed MS55K., as shown in Figure (3.15). This camera gives high-quality videos and images and the ability to load and save files. Moreover, this camera can connect to personal computers as the package includes a pre-set computer, software, lighting, power supply, camera cables, etc. [74].

Figure (3.15) High-Speed Camera

3.2.10 CO_2 Gas Cylinder

As shown in Figure (3.16), a carbon dioxide cylinder is used to inject CO_2 gas into the flow loop to mix it with liquid.

Figure (3.16) Carbon Dioxide Cylinder

3.3 Rheology Measurement Equipment

3.3.1 Electronic Scale

The Xanthan gum concentration is defined as a gram of Xanthan gum per litter of water; therefore, the mass of Xanthan gum is measured by this scale as in Figure (3.17).

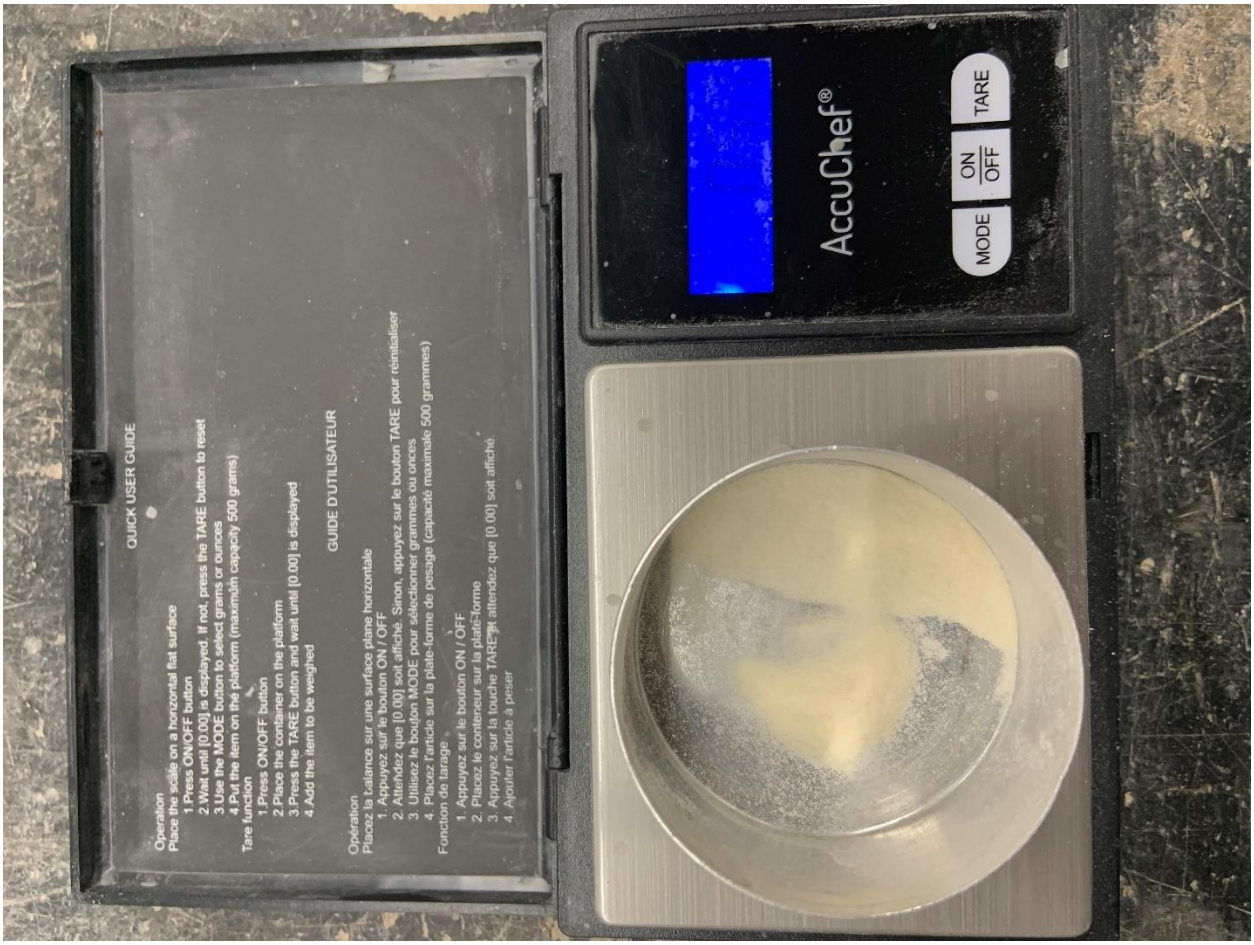

Figure (3.17) Electronic Scale

3.3.2 Graduated Beakers

To measure the volume of water needed to mix with Xanthan gum powder to make accurate concentrations, as seen in Figure (3.18),

3.3.3 High-Speed Mixer

The xanthan gum solution must be mixed homogeneously using the high-speed mixer displayed in Figure (3.19).

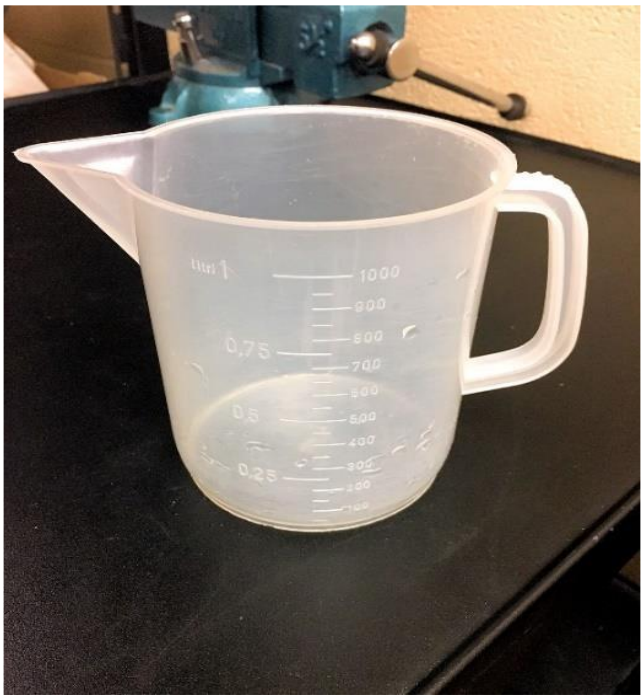

Figure (3.18) Graduated Beaker

3.3.4 Rotary Viscometer

Figure (3.20) shows the Rotary viscometer required to determine the viscosity of the xanthan gum solutions by giving the share rate and shear stress at different speeds.

Figure (3.19) High-Speed Mixer

Figure (3.20) Rotary Viscometer

3.4 Experimental Procedure

3.4.1 Calibration of Pressure Sensors

Calibration is the process by which the sensor's electrical signal is adjusted to have a known relationship to the applied pressure. After calibration, the electrical signal can be measured, and that can be used to determine the pressure at the sensor.

A metal adapter was designed and constructed to connect the sensor to the set-up to calibrate the omega pressure sensors used in the experimental set-up. The technical service team of Memorial University created the designed adapter, as shown in Figure (3.21). On one side, the adapter is connected to the Festo pressure hose system, while on the other side, there is a ¼ national pipe thread (NPT) to join the Omega pressure sensor to the calibration set-up.

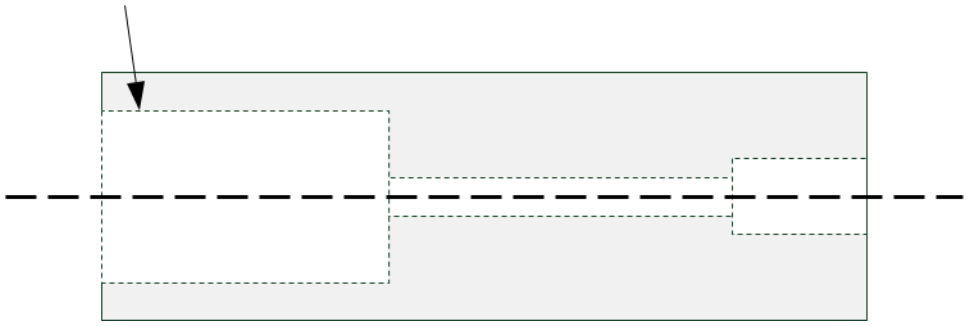

Figure (3.21) Scheme of the adapter for the pressure sensor calibration

The calibration setup, shown in Figure (3.22), consists of a pressure bottle filled with compressed air at 2,000 psi, a Festo LR-D-MINI pressure regulator, and a small Festo valve to remove the pressure of the system after the calibration. The regulator works in the pressure range from 0.5 to 12 bar and has a maximal hysteresis of 0.2 to 0.4 bar. All the parts are connected with Festo pressure hoses. The calibration is carried out as follows. Different pressures are generated with the regulator, and the outcoming voltage of the sensor is measured by a volt

meter. The calibration was carried out over the entire pressure range of a sensor. The pressure range is 9 bar for all sensors.

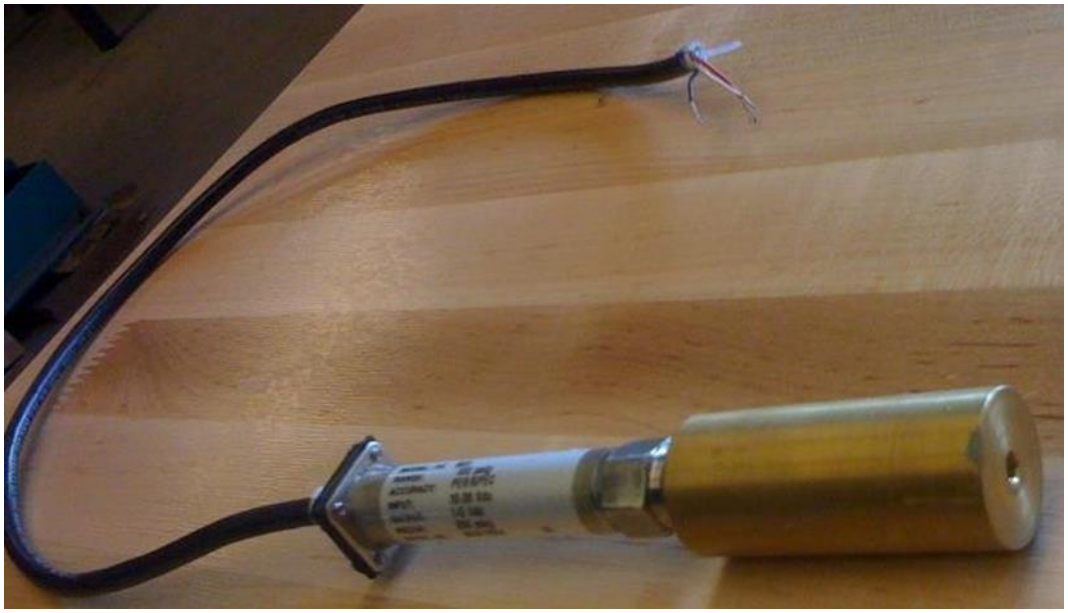

Figure (3.22) Adapter for the pressure sensor calibration

3.4.2 Single-Phase Flow Experiments

First, the flow loop was tested by single-phase flow using all the fluids involved in the project. This step is very important to ensure that all instruments work perfectly and calibrate all the sensors. Then, water was used as a liquid medium, and the strategy was selected to keep increasing the liquid flow rate and observe the pressure and temperature behavior. The gases used in the experiments are air, CO_2, and boat gases experimented in single-phase flow. The procedure for gas experiments started with a minimum gas flow rate and then raised the flow rate towards a maximum flow rate. The results are shown in Figure (3.23) and Figure (3.24).

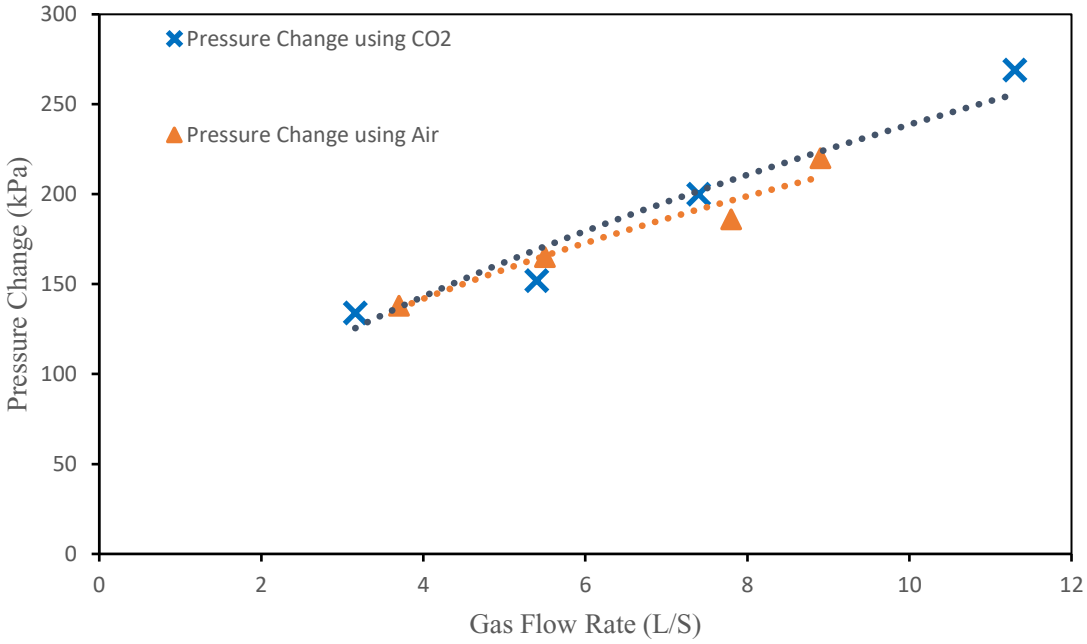

Figure (3.23) Pressure for Air and CO_2 flow versus gas flow rate.

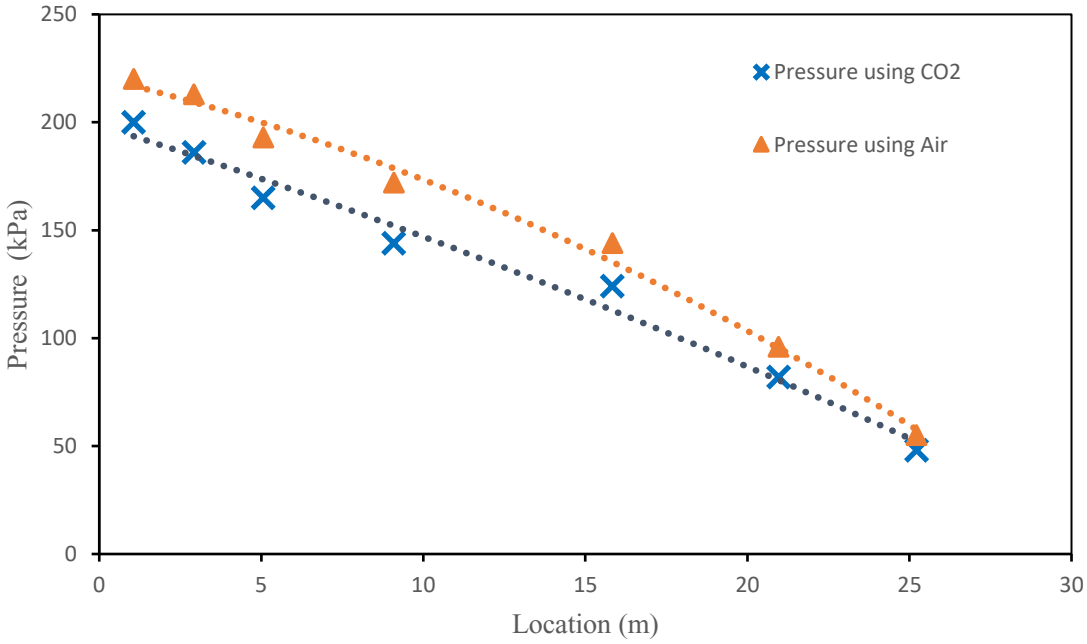

Figure (3.24) Pressure comparison (Air – CO_2) at 5.4 (L/S) CO_2 flow rate & 6.5 (L/S) Air flow rate.

3.4.3 Two-Phase Flow Experiments

The two-phase flow experiments have been done as a gas/liquid flow. The gases used in the experiments are air and carbon dioxide, while the liquids are water and Xanthan gum. We used Xanthan Gum as it's easy to experiment with, and its solution can be power-low or Herschel Bulkly fluid. Xanthan gum used in the experiments contains four concentrations, which are 1-2-3 and four g/L. The experimental process starts with fixed liquid velocity and increases gas velocity several times to reach high velocity with flow conditions recorded. The next step is increasing the velocity of Xanthan gum by raising the inlet pump pressure and changing the gas velocity numerous times for the same Xanthan gum velocity. Following this step, the liquid and gas velocities are changed many times, and the flow regime is investigated using a high-speed camera.

The limitations of the experiments were that the maximum pressure reached 496 kPa, and the minimum was 137. These values are considered regarding safety in the laboratory. In reality, the pressure will be higher.

3.4.4 Void Fraction Measurement Technique

The void fraction in this work is measured using the quick-closing valve technique. Two valves are installed in the experimental loop, one before the mixing point of gas and liquid and another at the end of the loop section before the tank. A quick closing of the two valves results in trapping a volume of two-phase mixtures inside the test section, measuring the volume of liquid by evacuating the liquid to the tank. The volume of gas trapped is the total volume of the tube section without the volume of liquid.

CHAPTER 4
Rheology

4.1. Rheology Tests and Non-Newtonian Fluid Properties

A rotary viscometer and high-speed mixer were used to record the rheology properties of all concentrations of Xanthan gum used in the experiments. Many models have been approved to describe the rheological behavior of non-Newtonian fluids based on the relationship between shear rate and shear stress. Generally, the models of most interest in the oil and gas industry and technology are power low, Bingham Plastic, and Herschel-Bulkley models, as shown in Fig (4.1).[75] However, most fluids don't conform properly to one model but a combination of models.

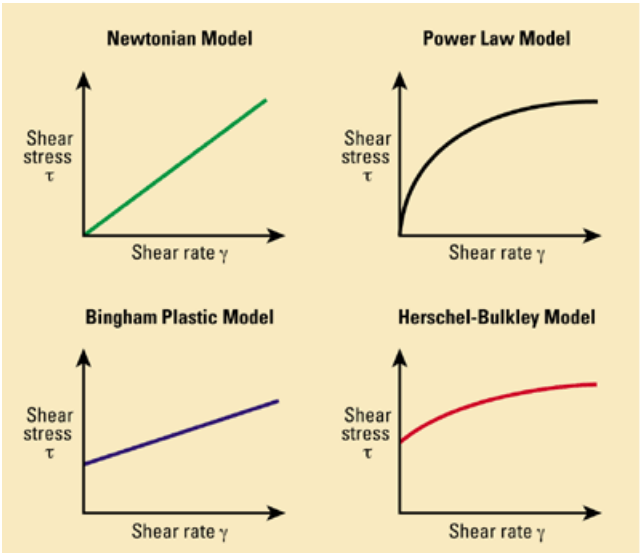

Figure. (4.1) Rheological models.[76]

4.1.1 Power-Law Model

This model is related to shear thinning fluids without exhibiting any yield stress. This model states that the following equation can describe the shear stress required to shear a fluid at a given rate:

$$\tau = k(\dot{\gamma})^{n-1} \quad (4.1)$$

n=1 → Newtonian Behavior

n<1 → Shear Thinning (Pseudoplastic) Behavior

n>1 → Shear Thickening (Dilatant) Behavior

(K) is the consistency index parameter

4.1.2 Bingham Model

This model is applicable when there is a yield stress on the fluid, and the viscosity is constant at stresses higher than the yield stress.

$$\tau = \tau_0 + \mu \dot{\gamma} \quad (4.2)$$

If τ_0=0→ Newtonian Behavior

If τ_0>1→ Bingham Behavior

4.1.3 Herschel-Bulkley Model

The Herschel–Bulkley fluid is a general model of a non-Newtonian fluid in which the relationship between shear stress and shear rate is nonlinear, as described in eq (4.3) [77].

$$\tau = \tau_0 + k(\dot{\gamma})^n \quad (4.3)$$

τ: shear stress

τ_0: yield stress

k: consistency factor

$\dot{\gamma}$: shear rate (sec^{-1})

n = flow index

τ_0=0 & n=1 → Newtonian Behavior

τ_0>0 & n=1 → Bingham Behavior

τ_0=0 & n<1 → Shear Thinning (Pseudoplastic) Behavior

τ_0=0 & n>1 → Shear Thickening (Dilatant) Behavior

The yield stress τ_0 is generally taken at 3 rpm of viscometer reading. In addition, *n* and *k* values are calculated from the 300 or 600 rpm values or can be obtained graphically.

The share rate $\dot{\gamma}$ It can be obtained as given below:

$$\dot{\gamma} = rpm \times 1.7034 \tag{4.4}$$

Here the (rpm) is the revolutions per minute.

The shear rate is the rate of change as the fluid layers move past one another per unit distance, which can be expressed as (v/h). V is the velocity of the moving geometry of the viscometer, and (h) is the separation of the plates or the thickness of the sample. Therefore, the dial reading is multiplied by 1.067 to give a reading in lb/100ft^{2,} and 1.7034 converts RPM into a speed to calculate the shear rate.

The rotation of the outer cylinder causes the fluid to stick onto the inner cylinder (Bob), and "Bob" is connected to a spring that produces a dial reading from the apparatus. Finally, the shear stress is correlated to the dial reading with this equation:

$$\tau = D.R.\times 1.067 \tag{4.5}$$

τ : Shear Stress (lb/100ft^2)

D.R. : dial reading

A conversion of shear stress to Pascals (Pa) by multiplying τ by 0.478803.

The apparent viscosity is defined as the viscosity of fluid that is measured at a given shear rate at a fixed temperature and calculated based on the relationship between shear stress and shear rate as shown below:

$$\mu = \frac{\tau}{\dot{\gamma}} \tag{4.6}$$

μ = Apparent viscosity in centipoise (cp)

τ = Shear Stress in milli pascals (mPa)

$\dot{\gamma}$ = Shear Rate (sec-1)

After plotting the relationship between shear rate and shear stress for all of the Xanthan gum samples tested by viscometer, our fluid behavior is precisely confirmed with the Herschel-Bulkley model as described in Figure (4.2).

Fig (4.2) shows the relationship between shear stress and shear rate, defined as apparent viscosity for Xanthan gum (1g/L), (2g/L), (3g/L), and (4g/L) concentration. The graphical model exactly confirms the Herschel-Bulkley model.

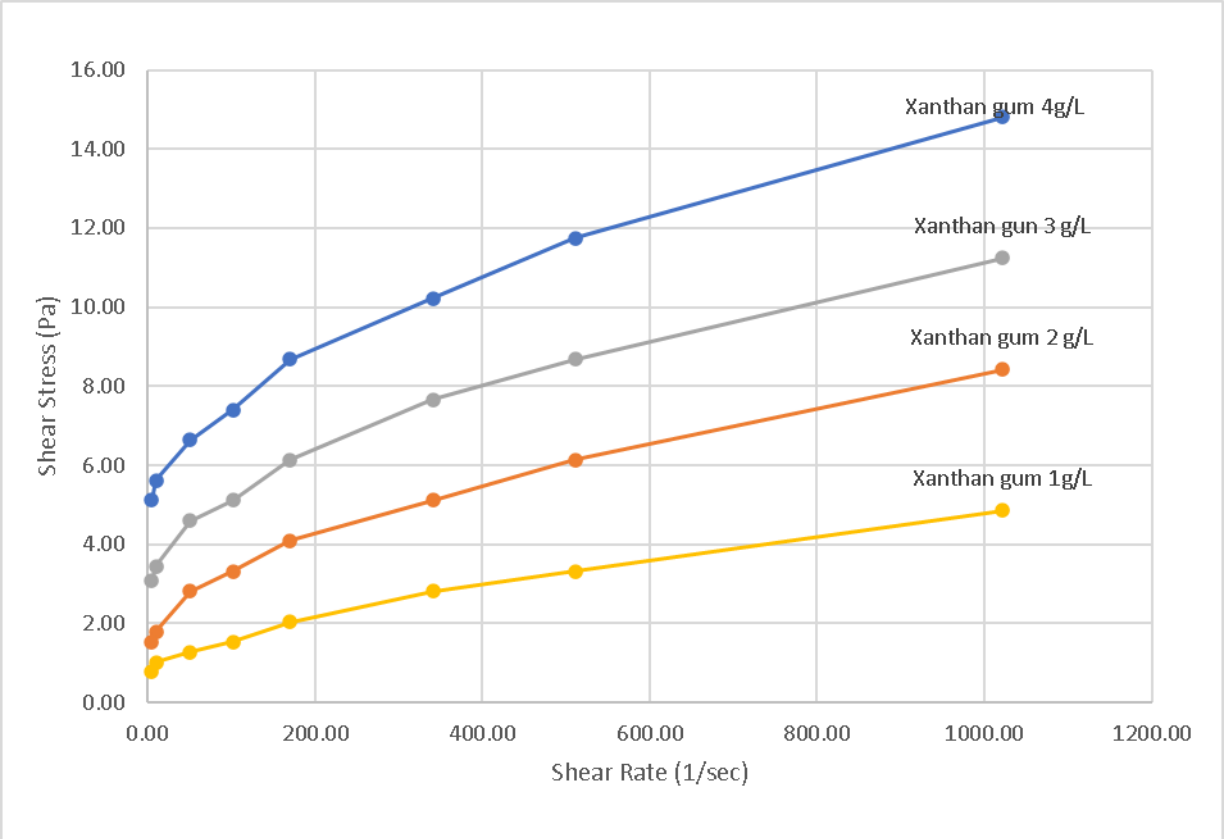

Fig. 4. 2 – Relationship between shear stress and shear rate for Xanthan gum four concentrations.

The graphical model exactly confirms the Herschel-Bulkley model, particularly at high Xanthan gum concentrations.

Yield stress (τ_0) can be obtained for each concentration at the interception of the relationship curve with the shear stress axes.

The Plastic viscosity (cp) = (600 rpm reading) – (300 rpm reading)

Bingham yield:

$Y_{.B.}$ (lb/100ft^2) = (300 rpm reading) – Plastic Viscosity

True yield:

$Y_t = ¾ \times Y_B$

Obtain the values of n and K of the Herschel–Bulkley model by changing the model equation into the log-log function so the equation becomes linear.

Solving equation (4.3) to obtain n and k by taking Log for both sides:

$$\text{Log}_{10}(\tau - \tau_0) = \text{Log}_{10} K + n \,\text{Log}_{10} \dot{\gamma} \qquad (4.7)$$

Using equation (4.7), we could obtain different plots at different Xanthan gum concentrations, which can be used to determine n and K values for different concentrations as illustrated in Figures (4.3), (4.4), (4.5), and (4.6). The obtained results of n and K for different Xanthan gum concentrations are given as follows:

Figure (1.5) shows equation (1.5) plotting to determine n and k values for Xanthan gum (1 g/L) concentration. In addition, figures (1.6), (1.7), and (1.8) indicate equation (1.5) plotting for Xanthan gum (2,3,4) g/L, respectively.

As a result of the figure (4.3), n = 0.52 and K = 10^ (-0.9856) = 0.1034 Pa.s^n.

As a result of the figure (4.4), n = 0.50 and K = 10^ (-0.6496) = 0.224 Pa.s^n.

As a result of the figure (4.5), n = 0.47 and K = 10^ (-0.491) = 0.323 Pa.s^n.

As a result of the figure (4.6), n = 0.42 and K = 10^ (-0.2556) = 0.55 Pa.s^n.

Liquid properties for each concentration of Xanthan gum were used in the tests and experiments have been summarized in Table (4.1)

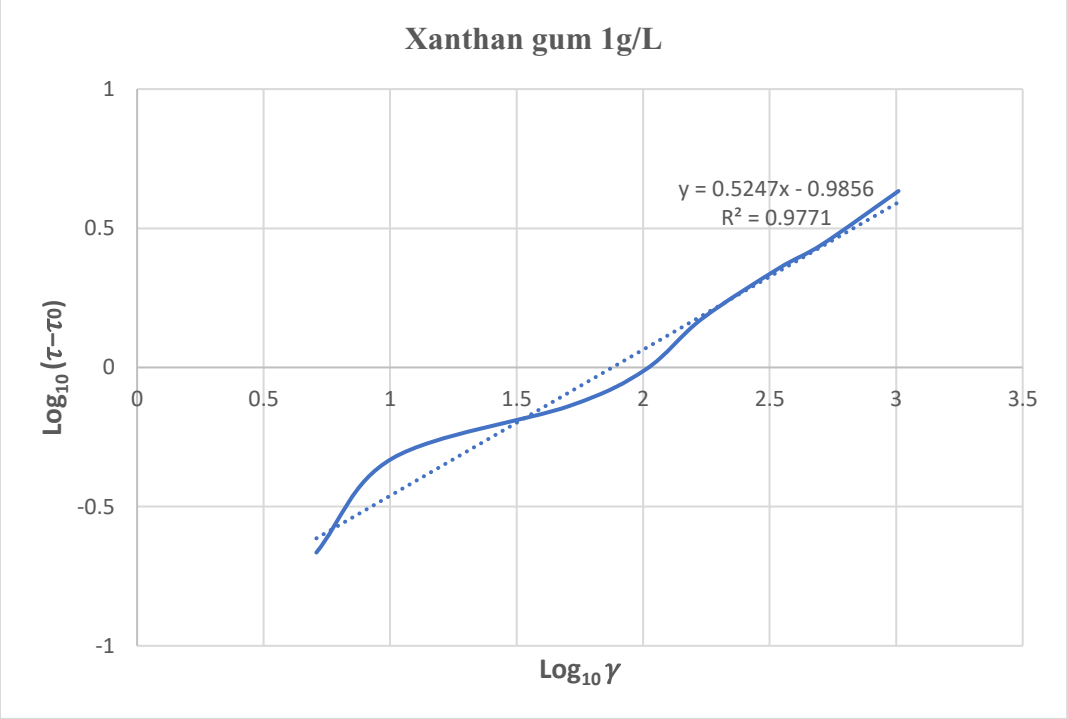

Fig. 4. 3 – Determination of n and k for Xanthan gum 1(g/L) concentration.

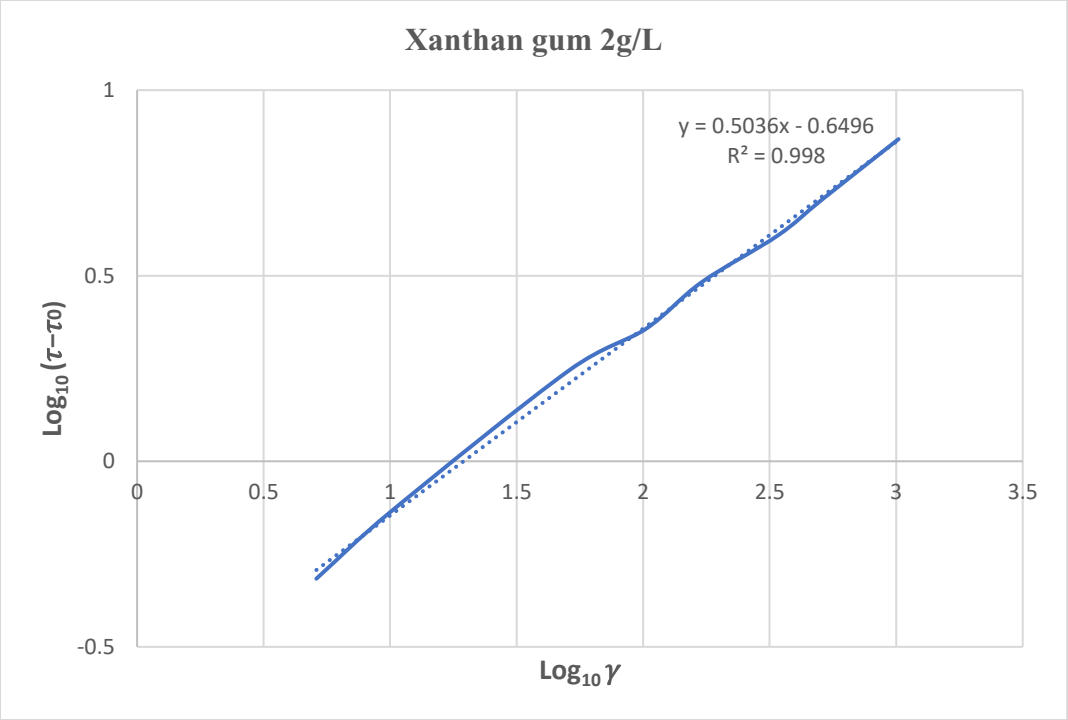

Fig. 4. 4 – Determination of n and k for Xanthan gum 2(g/L) concentration.

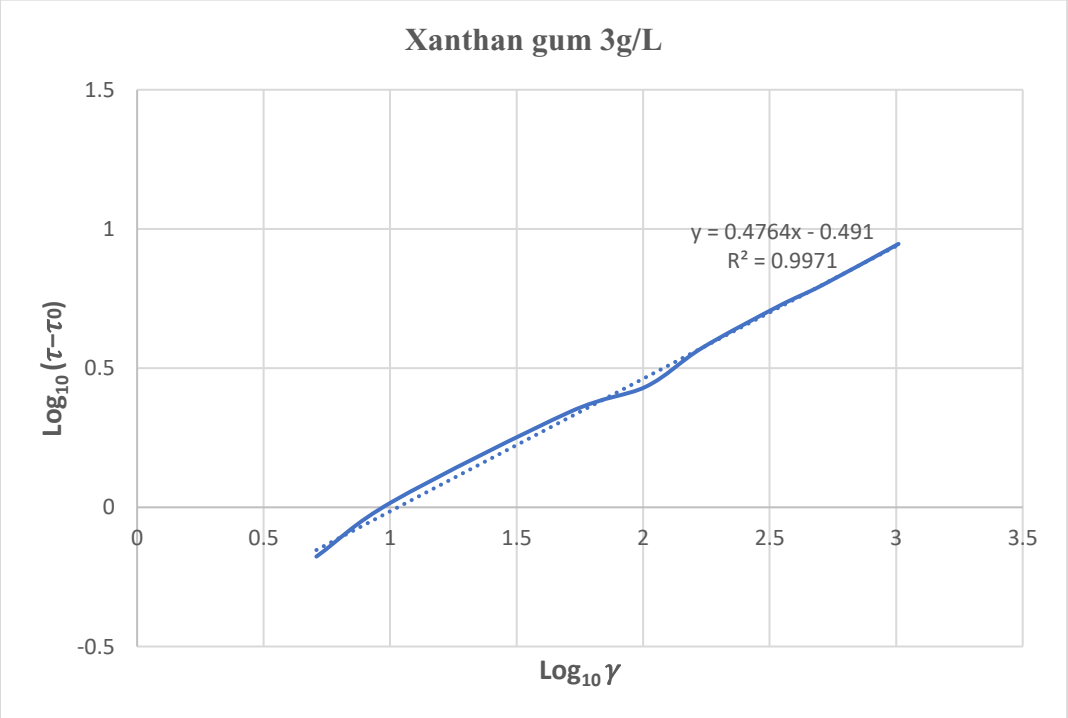

Fig. 4. 5 – Determination of n and k for Xanthan gum 3(g/L) concentration.

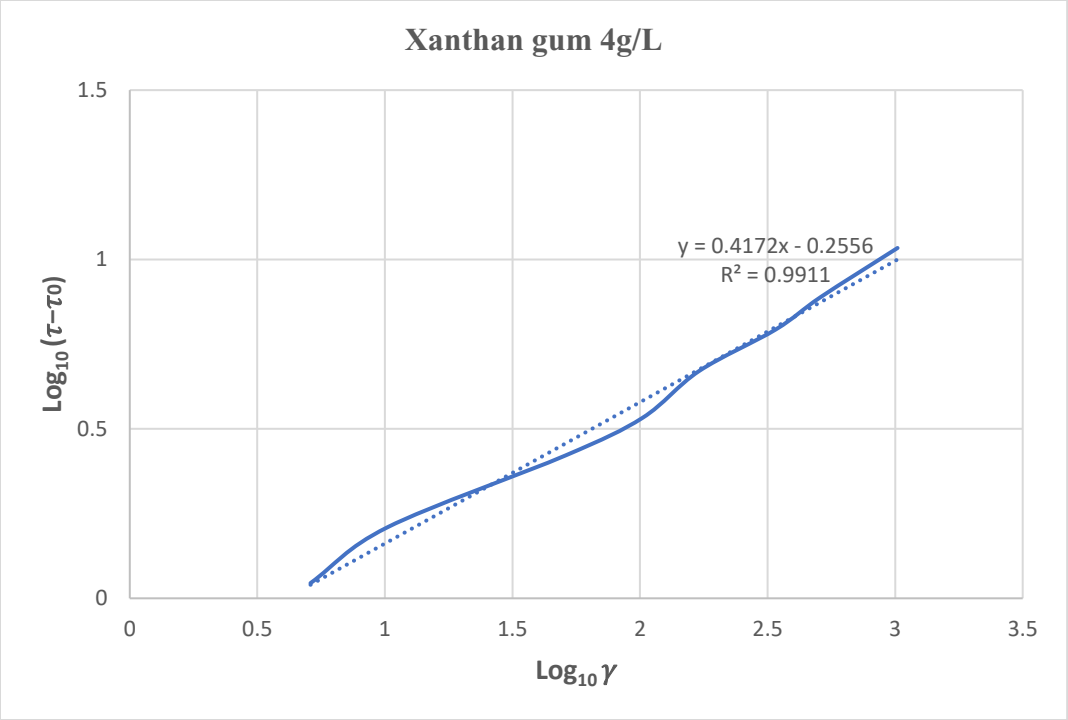

Fig. 4. 6 – Determination of n and k for Xanthan gum 4(g/L) concentration.

Table 4. 1 - Fluid Rheology Properties

Xanthan gum	τ_0 (Pa)	μ_P(cp)	Y_B (Pa)	Y_T (Pa)	n	K(Pa.S^n)
1 (g/L)	0.55	3	1.68	1.26	0.52	0.103
2 (g/L)	1.05	4.5	3.59	2.69	0.50	0.224
3 (g/L)	2.4	5	5.75	4.31	0.47	0.323
4 (g/L)	4	6	8.14	6.10	0.42	0.550

CHAPTER 5

PRESSURE DROP

5.1 Pressure Drop Overview

A pressure difference is needed to have flow in a pipe system, as fluids flow from a high-level pressure point to a low-level pressure point. A pressure drop in the multiphase flow system occurred due to friction or a physical obstacle in the pipeline. Therefore, maintaining pressure during the production and transportation of Newtonian and non-Newtonian products is critical to industry and the economy.

Maintaining pressure may be critical to the operation of the system, its equipment components, or the process output. Typical causes of pressure drop:

- Friction from the walls of the pipe against the gas particles
- Bends in or narrowing of the pipe
- Obstructions inside the pipe
- Sensors, probes, or other instruments inserted into the flow stream
- Leaks in the walls of the pipe
- Leaks from equipment installed on the pipe or in the process

Besides these factors, we need to know how flow rates and fluid concentrations impact pressure drop.

The main objective is to analyze the experimental results in order to explain the effect of many parameters on pressure drop. Each factor has been studied separately to conclude its effect ratio on total pressure drop.

5.2 Gas Flow Rate Effect on Pressure Drop:

As known, the pressure drop increases when the gas flow rate rises through pipelines. The rising pressure drop occurs because the increasing gas flow rate disturbs the flow, making waves go up and down through the pipelines and making the liquid film work as a very rough wall. Its roughness considerably affects the frictional part of the pressure drop Parsi et al. 2015 [20].

Fig.(5.1) shows the trend of pressure gradient along the flow direction through the pipelines for the (xanthan gum / CO_2) flow of 1g/L concentration. A wide range of gas flow rates has been used to describe the rising gas flow rate on pressure drop. As can be seen, the high-pressure reduction was observed at the high gas flow rates. Gas flow rates comparison of Xanthan gum concentrations of 2 and 3 (g/L) described in Fig.(5.2) and Fig.(5.3) for the range of gas flow rates between (3-19) L/s.

Fig. (5.4) describes the pressure gradient along the flow direction through the pipelines for the xanthan gum – CO_2 flow of 4g/L concentration for the 4-15 L/S CO2 flow rate range.

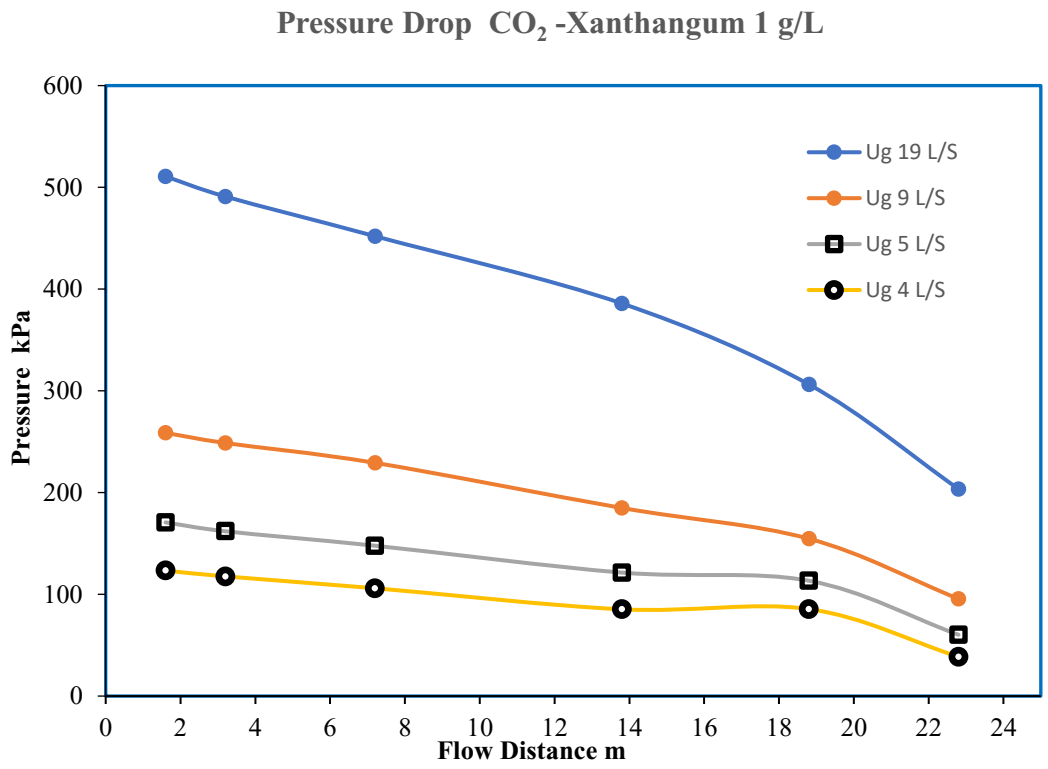

Fig. 5. 1 – Experimental Pressure Gradient of Xanthan gum – CO_2 (1g/L).

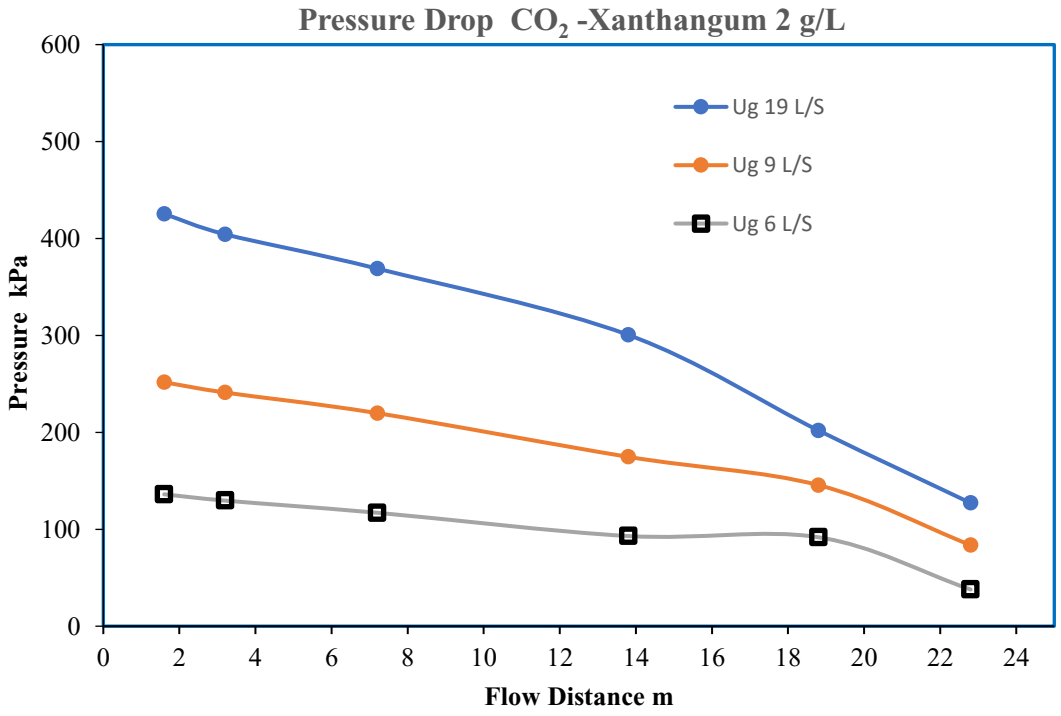

Fig. 5. 2 – Experimental Pressure Gradient of Xanthan gum – CO_2 (2g/L).

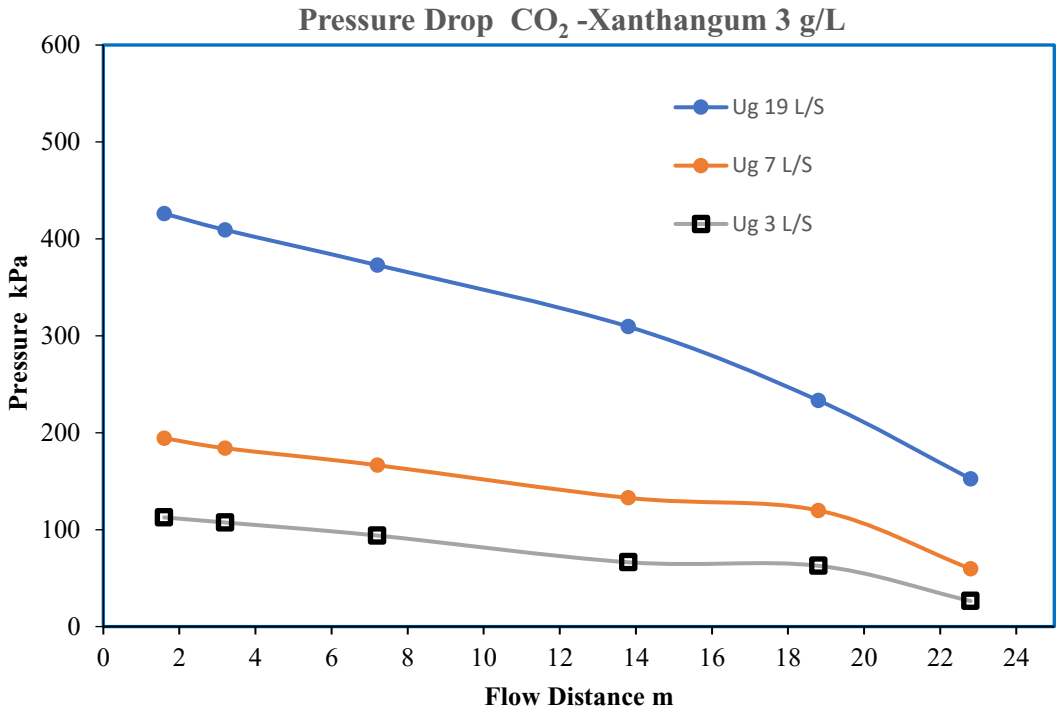

Fig. 5. 3 – Experimental Pressure Gradient of Xanthan gum – CO_2 (3g/L).

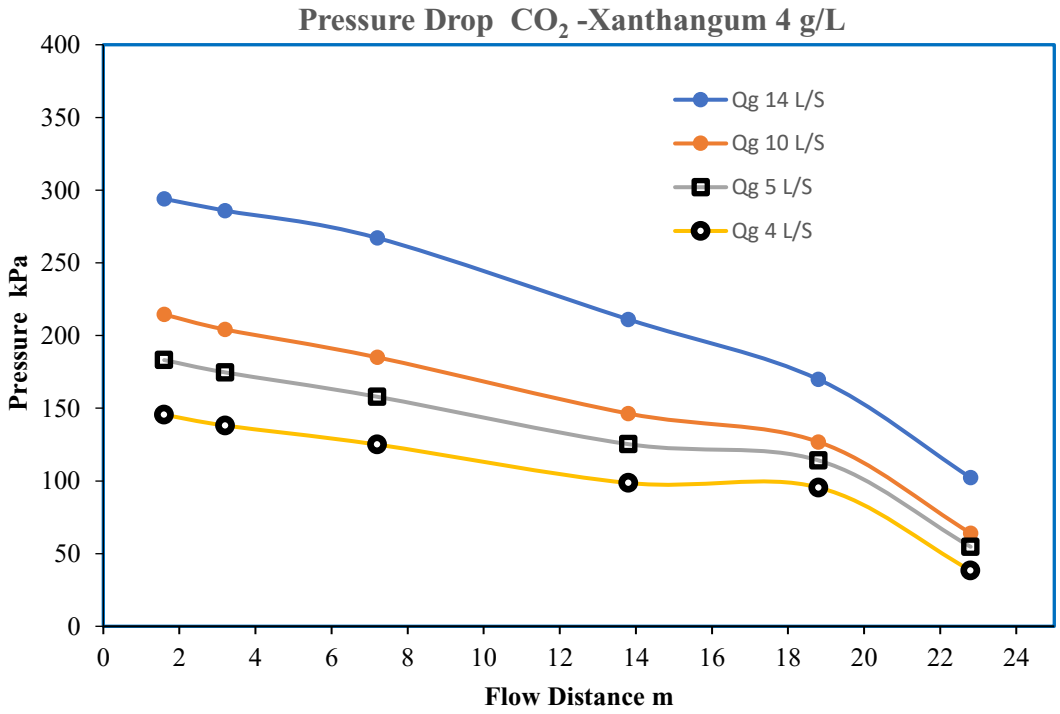

Fig. (5. 4) Experimental Pressure Gradient of Xanthan gum – CO_2 (4g/L)

In addition, the same experiments were repeated using air as a gas. Therefore, the following three figures indicate pressure gradients at different airflow rates for air–Xanthan gum flow. Fig.(5.5) describes the pressure gradient along the flow direction for the (Xanthan gum – air) flow for (1g/L) of Xanthan gum concentration and the range of 0.5-15 L/S air flow rate. Figures (5.6) and (5.7) show the pressure gradient along the flow direction for the (Xanthan gum – Air) flow for (2g/L) and (3g/L) of Xanthan gum concentration and the range of 3-19 L/S Air flow rate.

In conclusion, the gas flow rate can considerably affect Newtonian and non-Newtonian multiphase flow pressure drop. More gas injections cause slug flow and result in a huge pressure drop due to frictional pressure loss caused by wave formation.

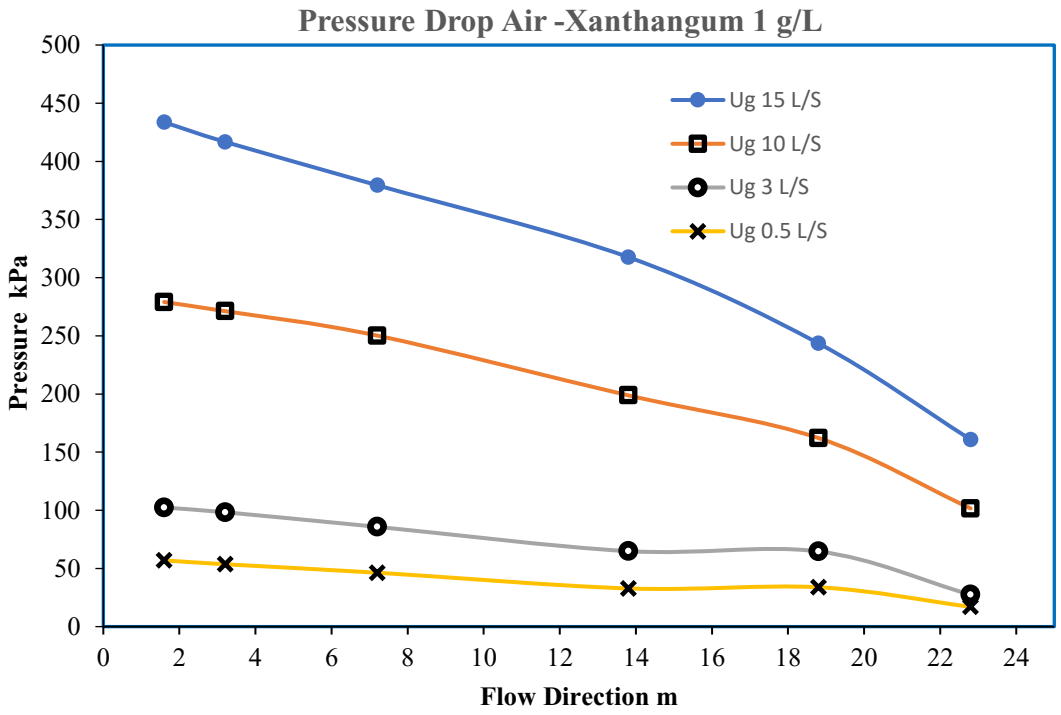

Fig. (5. 5) Experimental Pressure Gradient of Xanthan gum – Air (1g/L)

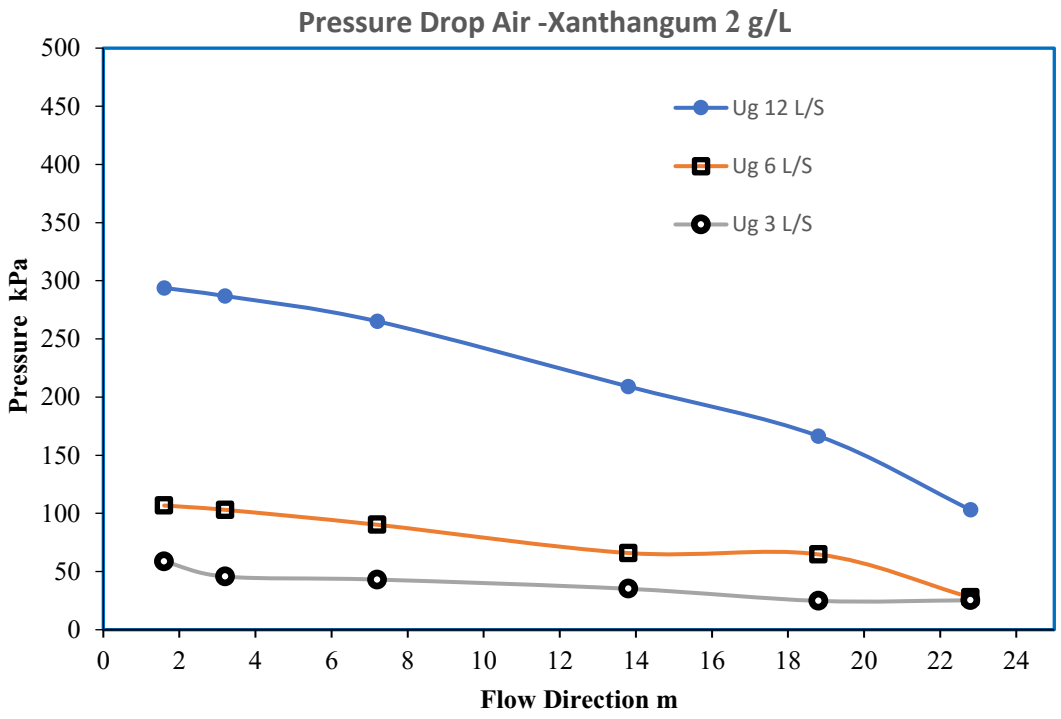

Fig. (5. 6) Experimental Pressure Gradient of Xanthan gum – Air (2g/L)

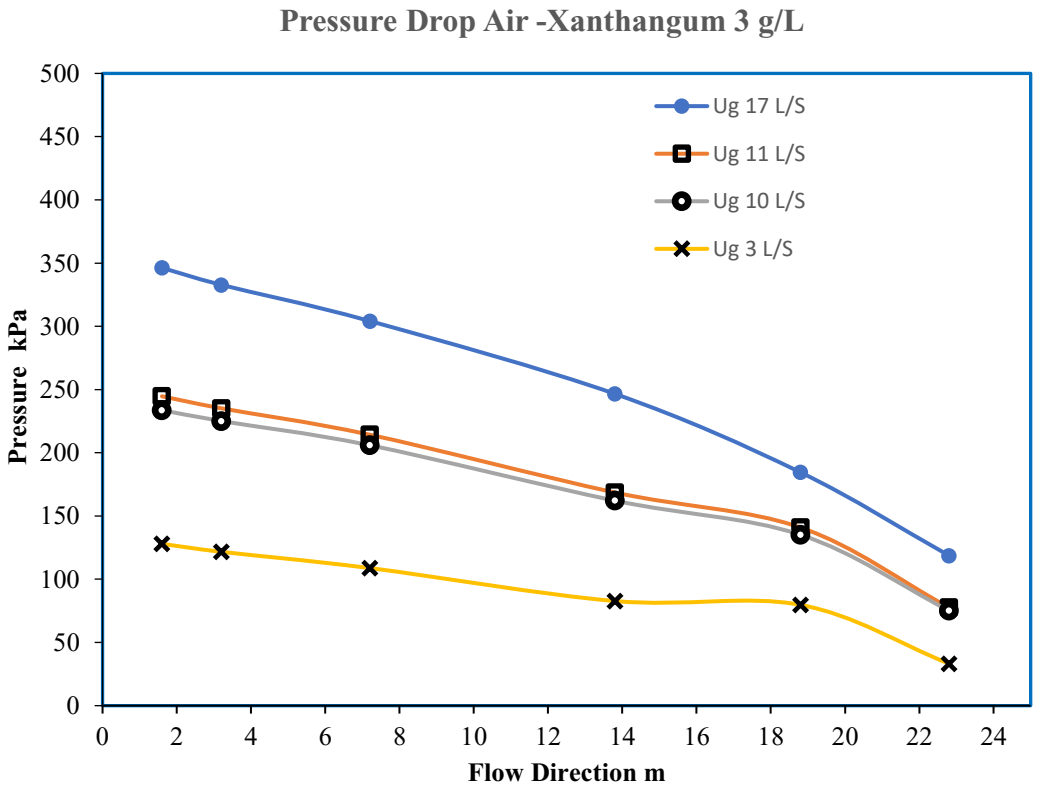

Fig. (5. 7) Experimental Pressure Gradient of Xanthan gum – Air (3g/L)

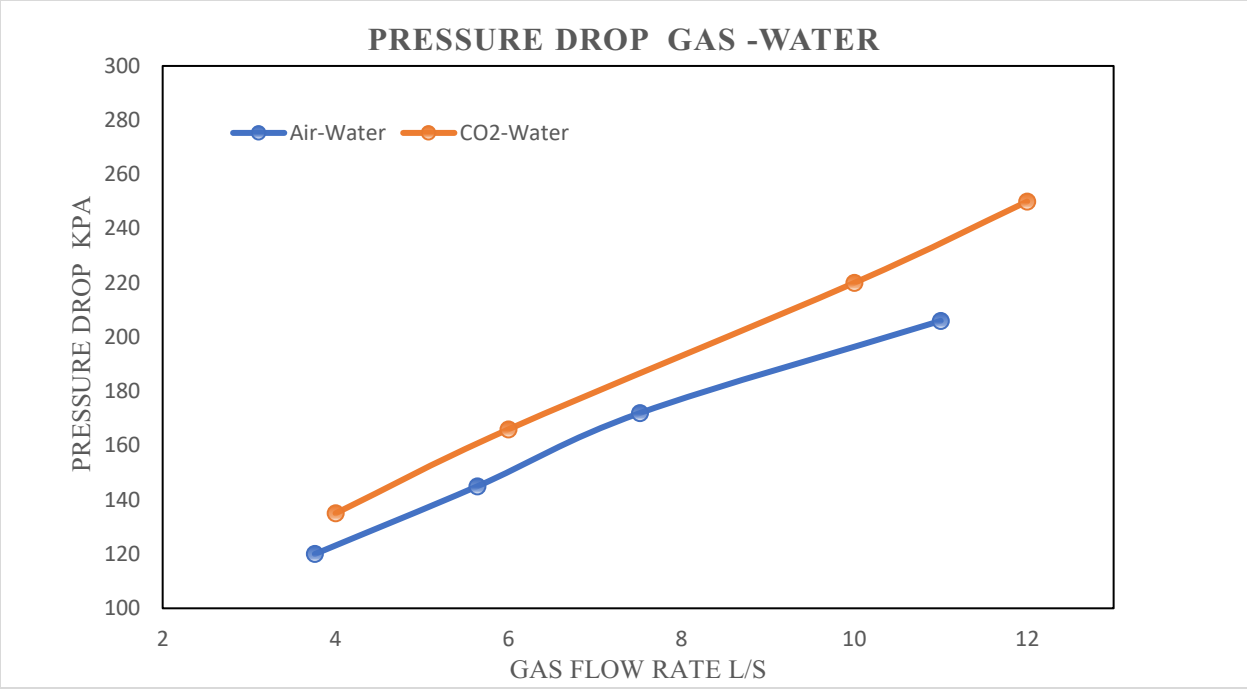

Fig. (5. 8) Experimental Pressure Drop Vs. Gas Flow Rate Newtonian/Gas Flow

Figure (5. 8) shows that pressure drops rise as the gas flow rate increases for the Newtonian/Gas flow system. However, increasing non-Newtonian concentration to be more shear-thinning will result in more pressure drop. As a result, the relationship between pressure drop and gas flow rate for non-Newtonian multiphase flow can be obtained, as shown in Figure (5. 9).

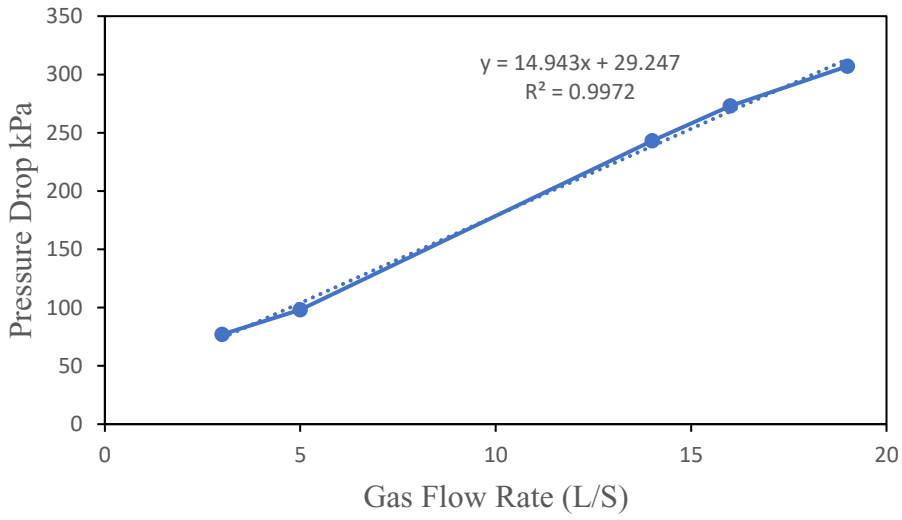

Fig. (5. 9) Gas Flow Rate Effect on Pressure Drop (Non-Newtonian Multiphase Flow)

5.3 Liquid Flow Rate Effect on Pressure Drop:

Like the gas flow rate, pressure drop increases when the liquid flow rate rises. However, increasing the liquid flow rate means increasing the liquid occupied in the tube, affecting flow patterns and raising friction loss. For example, Fig. (5. 10) shows pressure drop for (CO_2 - Xanthan gum) flow using different concentrations of Xanthan gum and many CO_2 flow rates. Fig. (5.10) indicates that two factors affect pressure drop under liquid flow investigation: the liquid flow rate and liquid concentration. As a result, a high-pressure drop was reached when a higher liquid flow rate and higher concentration were recorded. Fig. (5.11) presents the pressure drop equation regarding liquid flow rate.

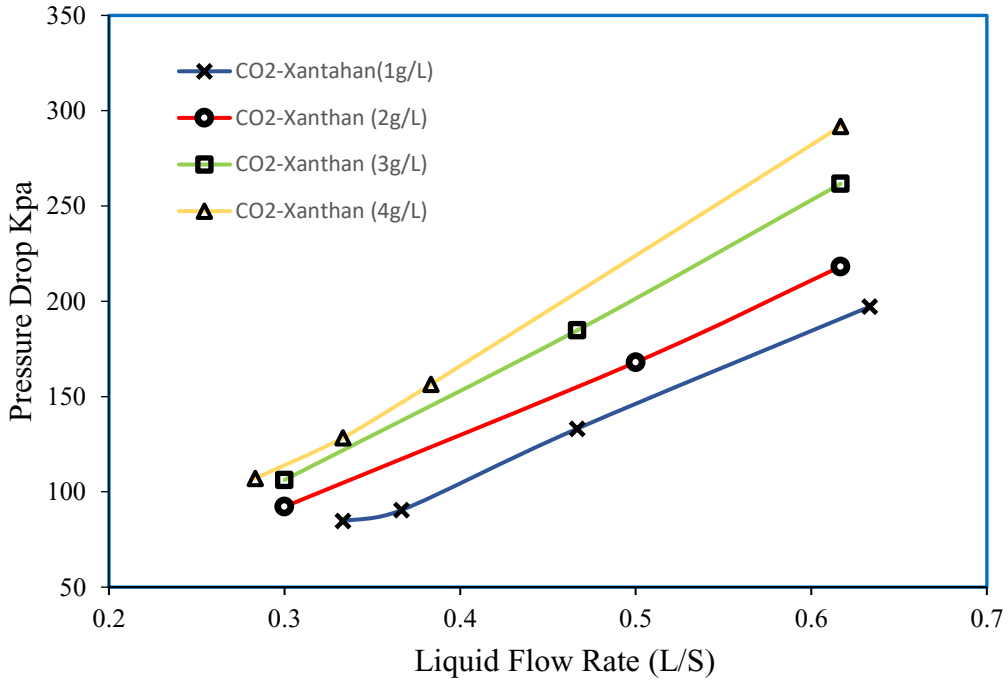

Fig. (5. 10) Liquid Flow Rate Effect on Pressure Drop (Non-Newtonian Multiphase Flow)

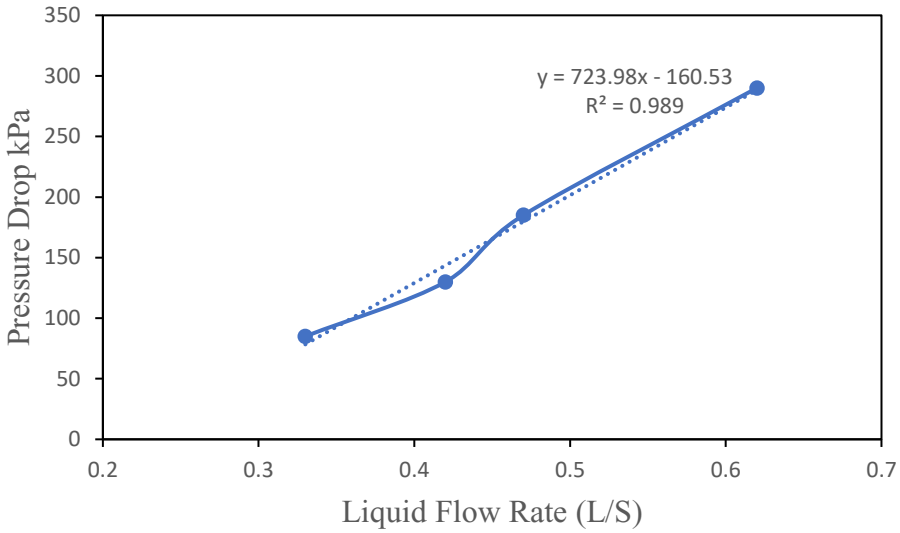

Fig. (5. 11) Liquid Flow Rate and Pressure Drop Relationship

5.4 Superficial velocities of gas and liquid:

Describe the flow effect on pressure drop for non-Newtonian multiphase flow based on superficial gas and liquid velocities, which is more efficient than the flow rate. Superficial velocity is the volumetric flow rate divided by a cross-sectional area considering the pipe diameter of flow. Superficial velocity is calculated as if the given phase were the only one flowing in a given cross-sectional area as follows[78]:

Liquid superficial velocity

$$U_{Ls} = \frac{q_L}{A} \tag{5.1}$$

The superficial velocity of the gas

$$U_{Gs} = \frac{q_G}{A} \tag{5.2}$$

Mixture Velocity:

Total of superficial velocities:

$$U_{mix} = U_{Ls} + U_{Gs} \tag{5.3}$$

The effect of both superficial velocities of gas and liquid on pressure drop is described in the figures below. Fig (5. 12) shows the relationship between air superficial velocity and pressure drop for air Xanthangum flow, starting with the superficial velocity of the gas. As can be seen, two factors affect pressure drop: the superficial velocity of gas and Xanthan gum concentration.

Pressure drop increases by increasing the superficial velocity of gas corresponding to the Bernoulli Equation. Similarly, Fig. (5. 13) describes pressure drop in terms of superficial velocity of CO_2 for CO_2 /Xanthangum Flow using different concentrations of Xanthan gum. The overall pressure drop per tube length is estimated for each concentration separately, considering the range of superficial gas velocity that has been tested.

Fig. (5. 14) explains pressure drop relationship estimation based on the superficial gas velocity for the range of (1-4) g/L Xanthangum concentration and two different gases.

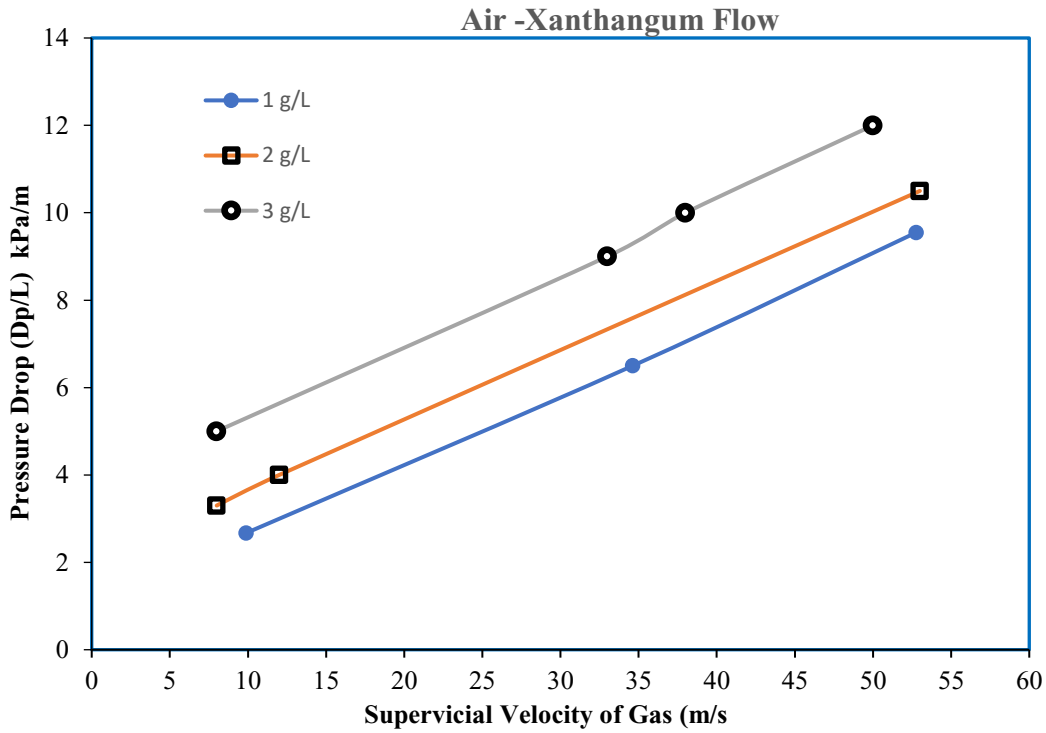

Fig. (5. 12) Pressure Drop and Superficial Velocity of Air-Xanthangum Flow

The effect of superficial liquid velocity on Pressure drop for both Air - Xanthan gum flow and CO_2 – Xanthan gum flow is described in Fig. (5. 15) and Fig. (5. 16), respectively. Figures (5. 15) and (5. 16) estimate the overall pressure drop related to each concentration's superficial liquid velocity range. Afterward, the general equation for pressure drops as a function of the superficial velocity of the liquid is generated in Fig. (5.17).

Since the fluid mixture velocities are the sum of the superficial liquid and gas velocities, the overall effect of mixture velocity on pressure drop for both air Xanthangum flow and CO_2 Xanthangum flow is shown in Figure (5. 18).

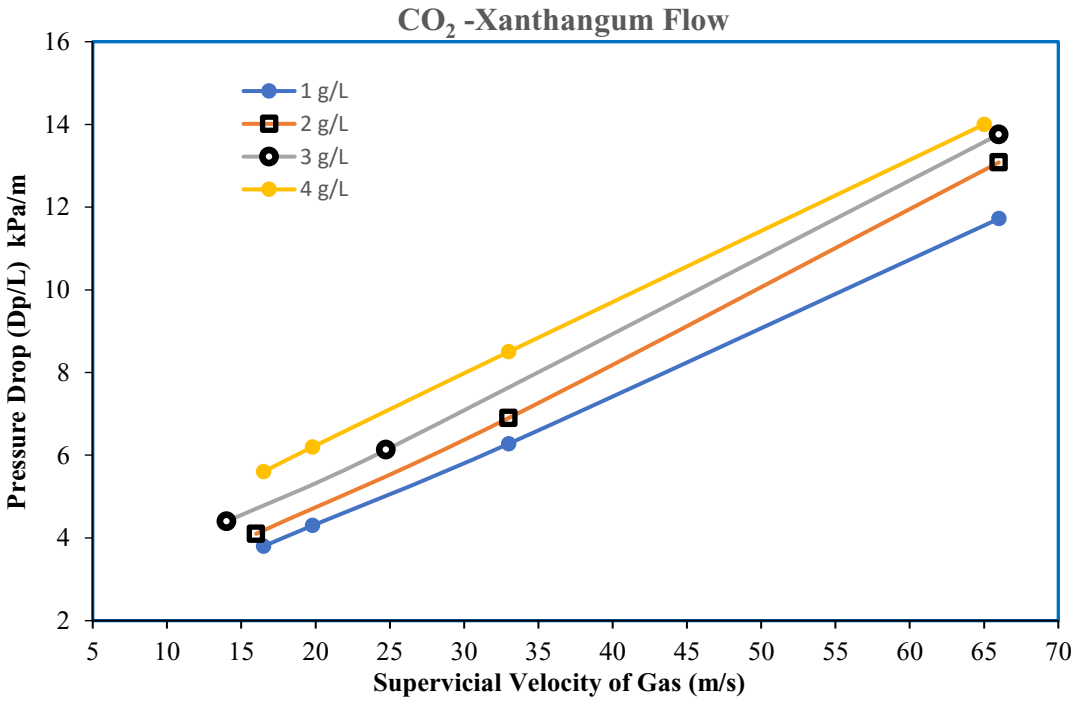

Fig. (5. 13) Pressure Drop and Superficial Velocity of CO_2 Xanthangum Flow

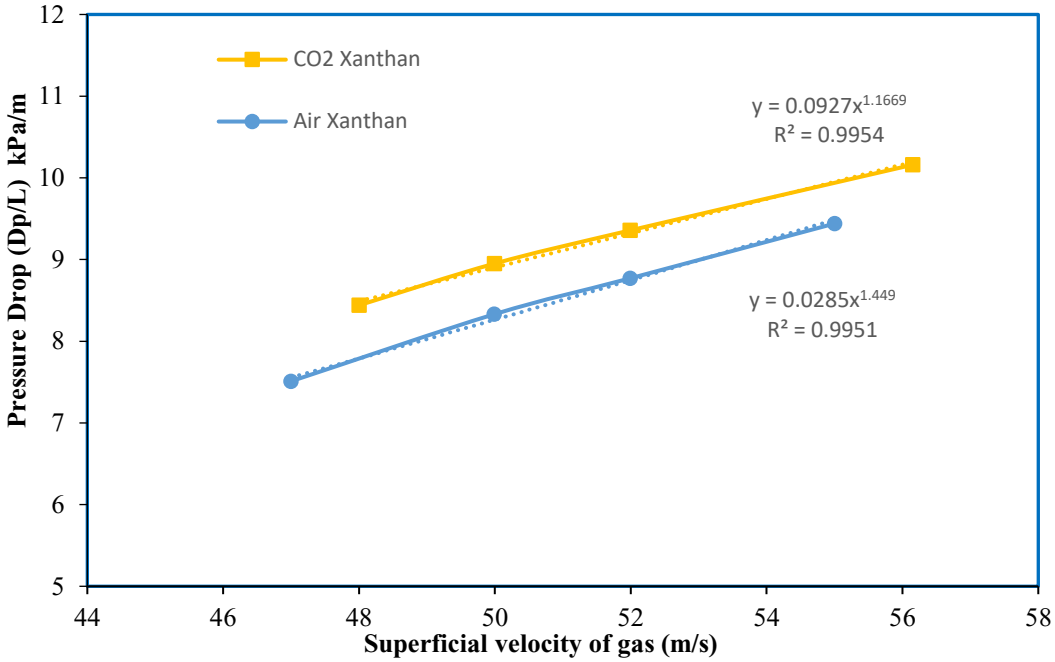

Fig. (5. 14) Pressure Drop and Superficial Velocity Relationship of Gas Non-Newtonian Flow

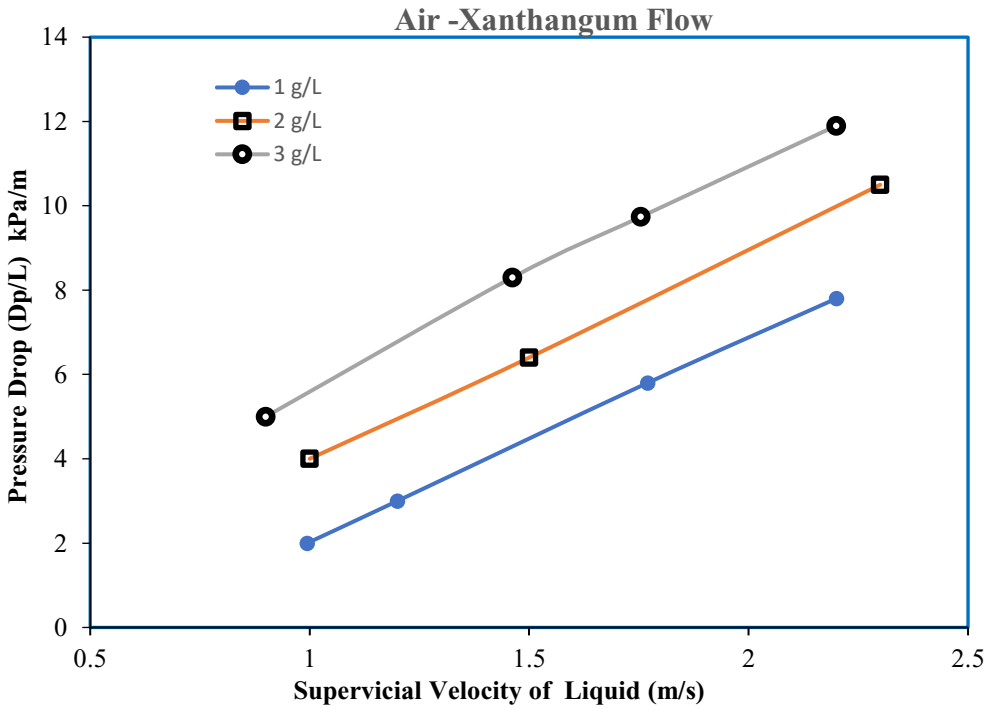

Fig. (5. 15) Pressure Drop and Superficial Velocity of Air-Xanthan Gum Flow

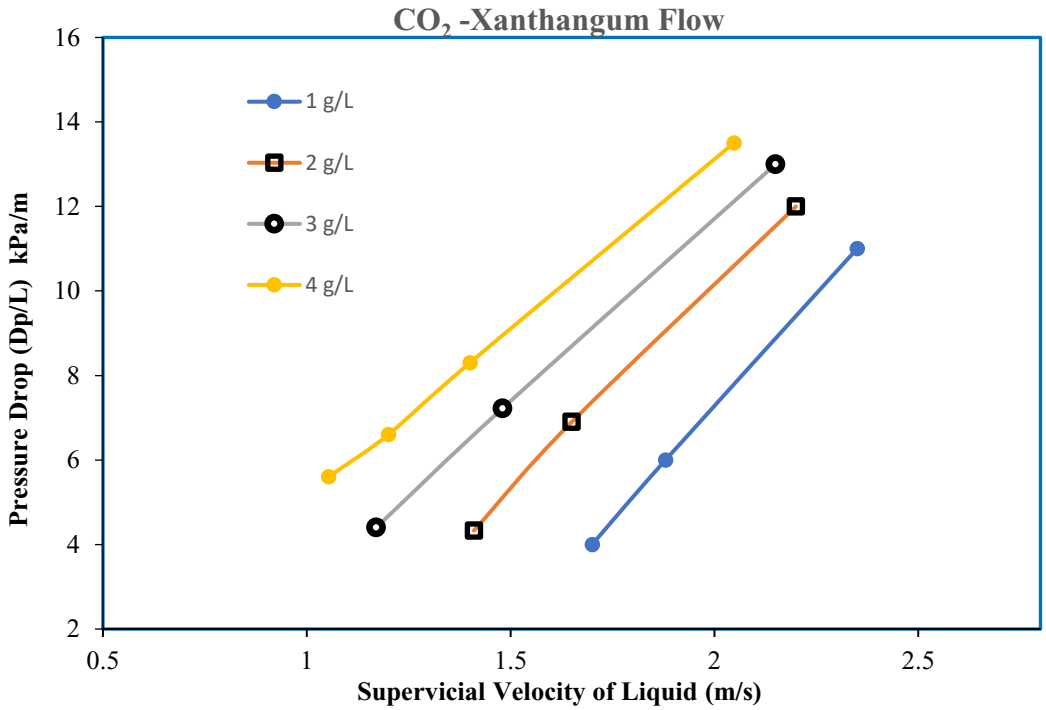

Fig. (5. 16) Pressure Drop and Superficial Velocity of CO_2-Xanthan gum Flow

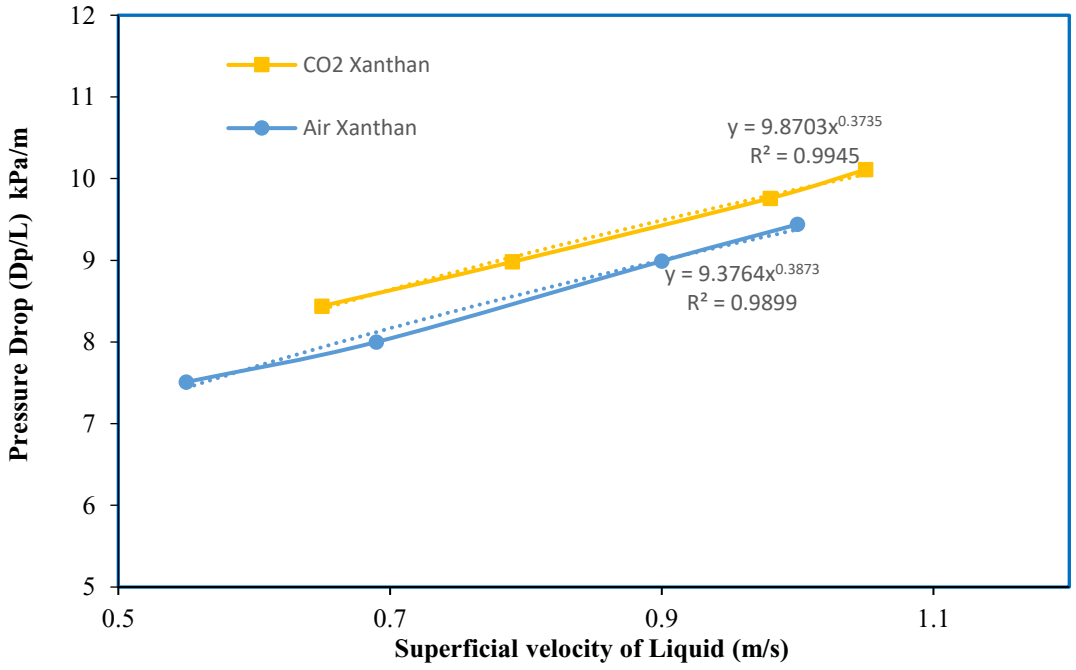

Fig. (5. 17) Pressure Drop and Superficial Velocity of Liquid Relationship

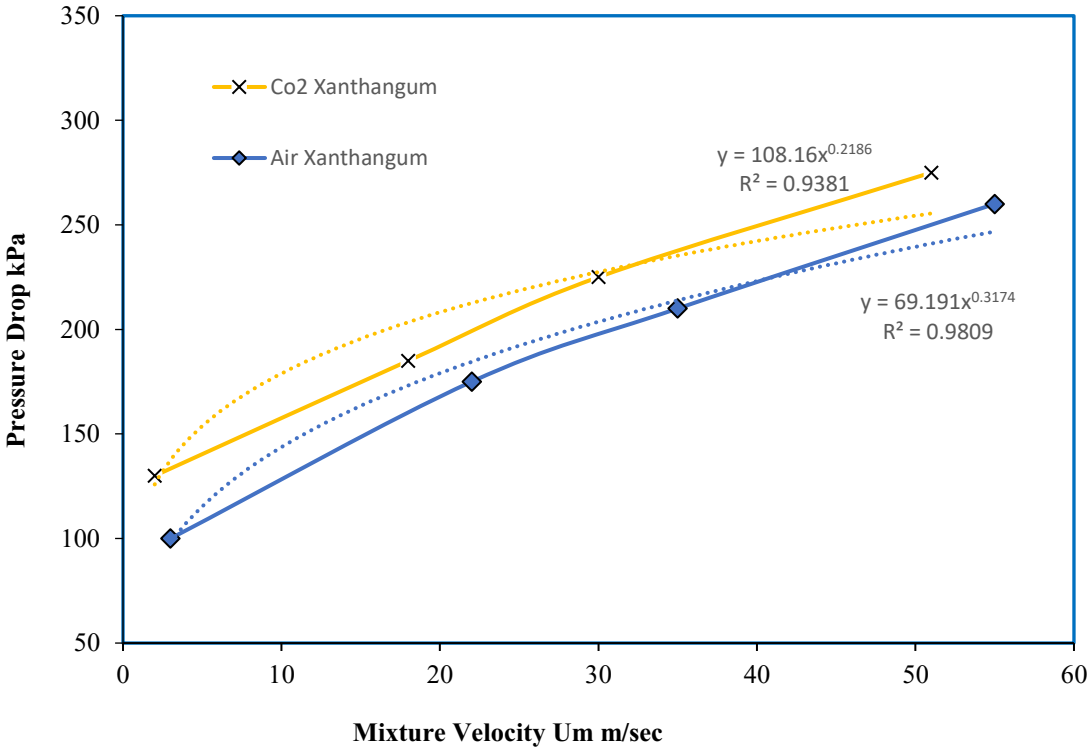

Fig. (5. 18) Pressure Drop and Mixture Velocity Relationship

5.5 Non-Newtonian Concentration Effect:

Three concentrations of Xanthan gum that were used for the experiments are 1, 2, 3, and 4 grams of Xanthan gum per litre of water. These concentrations have been used in all comparison aspects above. As shown from all figures above, the more shear-thinning fluid, the higher the pressure drop. Therefore, raising the concentration increases the viscosity and density of the fluid, and that will increase the friction loss towards more resistance of fluid flow. Fig. (5. 19) shows pressure drops related to the concentration of Xanthan gum for both CO2-Xanthangun flow and Air-Xanthan gum flow. On the other hand, the density of Xanthan gum can be used for comparison instead of concentration. Table 5.1 lists the density of all Xanthan gum solutions and the densities of water, Air, and CO_2 used in experiments.

Fig. (5. 20) Describe the relationship between Xanthan gum density and pressure drop of Air Xanthan gum flow and CO_2 Xanthan gum flow. Finally, the relation between pressure drop and density of the mixture for gas non-Newtonian flow is shown in Fig. (5. 21).

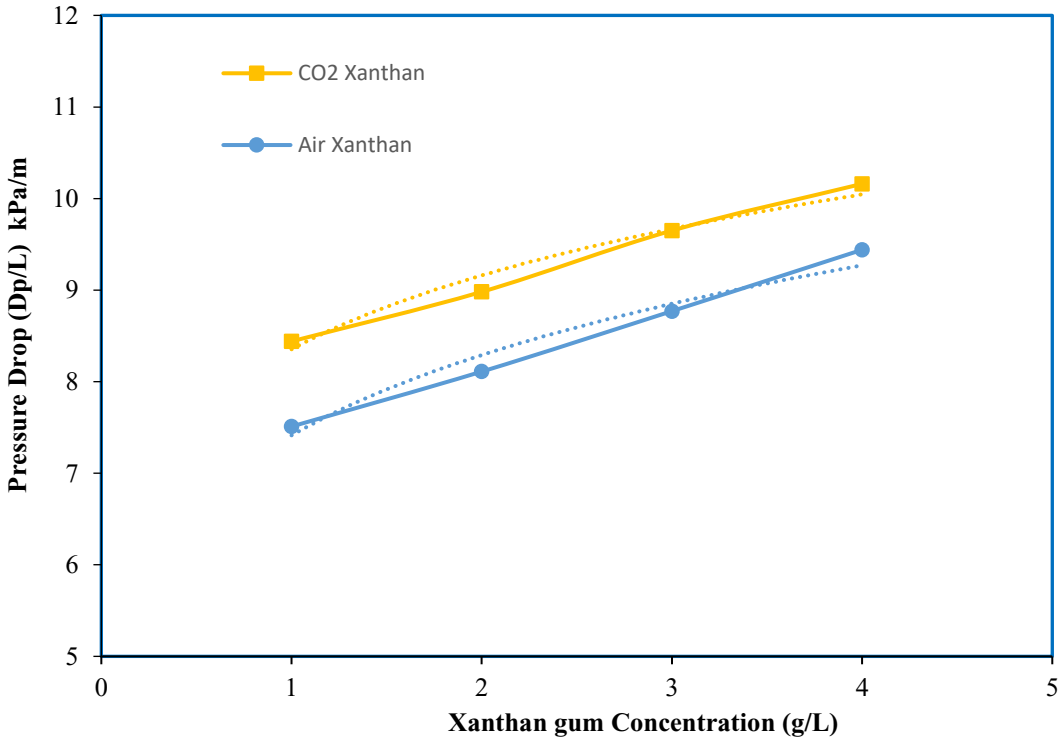

Fig. (5. 19) Xanthan Gum Concentration Effect on Pressure Drop

Table 5. 1 – Densities of Liquids and Gases

Xanthan gum	$\rho_{Xanthan}$ (Kg/m^3)	ρ_{water} (Kg/m^3))	ρ_{Air} (Kg/m^3)	ρ_{CO2} (Kg/m^3)
1 (g/L)	999.198	998.2	1.204	1.815
2 (g/L)	1000.196	998.2	1.204	1.815
3 (g/L)	1001.195	998.2	1.204	1.815
4 (g/L)	1002.193	998.2	1.204	1.815

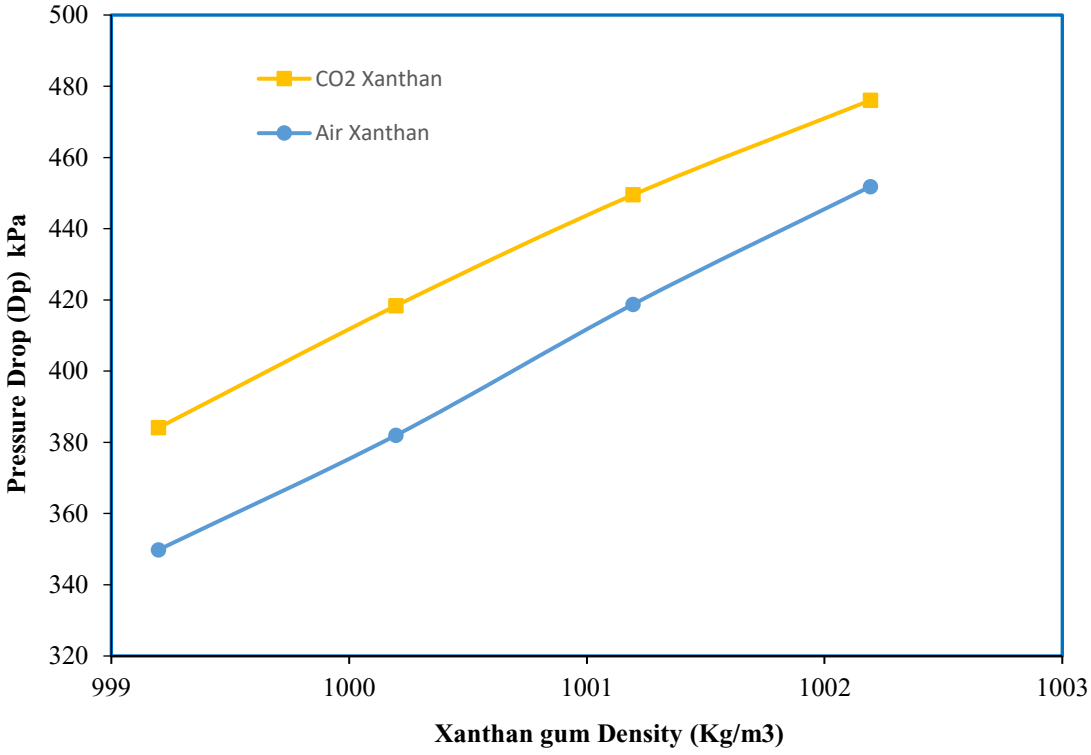

Fig. (5. 20) Relationship Between Xanthan Gum Density and Pressure Drop

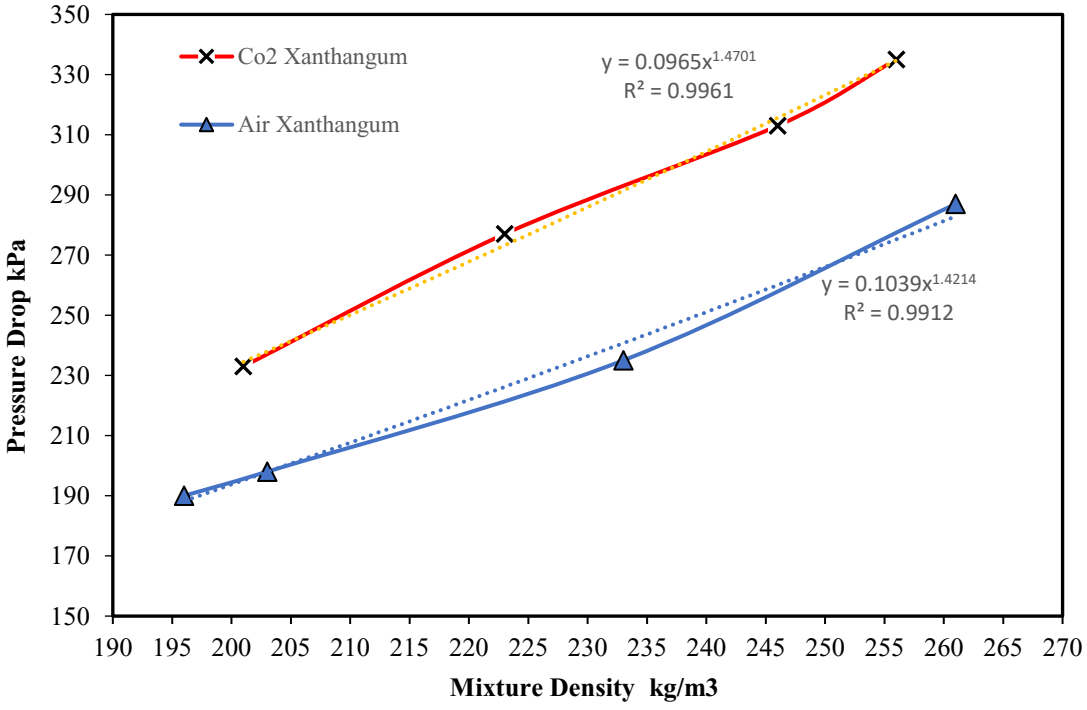

Fig (5. 21) Relationship Between Pressure Drop and Mixture Density

5.6 **Friction Loss:**

The friction loss represents the fluid's pressure loss in a pipe due to the interactions between the liquid and the inner surface of the pipe. The Darcy method commonly estimates the friction factor of single-phase flow [30].

The friction factor for smooth pipes depends entirely on the Reynolds number, but for rough pipes, it also depends on the relative roughness [79]. The PVC tubes are used during the experiments, and the average roughness for these tubes is about 0.0015(mm)

Two-phase mixing rules are used to estimate the mixture properties and Reynolds number.

Starting with the mixture density

$$\rho_m = \rho_L \varepsilon_L + \rho_G \varepsilon_G \tag{5.4}$$

Mixture Reynolds number:

$$Re_m = \frac{\rho_m u_m D}{\mu_m}. \tag{5.5}$$

After all, the friction factor is estimated as a Reynolds number and roughness function.

The Head loss due to friction $H_{L.}$ can be calculated as:

$$h_L = f\frac{L u_m^2}{2gD}. \tag{5.6}$$

Three components can characterize the pressure difference:

- Hydrostatic pressure loss
- Frictional pressure loss
- Kinetic pressure loss

For nearly all applications, minimal kinetic pressure loss can be neglected. As a result, the overall pressure loss equation can be expressed as the sum of two terms:

$$\Delta P_T = \Delta P_H + \Delta P_f$$

The hydrostatic pressure occurs only when there are differences in elevation from the inlet to the outlet of a pipe, and this component is zero for horizontal pipes. Therefore, the total pressure loss in our experimental horizontal setup is the only frictional pressure loss. The pipe fittings are the other cause of pressure drop. The main causes of pressure losses in pipe fittings are the direction and cross-sectional area changes. Both of these changes result in the fluid's acceleration, which consumes energy. Table 5.2 explains the equivalent length of pipe fittings used in the loop[80].

Table 5. 2 – Equivalent Length of Pipe Fittings on The Loop

Pressure sensor Location	**Distance (m)**	**Number of elbows**	**Equivalent length (m)**
1	0.96	3	2.79
2	2.71	4	5.15
3	4.06	4	6. 50
4	5.86	8	10.74
5	5.36	8	10.24
6	3.75	8	8.63
7	0.97	3	2.80

Fig. (5. 22) Describe the relationship between Reynolds number and friction factor for CO_2 Xanthan gum flow. The friction factor decreases as the Reynolds number increase, and this is because the thickness of the laminar sublayer (viscous sublayer) decreases with increasing Reynolds number.

The pressure loss is due to the friction factor shown in Fig. (5. 23). Two types of friction loss occur when fluid flows through pipes. Wall friction is due to friction between the inner pipe surface and the fluid. The other kind of friction is internal friction between viscose fluid layers.

The internal friction is greater as the fluid flow goes faster. As a result, more flow losses are caused by turbulence in the fluid, mainly at fittings, which act as obstacles to the flow.

After all, Fig. (5. 24) displays the equation representing the relationship between pressure loss and friction factor for the gas non-Newtonian flow system.

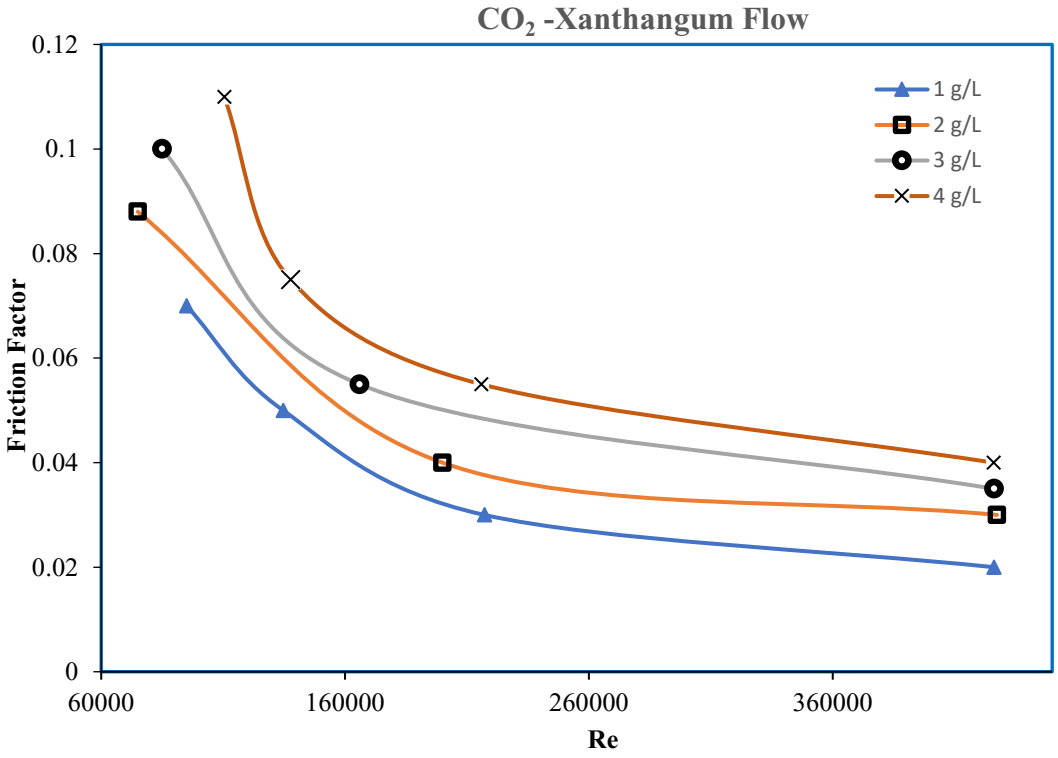

Fig. (5. 22) Relation between Reynolds number and Friction Factor for CO_2 Xanthangum Flow

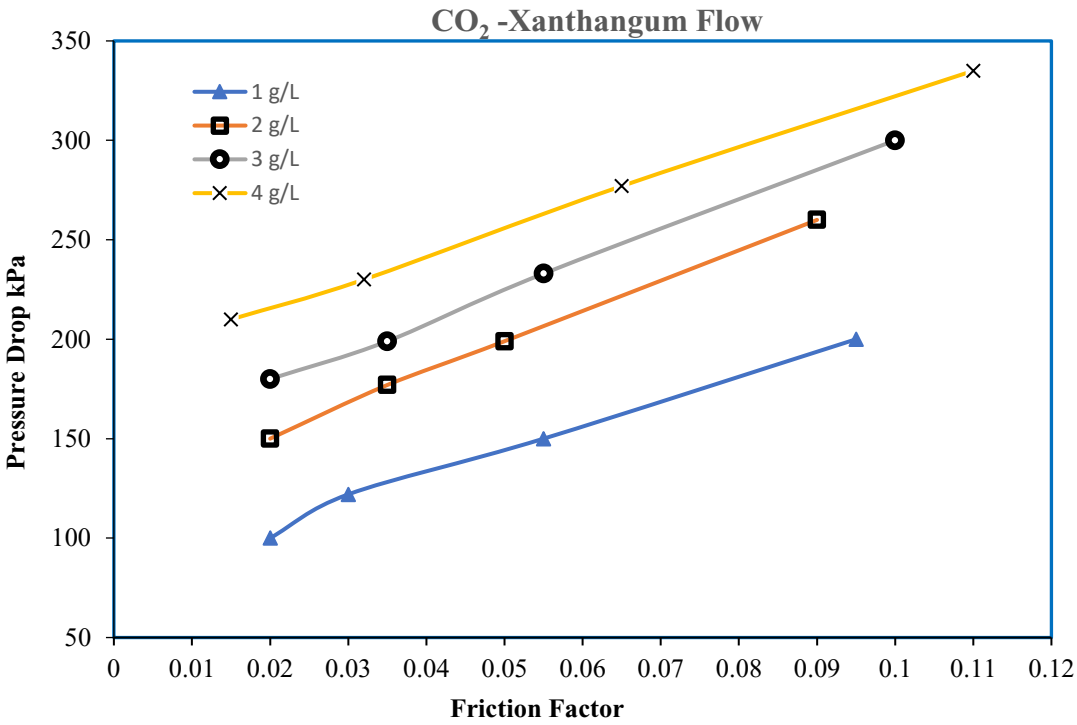

Fig. (5. 23) Relationship between Pressure Drop and Friction Factor for CO_2 Xanthangum Flow

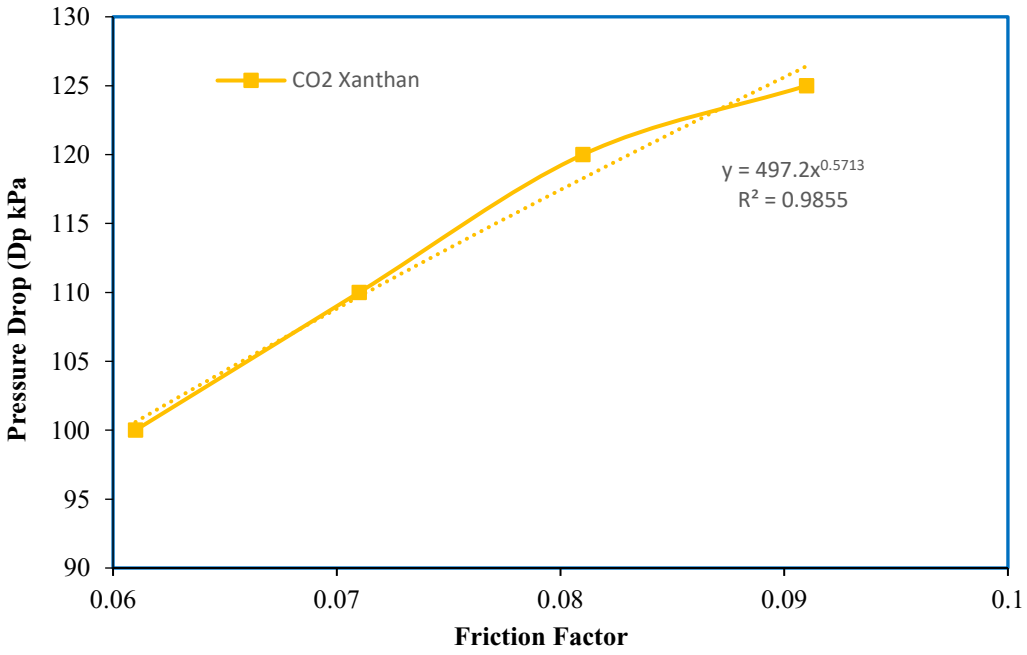

Fig. (5. 24) Pressure Drop Equation Based on Friction Factor for CO_2 Xanthangum Flow

Fig (5.25) concludes the effect of flow conditions and fluid properties of the fluids on the pressure drop for gas/non-Newtonian liquid flow. Results show that the mixture density significantly affects pressure drop with about 50% more than the mixture velocity, which gives up to 40% of the total effect. The effect of the friction factor and bends is about 10%.

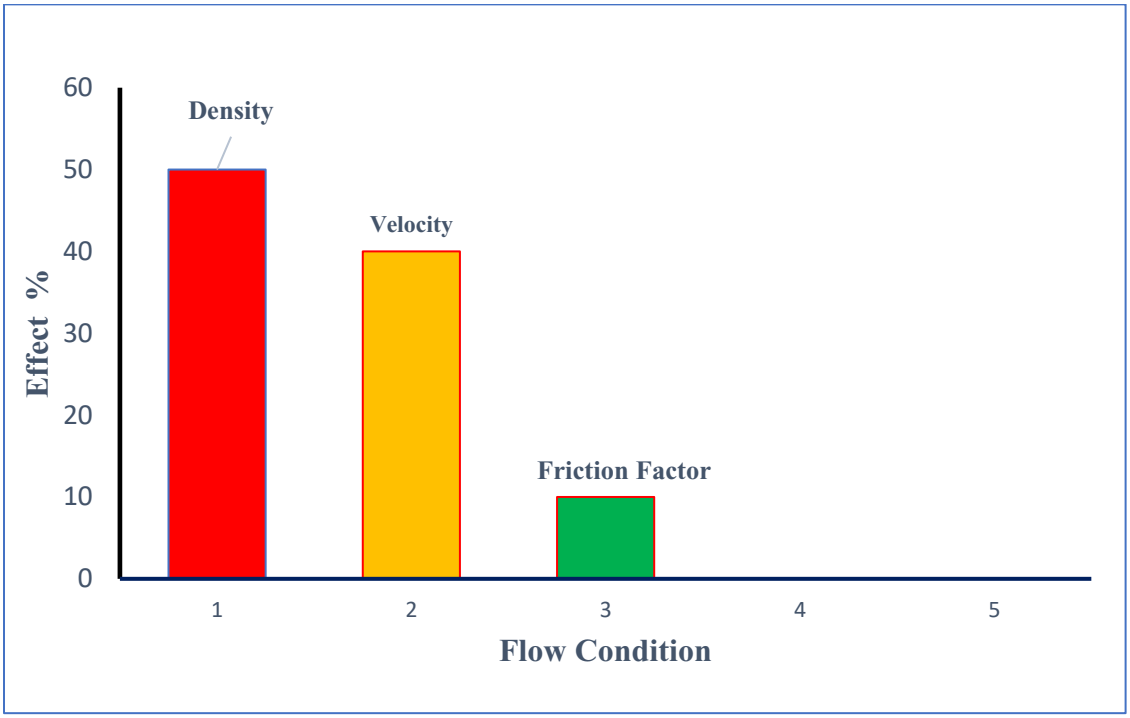

Fig (5. 25) Percentage Effect of Flow Condition on Pressure Drop

5.7 Experimental Pressure Drop Models:

Based on theoretical studies, many correlations to predict pressure drop in gas / non-Newtonian flow have been developed or modified from Newtonian correlations. However, there are currently only a few pressure loss models that have been generated from experimental investigations. Experimental work can help create pressure drop models for gas / non-Newtonian flows with smaller error percentages than theoretical derivations since predictions about the

behavior of non-Newtonian liquids are theoretically complex. The experimental model in this work is developed based on all the above-created models. It is a combination of the models after considering the effect of each parameter on pressure drop.

The experimental pressure drop data compared with pressure drop estimated from other empirical known correlations to conclude which correlation is better for Herschel-Bulkleyfluids. Fig(5.26) compares the experimental results with results achieved by other known empirical correlations. The Xu et al. model provides a better predictive ability than some of the correlations, and the overall performance of the evaluation has shown an acceptable percentage of error.

Following is the review of the correlations that were used for the comparison and their advantages and disadvantages:

Ideal Plug Model: This model is suitable for a gas/power law system and good for a laminar regime. This model ignores the pressure drop across the gas slug, as well as the gas slip, and the two-phase pressure drop is reduced to the simple expression[3] :

$$\left(\frac{dP}{dL}\right)_{tp} = \left(\frac{dP}{dL}\right)_{1} \lambda_1^{1-n} \tag{5.7}$$

Here λ is the liquid volume fraction, and n is the flow behavior index.

Dziubinski and Chhabra [36] empirically modified the liquid volume fraction term λ in the ideal plug model as follows:

$$\left(\frac{d_p}{d_l}\right)_{tp} = \left(\frac{d_p}{d_l}\right)_{l} \left(J + \frac{C_0}{x} + \frac{J}{x^2}\right) \tag{5.8}$$

This model has an approximate 40% error when used for turbulent flow because it is related to laminar flow.

Dziubinski Model [21] Dziubinski created an empirical correlation to predict pressure drop in intermittent horizontal flow as:

$$\left(\frac{d_p}{d_l}\right)_{tp} = \left(\frac{d_p}{d_l}\right)_{l} \left[\frac{1 + 1.036 \times 10^{-4} \left(\frac{D^n u_m^{2-n} \rho_m}{8^{n-1} K}\right)^{1.235}}{1 + 1.036 \times 10^{-4} \left(\frac{D^n u_1^{2-n} \rho_1}{8^{n-1} K}\right)^{1.235}}\right] \lambda_1 \tag{5.9}$$

This model has about 15% error and considers all the flow parameters that affect pressure drop but not friction factor.

Two-Fluid Model: This model considers each phase as a separate flow. The total pressure drop consists of the pressure drop across the liquid slugs and the pressure drops across the gas slugs and can be calculated as:

$$\left(\frac{dP}{dL}\right)_{tp} = \left(\frac{dP}{dL}\right)_{L} + \left(\frac{dP}{dL}\right)_{g} \tag{5.10}$$

Xu et al. Model: Xu et al. modified the Two-Fluid Model for gas/Newtonian fluid slug flow to include power-law fluids [13]. Xu et al. assumed that the film does not contain bubbles and that both liquid and gas are incompressible by ignoring pressure drop across the gas slug.

The pressure drop can be calculated as:

$$\left(\frac{dp}{dl}\right)_{tp} = \left(\frac{dp}{dl}\right)_{ls} = 2\frac{f_{ls}}{D}\rho_{ls} u_m^2 k \tag{5.11}$$

This model exhibits an average error of about 14% of 696 data points. However, it used liquid density and liquid phase friction factor instead of mixture properties.

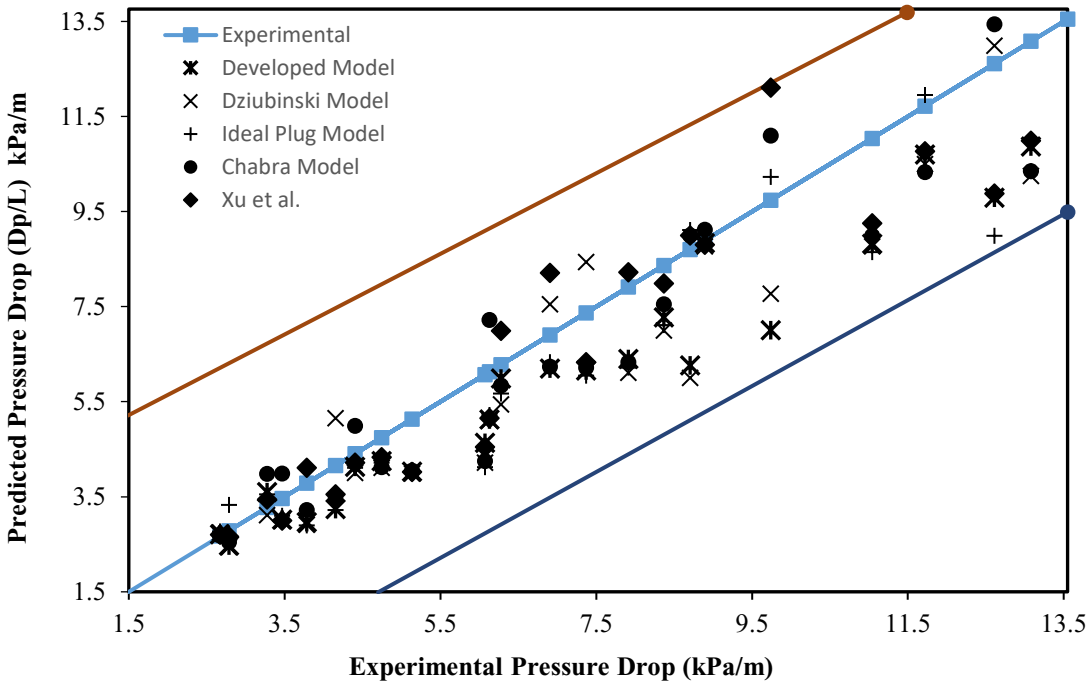

Fig. (5. 26) Comparison of Developed Model Results With Other Correlations

The percentage error for each model used for comparison above is estimated based on the experimental results. Figures (5. 27), (5. 28), and (5. 29) clarify the percentage error for pressure drop that we got from the experiments and the pressure estimated from other models for the Air Xanthangum flow system. The three figures are for the three concentrations of Xanthan gum.

Figures (5. 30), (5. 31), (5. 32), and (5.33) are for the Carbon dioxide Xanthangum flow system with four concentrations. As can be seen, the developed model and the model by Xu et al. are the best models that can give a good estimate of pressure drop.

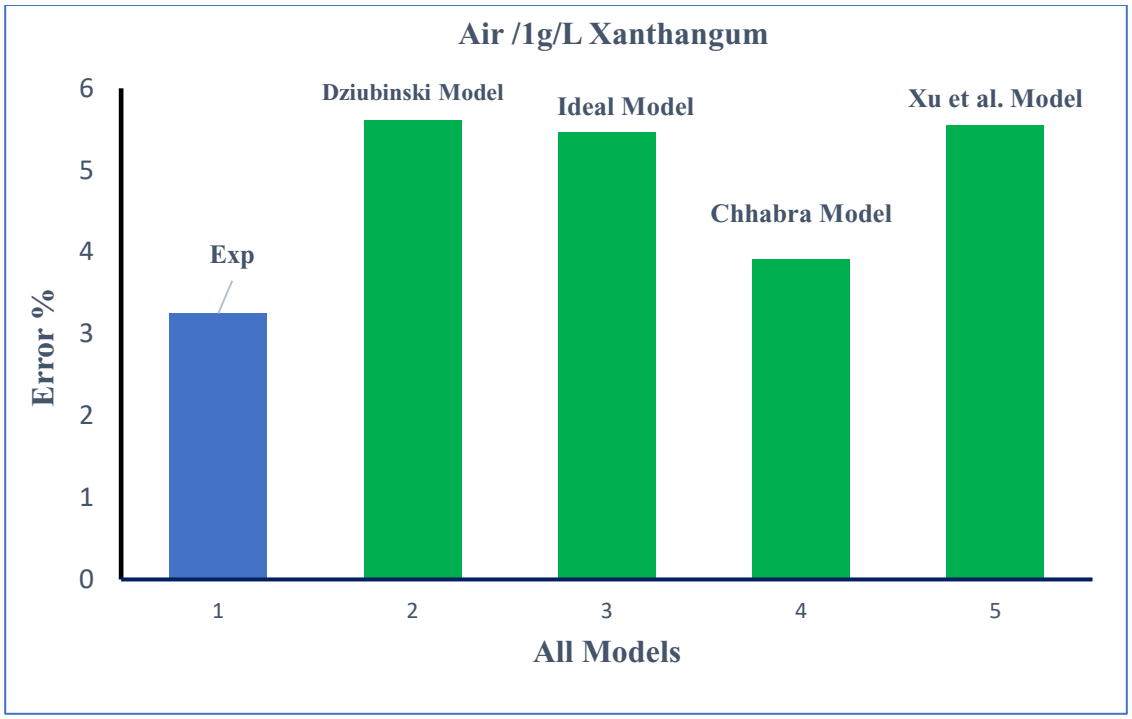

Fig. (5. 27) Error % for Developed Model and Other Correlations (Air/Xanthan gum)(1g/L)

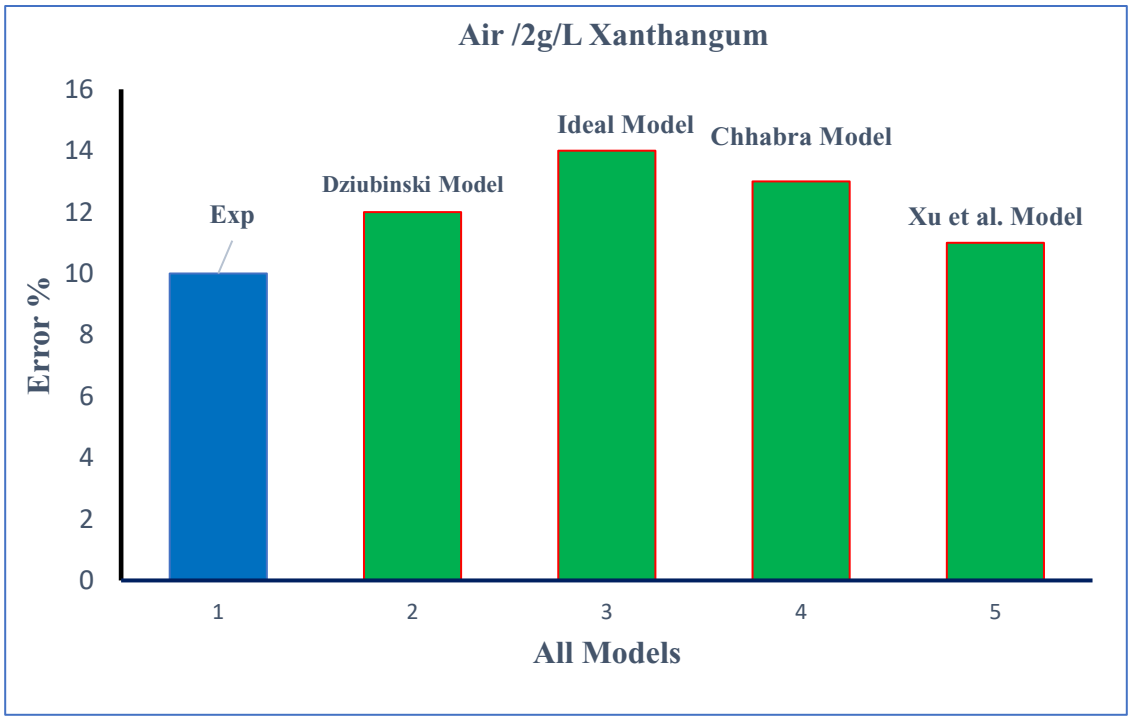

Fig. (5. 28) Error % for Developed Model and Other Correlations (Air/Xanthan gum)(2g/L)

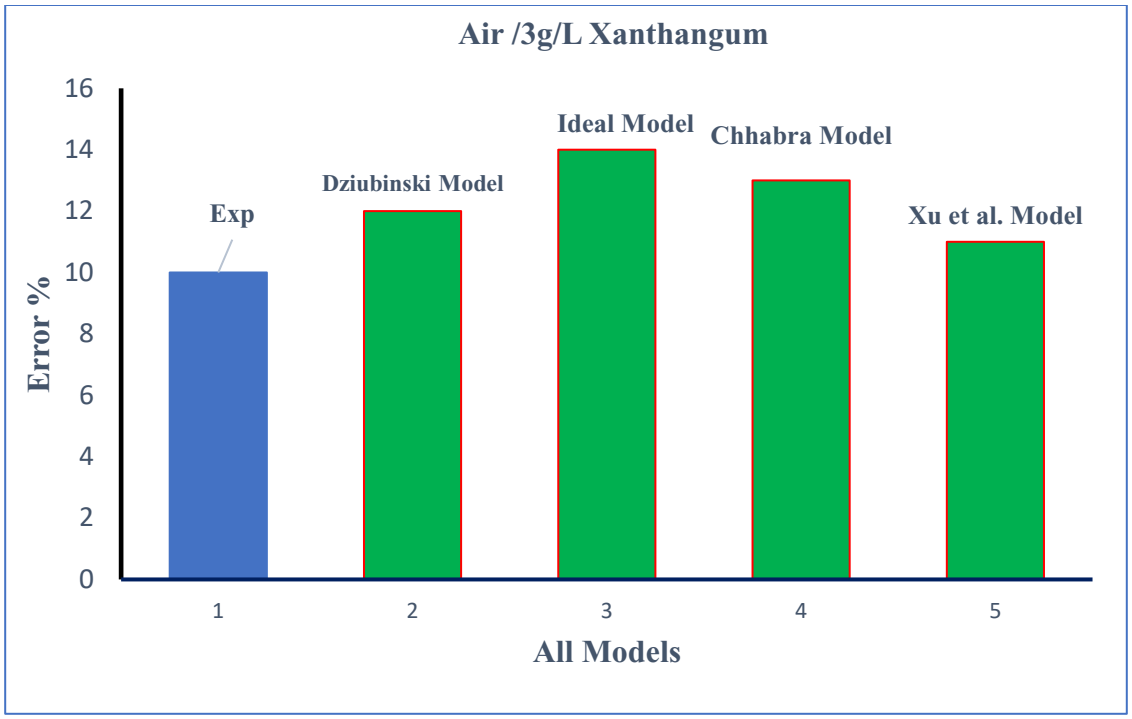

Fig. (5. 29) Error % for Developed Model and Other Correlations (Air/Xanthan gum)(3g/L)

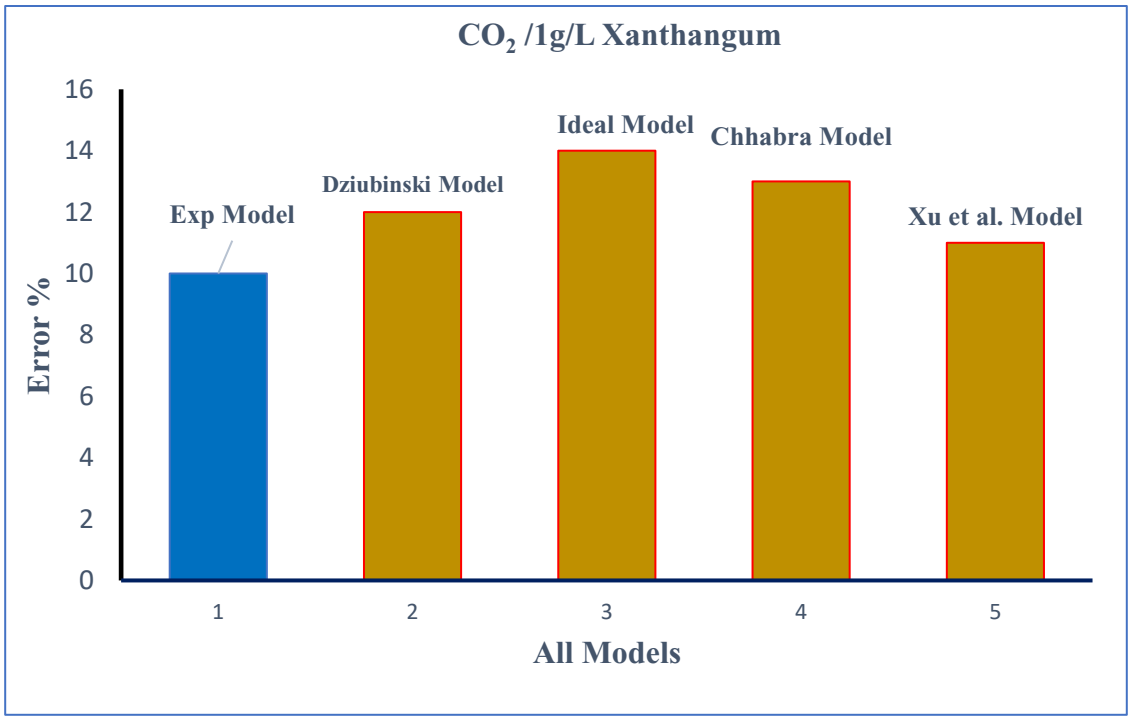

Fig. (5. 30) Error % for Developed Model and Other Correlations (CO_2/Xanthan gum)(1g/L)

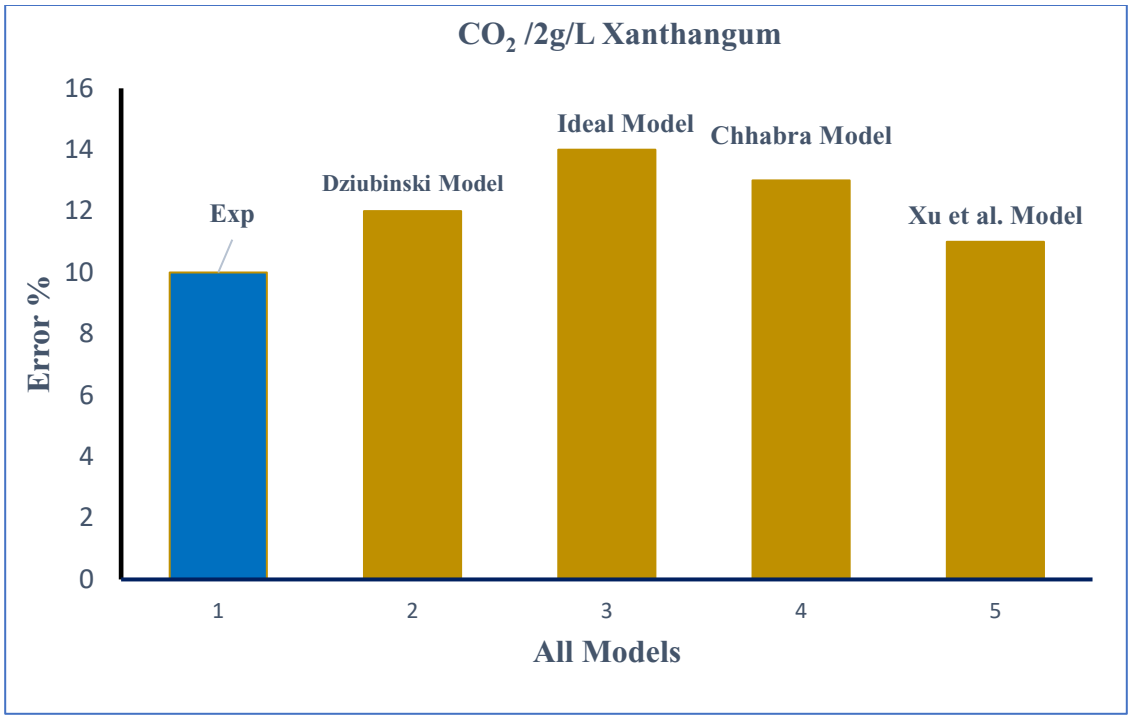

Fig. (5. 31) Error % for Developed Model and Other Correlations (CO_2/Xanthan gum)(2g/L)

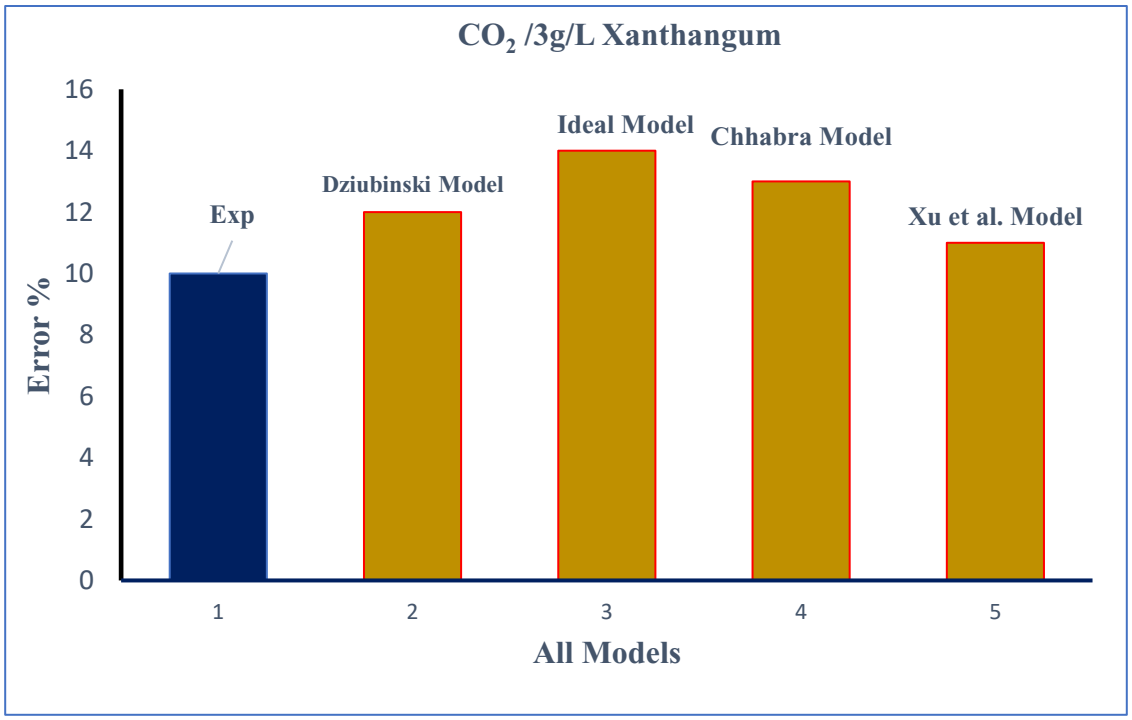

Fig. (5. 32) Error % for Developed Model and Other Correlations (CO_2/Xanthan gum)(3g/L)

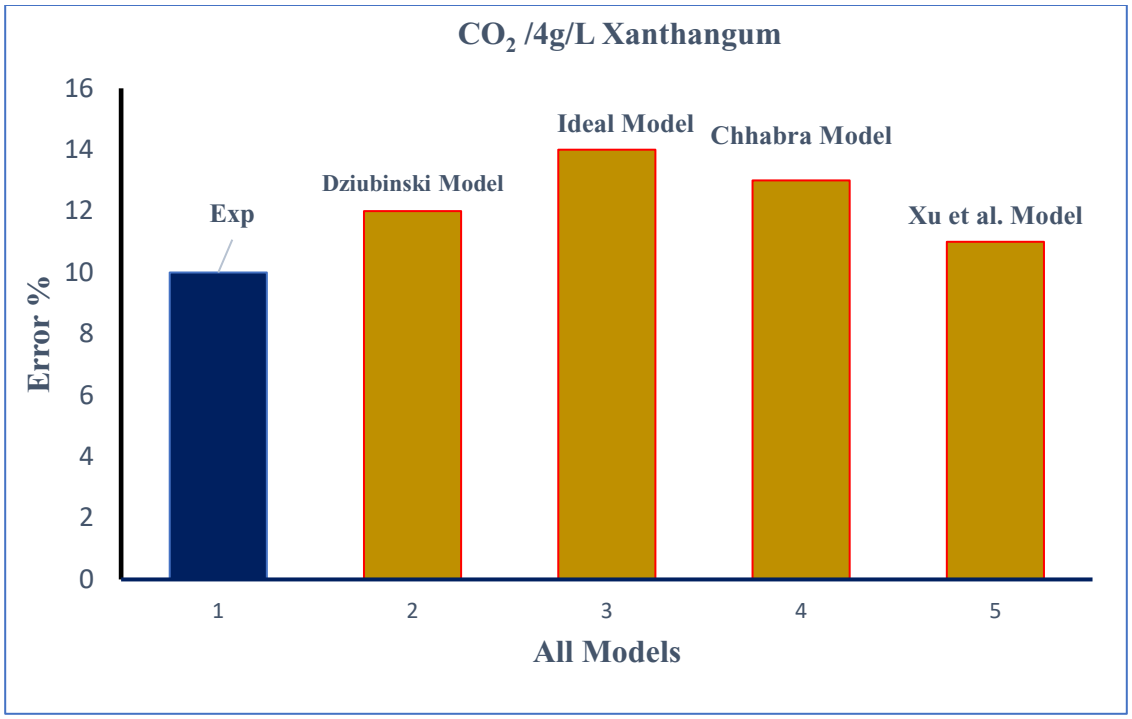

Fig. (5. 33) Error % for Developed Model and Other Correlations (CO2/Xanthan gum)(4g/L)

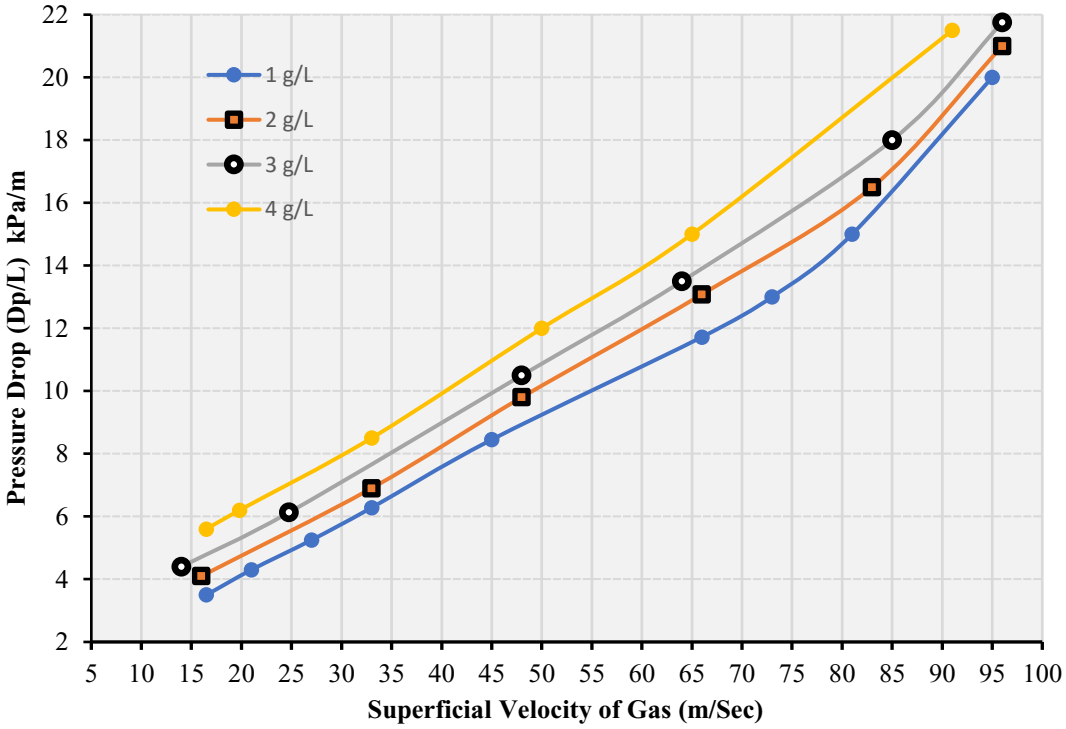

Fig. (5. 34) Predicted Model Curves of Pressure Drop Against the Gas Velocity

5.8 **Conclusion:**

This study conducted an experimental investigation of gas/non-Newtonian two-phase flow. Four concentrations of Xanthan gum have been used for air/Xanthan gum and CO_2/Xanthan gum flow in a pipe system. The effect of flow conditions and the fluid properties on the pressure drop is analyzed, and the results show that:

- The higher the velocity of a fluid (liquid or gas), the higher the pressure drop. This is because of Bernoulli's Principle. The random motion of the fluid molecules causes fluid pressure. When the fluid speeds up, some of the energy from that random motion is used to move faster in the fluid's direction of movement. This results in lower fluid pressure and more pressure drop.
- The pressure drop caused by carbon dioxide Xanthan gum flow is higher than that caused by air Xanthan gum flow, which the Darcy equation proves since carbon dioxide density is higher than Air.
- The pressure drop goes high when the non-Newtonian concentration goes up. That occurs because two types of friction loss occur when fluid flows through pipes. Wall friction is due to friction between the inner pipe surface and the fluid. The other kind of friction is internal friction between viscose fluid layers.
- Results show that the mixture density significantly affects pressure drop with about 50% more than the mixture velocity, which gives up to 40% of the total effect. The effect of the friction factor and bends is about 10%.

- The experimental pressure drop data compared with pressure drop estimated from other empirical known correlations to conclude which correlation is better for Herschel-Bulkleyfluids.
- Finally, the experimental pressure drop was compared with the pressure drop estimated using commonly used models. The results show that the Xu et al. model exhibits an appropriate average error compared to other models. Figure (5.34) concludes the Xu et al. model curves of pressure drop against the gas velocity.
-

CHAPTER 6

Void Fraction

6.1 Void Fraction Overview (ε)

The void fraction is considered one of the most important flow parameters describing two-phase flows in tubes. Void fraction is a critical process variable for the volume and mass calculation required for transporting gas-liquid mixture in pipelines, storage in tanks, metering, and custody transfer. Furthermore, it is important for determining other flow parameters such as two-phase density and viscosity or the average velocities of gas and liquid mixture. In addition, it plays a significant role in estimating and modeling two-phase pressure drop and flow pattern transitions.

The void fraction in the multiphase flow of gas and liquid can be defined as the volume fraction of gas that is occupied in the channel flow. In particular, the void fraction of gas-liquid flow is the fraction of the gas flow rate to the total gas and liquid flow rates. The void fraction value varies from zero for a single phase of liquid flow to one for a single phase of gas flow. Void fraction could be evaluated experimentally by several methods, such as trapping a section of the flow stream between two quick closing valves and measuring the gas or liquid trapped volume. The comparative volume of liquid is called liquid holdup $H_{L.}$ and is expressed as:

$$H_{L.} = 1 - H_G$$

A value for void fraction cannot be estimated analytically but from empirical correlations. It is a function of many variables, such as liquid and gas properties, flow pattern, pipe diameter, and liquid and gas velocities.

Many void fraction correlations are created based on the liquid and gas superficial velocities, and the most simple correlation to estimate void fraction depending on mixture velocity is the Hughmark correlation [41]:

$$\boldsymbol{\varepsilon} = \frac{V_{sg}}{1.2V_{mix}} \tag{6.1}$$

V_{sg} is the superficial gas velocity, and V_{mix} is the average liquid and gas mixture velocity.

In this work, the void fraction for the experimented Newtonian and non-Newtonian multiphase flow is experimentally estimated and calculated based on the basic void fraction correlations. Results were plotted against the flow parameters to determine each flow variable's effect and develop a void fraction prediction correlation.

6.2 Superficial Velocity of Gas Effect:

Fig. (6. 1) describes the void fraction of Air-water and Air Xanthangum flows as the superficial velocity of gas increases. Similarly, Fig. (6. 2) explains the void fraction of CO_2-water and CO_2 Xanthangum flows as the superficial velocity of gas increases.

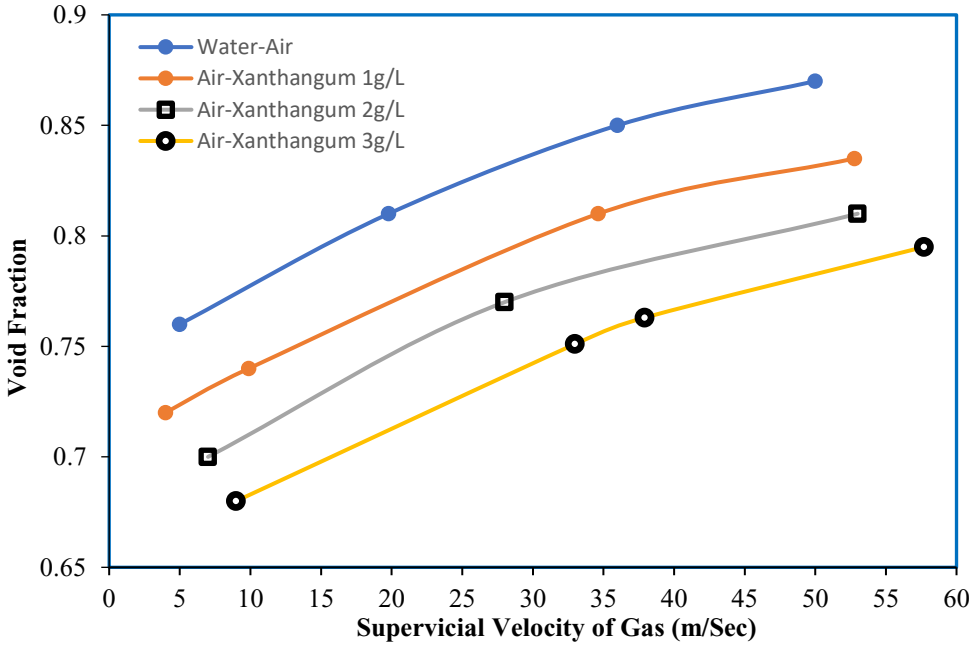

Fig. (6. 1) Void Fraction and Superficial Velocity of Gas (Water-Air-Xanthan gum)

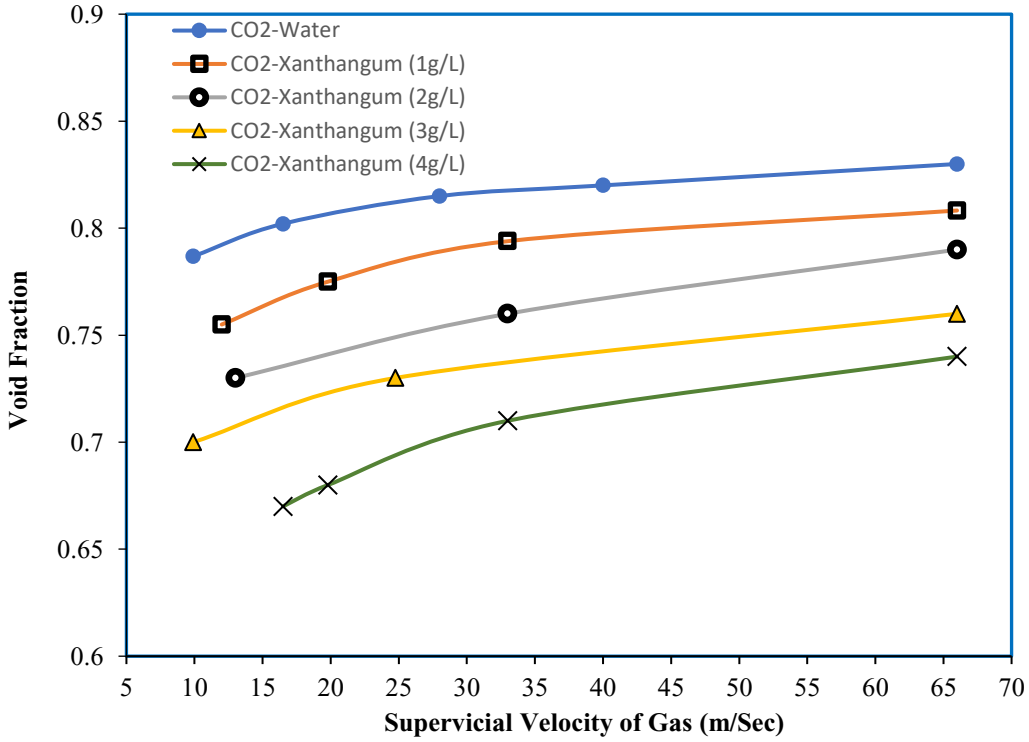

Fig. (6. 2) Void Fraction and Superficial Velocity of Gas (Water-CO_2-Xanthan gum)

The above two figures conclude that the void fraction grows as gas velocity increases, which is consequential to Parsi et al. [20]. Additionally, there are reductions in void fraction at higher shear-thinning behavior when the non-Newtonian fluid flows at high concentrations.

The general equation of estimating void fraction of the system can be created after developing the relationship between the void fraction and each flow parameter separately. Figure (6. 3) shows the effect of the superficial velocity of gas on the void fraction when the other flow parameters are fixed. The two flow systems of Air Xanthangum flow and CO_2 Xanthangum flow exhibit nearly the same void fraction equation with a high void fraction for Air Xanthangum flow.

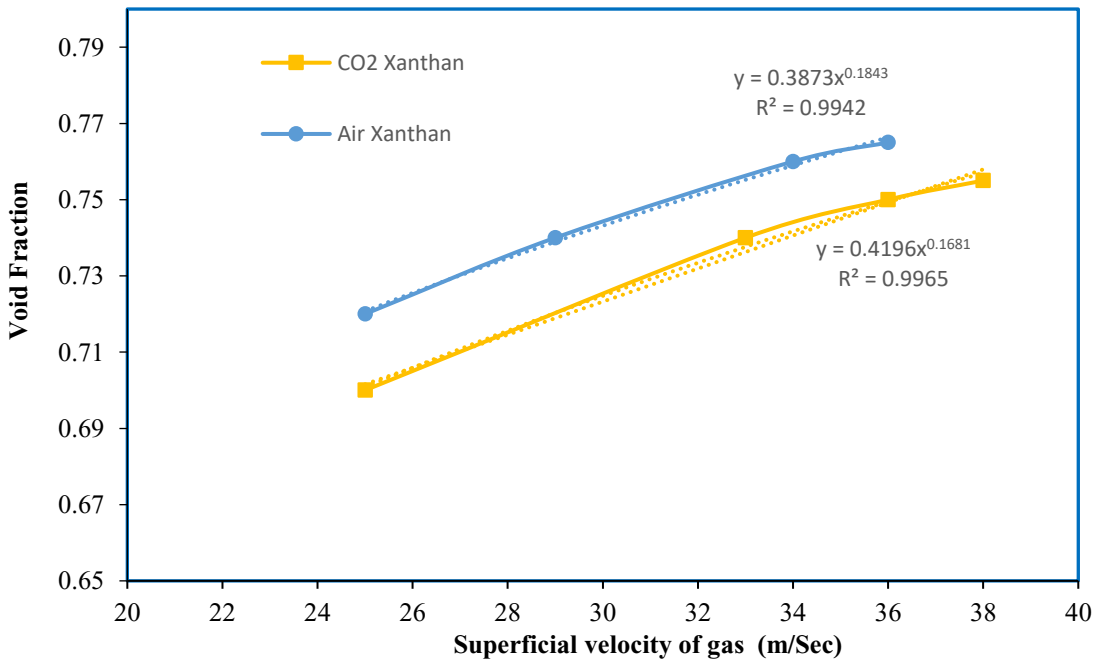

Fig. (6. 3) Void Fraction and Superficial Velocity of Gas Relationship

6.3 Superficial Velocity of Liquid Effect:

As the superficial velocity of liquid rises, the liquid holdup will increase while the void fraction or gas holdup will decrease. Fig. (6.4) and Fig. (6.5) describe the effect of the superficial velocity of liquid on the void fraction for the Air Xanthangum flow and CO_2 Xanthangum flow, respectively.

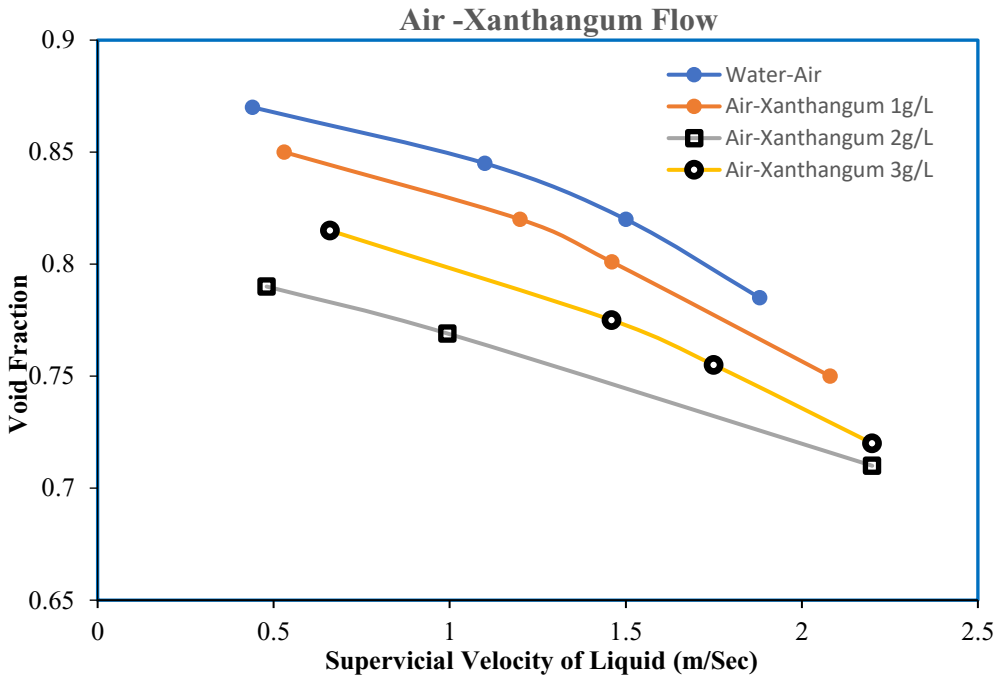

Fig. (6. 4) Void Fraction and Superficial Velocity of Liquid (Air-Xanthan gum)

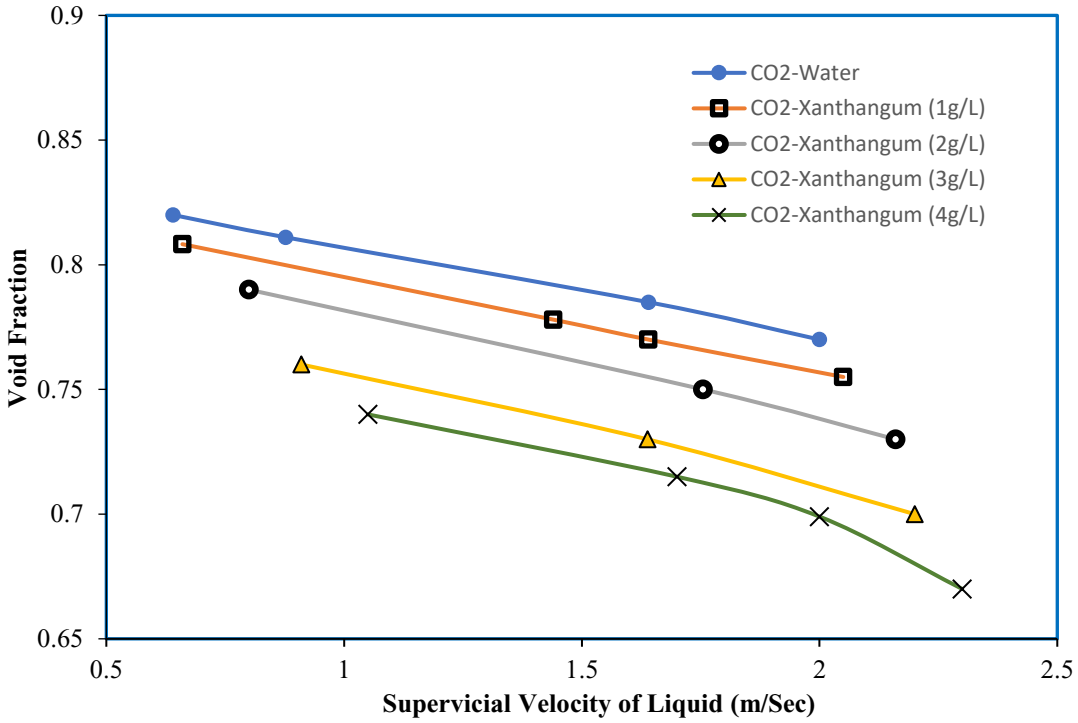

Fig. (6. 5) Void Fraction and Superficial Velocity of Liquid (CO_2-Xanthan gum)

The last two figures introduce the reduction in void fraction as liquid velocity increases, which is consequential with Jing-yu Xu. [5]. Similarly, there are reductions in void fraction at higher shear-thinning behavior when the non-Newtonian fluid flows at high concentrations.

Fig. (6. 6) shows the void fraction equation based on the superficial velocity of liquid when the other flow parameters were fixed. The two flow systems of Air Xanthangum flow and CO_2 Xanthangum flow exhibit different but similar void fraction trends.

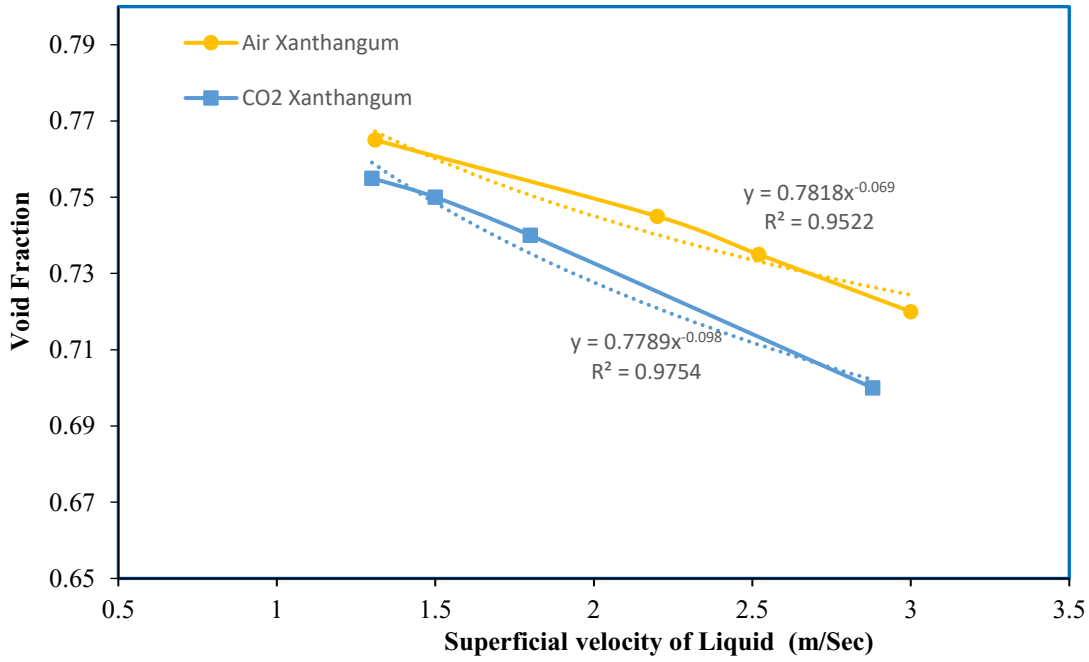

Fig. (6. 6) Void Fraction and Superficial Velocity of Liquid Relationship

6.4 Liquid and Gas Density Effect:

For the void fraction estimations, most empirical correlations involve gas density ρg to liquid density ρl ratio is an essential factor in their equations. This is because liquid resistance to the gas passing through it increases with the increase of the density of the liquid due to viscous forces.

Fig. (6. 7) introduces the effect of four Xanthan gum densities on void fraction, as four concentrations of Xanthan gum were used during the experiments in this work.

The effect of gas density ρ_G on the void fraction is not considered that much for the void fraction estimations because the gas density is negligible compared to the liquid density. However, the results show that increasing liquid density produces a high void fraction, which is compatible with empirical correlations as dressed in Fig (6.7)

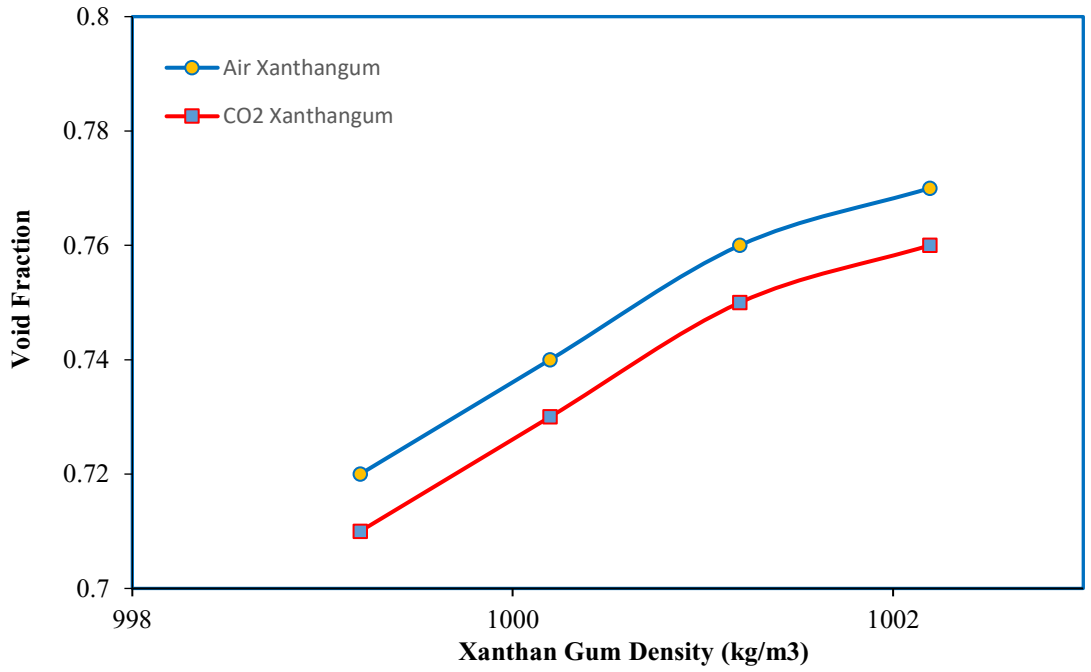

Fig (6. 7) Void Fraction and Liquid Density effect

In general, many void fractions estimating correlations combine the effect of gas and liquid density in one term. Fig. (6.8) shows the void fraction of Air Xanthan gum flow as a function of the gas-liquid density ratio. Similarly, Fig. (6.9) shows the void fraction of CO_2 Xanthan gum flow as a function of the gas-liquid density ratio. The results indicate that the void fraction increases as the gas-liquid density ratio increases. The general form of the void fraction equation related to the gas-liquid density ratio is created based on the two equations.

In summary, fluids with more mass per unit volume are heavier and require more energy to move them, and they shear less easily. Increasing liquid density will reduce the quantities of liquid transferred in tubes. As a result, the amount of gas will rise.

6.5 Liquid and Gas Viscosity Effect:

Fig. (6.10) displays how the void fraction changes while the liquid-to-gas viscosity ratio changes. The concentration-effect section explains that the void fraction decreases as the liquid-to-gas viscosity ratio increases.

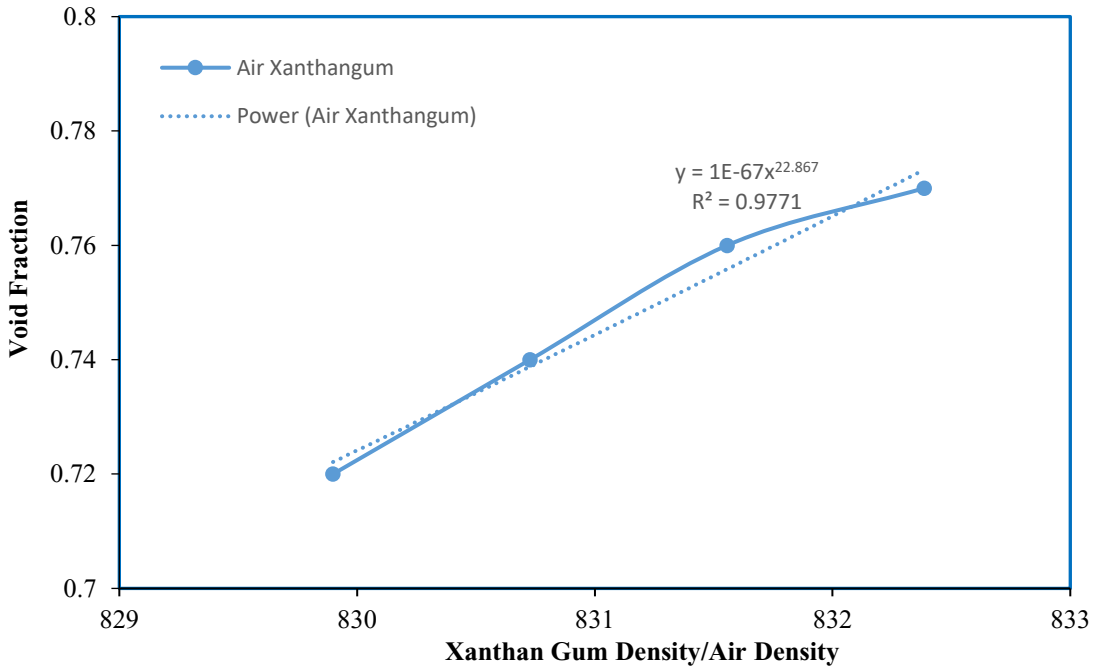

Fig. (6. 8) Void Fraction and Liquid Density effect

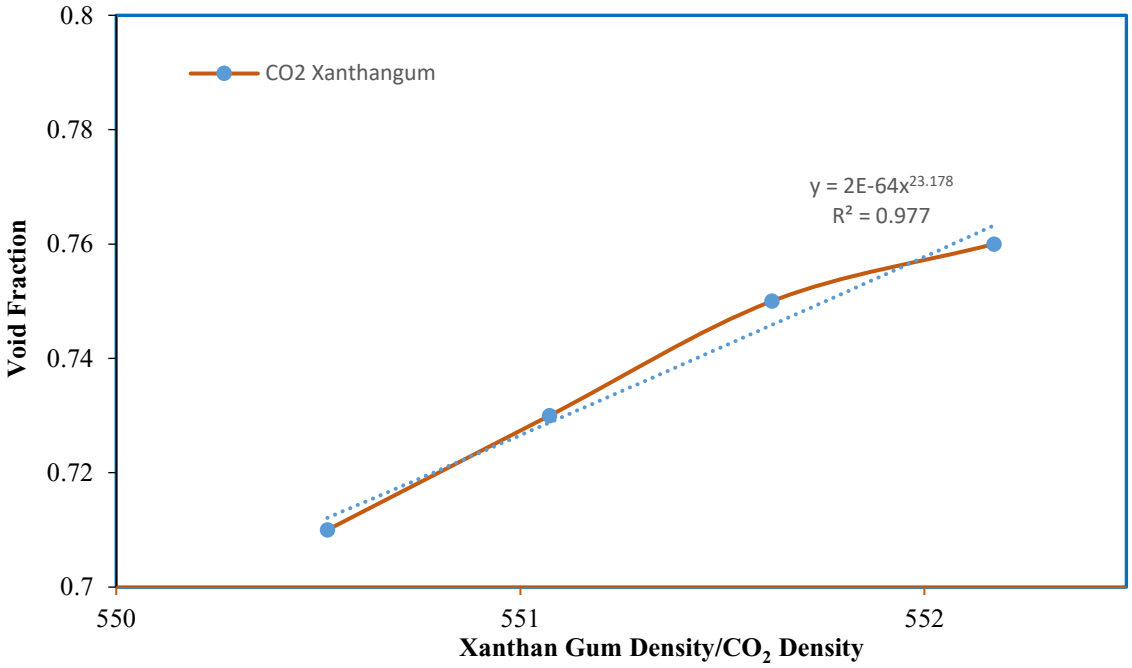

Fig. (6. 9) Void Fraction and Liquid Density effect

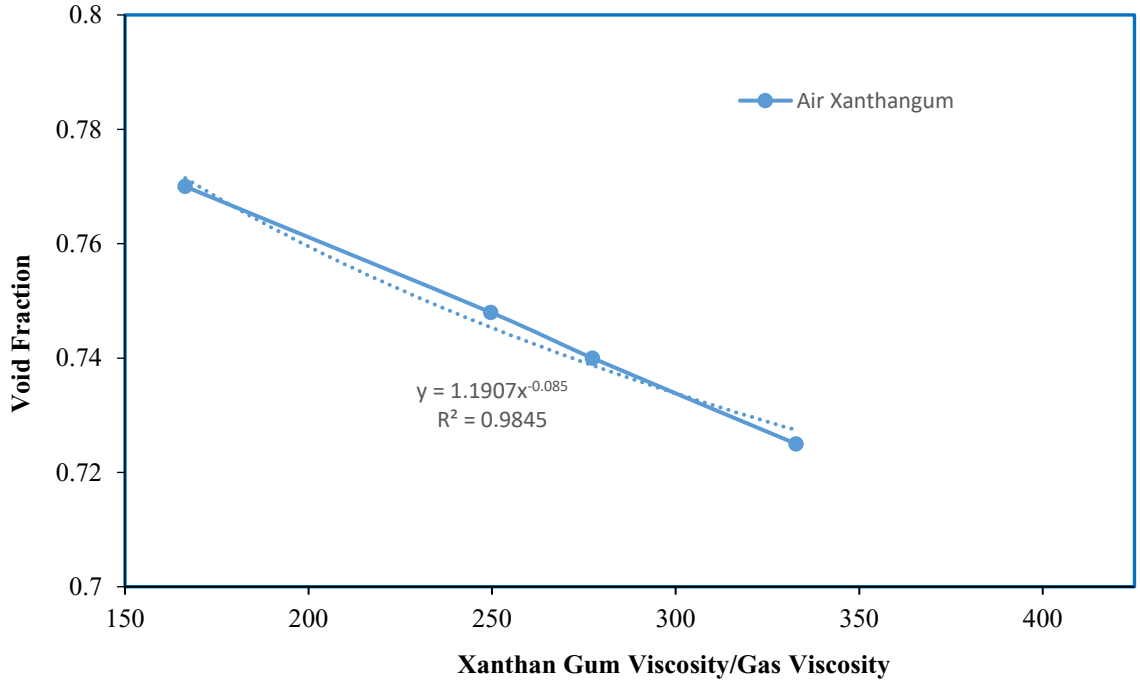

Fig. (6. 10) Void Fraction Against Viscosity Ratio

We can infer that the more viscous or less slippery a fluid, the harder it is to get shearing between layers. The high viscosity prevents rapid velocity from occurring between layers. Therefore, the gas void fraction decreases with the increase in liquid viscosity. Because an increased liquid viscosity causes an increase in the thickness of the liquid film, which separates gas bubbles from the channel wall, the effective cross-section gas flow decreases. The effect of the viscosity of gas is negligible because it is so small compared with liquid viscosity.

6.6 Flow Quality

In two-phase gas-liquid flow, the flow quality indicates the ratio of the gas quantity to the total gas and liquid quantities in the tube. The flow quality (x) in a two-phase flow is defined as:

$$x = \frac{\dot{m}_G}{\dot{m}_G + \dot{m}_L} \tag{6-2}$$

It is the fraction of gas mass flow to the total gas and liquid mass flow.

As a result, the gas-liquid mass flow ratio is defined as :

$$\frac{\dot{m}_G}{\dot{m}_L} = \frac{x}{1-x} \tag{6-3}$$

The liquid-to-gas mass flow ratio (1-x)/x is used during derivative void fraction equations. It is preferred as the liquid mass flow rate is greater than the gas mass flow rate, and the void fraction decreases as the liquid mass flow rate increases.

Fig. (6.11) explains how the void drops down as the ratio of liquid to gas mass flow rate increases for the Air Xanthan gum flow. When the liquid flow rate increases or the gas flow rate decreases, the gas fraction decreases. Fig. (6.12) is for the CO_2 – Xanthangum flow and is

compared with CO_2 water flow. Finally, the relation between the flow quality (x) and the void fraction of Newtonian and non-Newtonian multiphase flow is expressed in Fig (6.13).

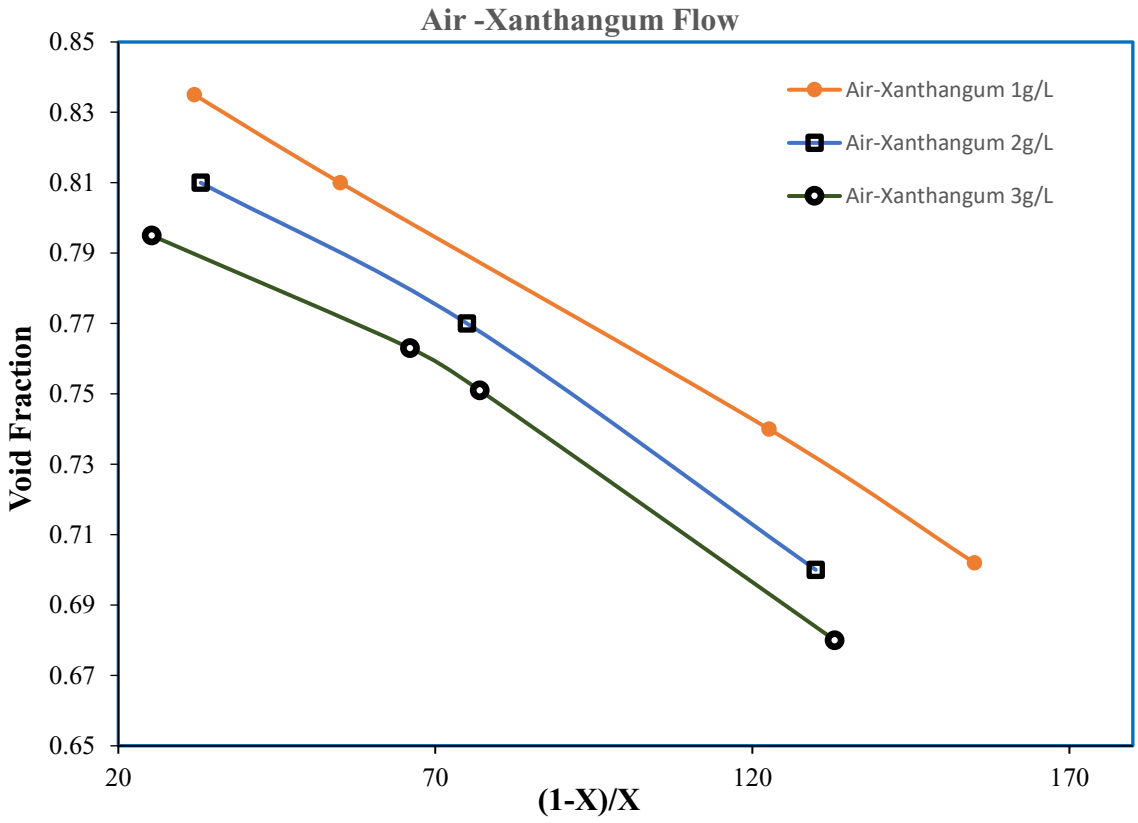

Fig. (6. 11) Void Fraction and Liquid to Gas Mass Flow Ratio (Air Xanthan gum)

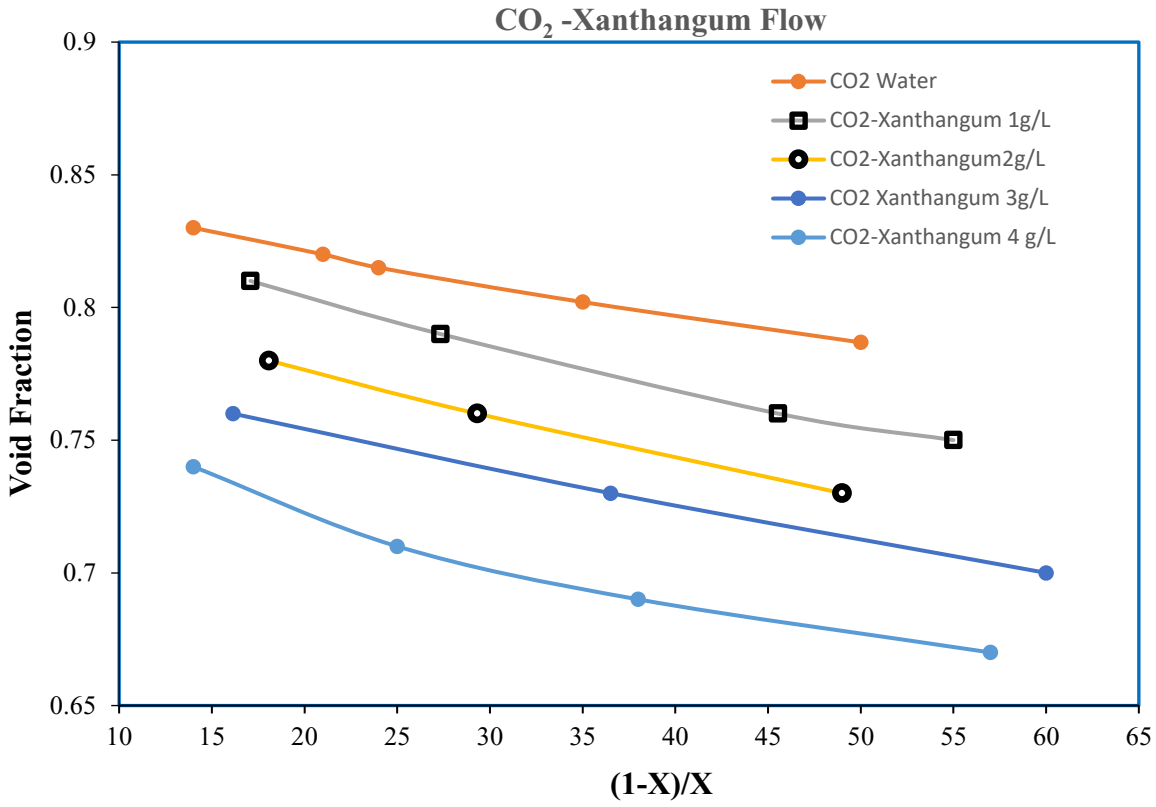

Fig. (6. 12) Void Fraction Against Liquid Gas Mass Flow Ratio (CO_2 Xanthan gum)

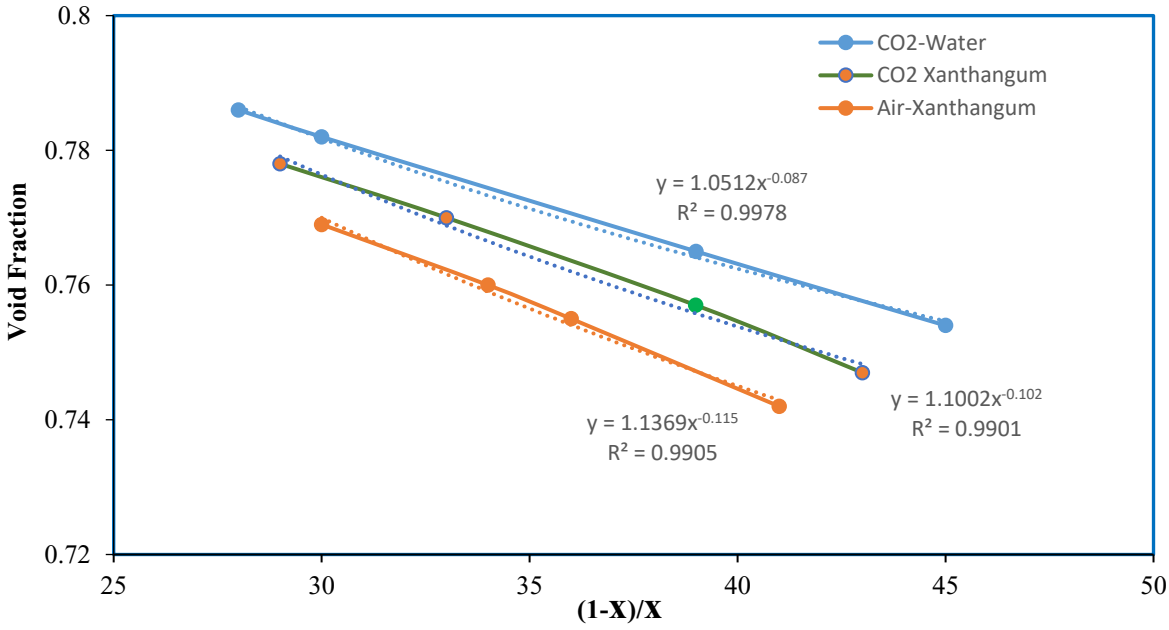

Fig. (6. 13) Void Fraction Equation with Flow Quality

6.7 Slip Ratio Effect:

The slip ratio is the ratio of the velocity of the gas phase to the velocity of the liquid phase for gas-liquid flow. Determining the phase distribution from given input conditions of multiphase flow through pipes is complicated due to the slippage between the gas and the liquid phases. However, many void fraction correlations consider no-slip conditions, which means the two phases travel at the same velocity. Experimentally, This assumption can only occur in a very limited range of flow situations like bubbly, dispersed, or mist flow. In addition, most industrial two-phase flows have different velocities for the gas and liquid phases. Fig. (6. 14) and Fig. (6. 15) show the slip ratio effect on void fraction for Air Xanthangum flow and CO_2 Xanthangum flow, respectively. Void fraction increases when the slip ratio increases because gas slippage raises gas velocity and gas quantities in the pipe.

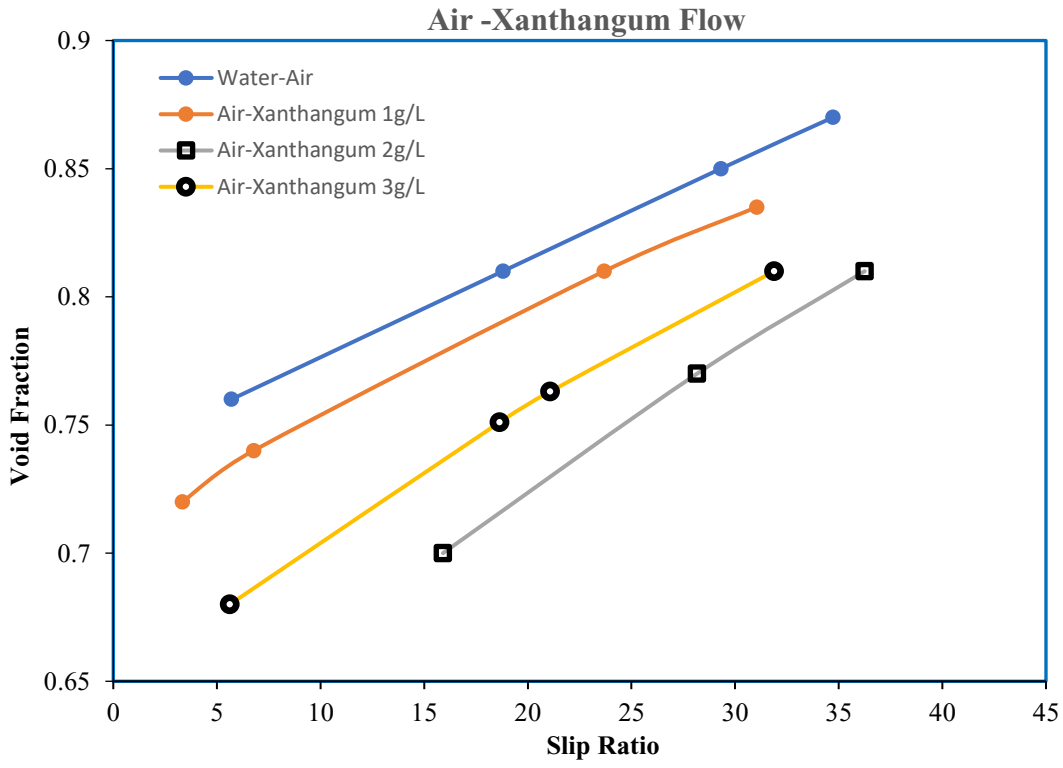

Fig. (6. 14) Void Fraction and Slip Ratio for Air Xanthangun Flow

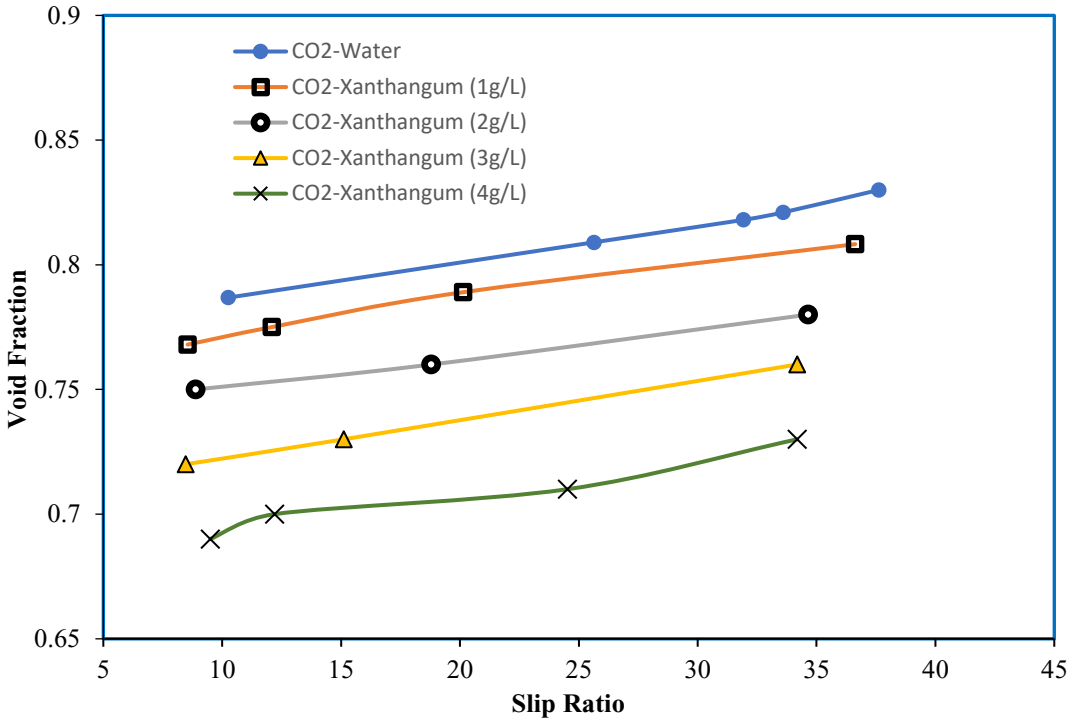

Fig. (6. 15) Void Fraction and Slip Ratio for CO_2 Xanthangun Flow

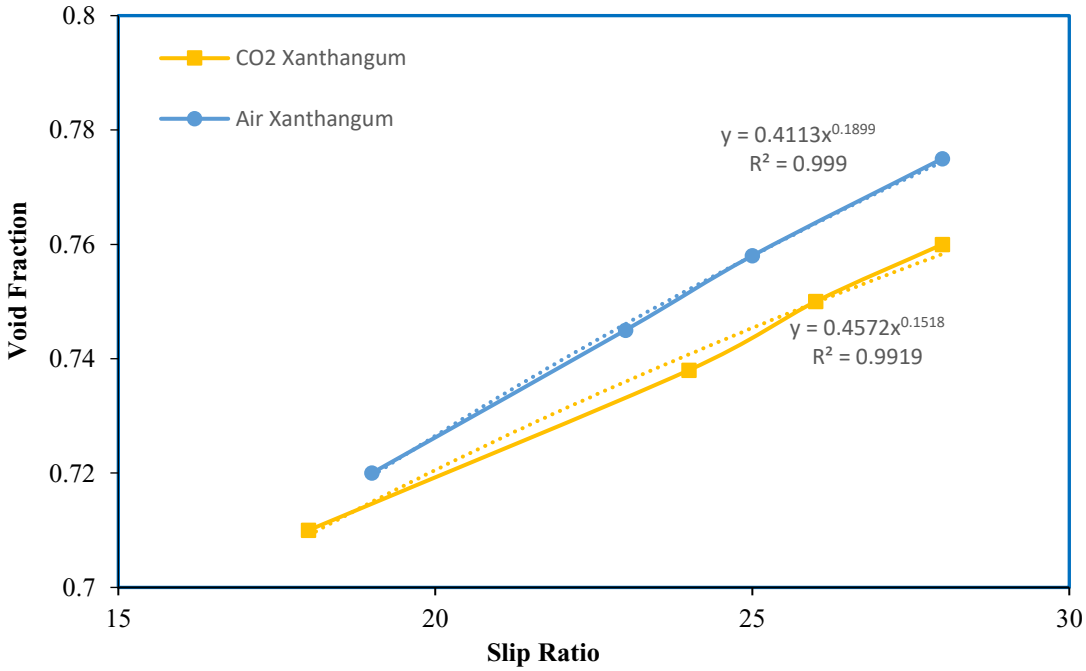

Fig. (6. 16) Void Fraction and Slip Ratio Equation

The developed void fraction equation based on the slip ratio is presented in Fig. (6.16).

Defining the void fraction and the slip ratio is important because they can also play an essential role in calculating the pressure drop of the two-phase flow.

The similarity between the existing models of predicting void fraction for gas-liquid flow

Such (Lockhard & Martinelli [11]; Baroczy [12]; Turner & Wallis [13]) has been studied by Butterworth.

The predicted void fraction for liquid gas flow is expressed in the general form by Butterworth (1975), which simulates all cases as shown in equation (6.4).

$$\boldsymbol{\varepsilon} = \left[1 + K\left(\frac{1-x}{x}\right)^{a}\left(\frac{\rho_g}{\rho_L}\right)^{b}\left(\frac{\mu_L}{\mu_g}\right)^{c}\right]^{-1} \tag{6.4}$$

The constants K, a, b, and c are different from one model to another and can be determined experimentally. Therefore, the developed model parameters are estimated based on the equations derived from experimental results for each general equation term. Four equations is obtained from Fig(6.9), Fig(6.10), Fig(6.13),and Fig(6.16) as listed below:

$$\mathbf{1}/\boldsymbol{\varepsilon} = 3 \times 10^{6}\left(\frac{\rho_g}{\rho_L}\right)^{22} \tag{6.5}$$

$$\mathbf{1}/\boldsymbol{\varepsilon} = 1.25\left(\frac{\mu_L}{\mu_g}\right)^{0.095} \tag{6.6}$$

$$\mathbf{1}/\boldsymbol{\varepsilon} = 1.12\left(\frac{1-x}{x}\right)^{0.11} \tag{6.7}$$

$$\boldsymbol{\varepsilon} = 0.43S^{0.17} \tag{6.8}$$

.

The overall void fraction equation can be developed based on the above four equations and the percentage effect of each parameter on the void fraction value to get the following equation:

$$\boldsymbol{\varepsilon} = \left[1 + \left(\frac{\rho_g}{\rho_L}\right)^{0.78} \times \left(\frac{\mu_L}{\mu_g}\right)^{0.12} \times \left(\frac{1-x}{x}\right)^{0.82}\right]^{-1} \tag{6.9}$$

Equation (6.9) is the created model to estimate the void fraction for a gas non-Newtonian flow system. This model predicts the void fraction with a small error percentage, as shown in Fig. (6.17). Moreover, we can estimate the general form equation (6.4) constants based on the created model equation. Fig(6.18) describes the estimated general equation constants a, b, and c for the CO2 Xanthangum flow. As can be seen, we got the same values of constants (b) and (c) for all Xanthan gum concentrations used for the experiments. There are minor fluctuations for constant (a) values with only slight difference amounts. This is a good indicator that these constants can be used for such systems to estimate the void fraction using the general equation form. The similarity between the constants of the developed model and existing correlations like Lockhard & Martinelli [11][81], Baroczy [12], and Turner & Wallis [13] are tabulated in Table 6. 1.

`

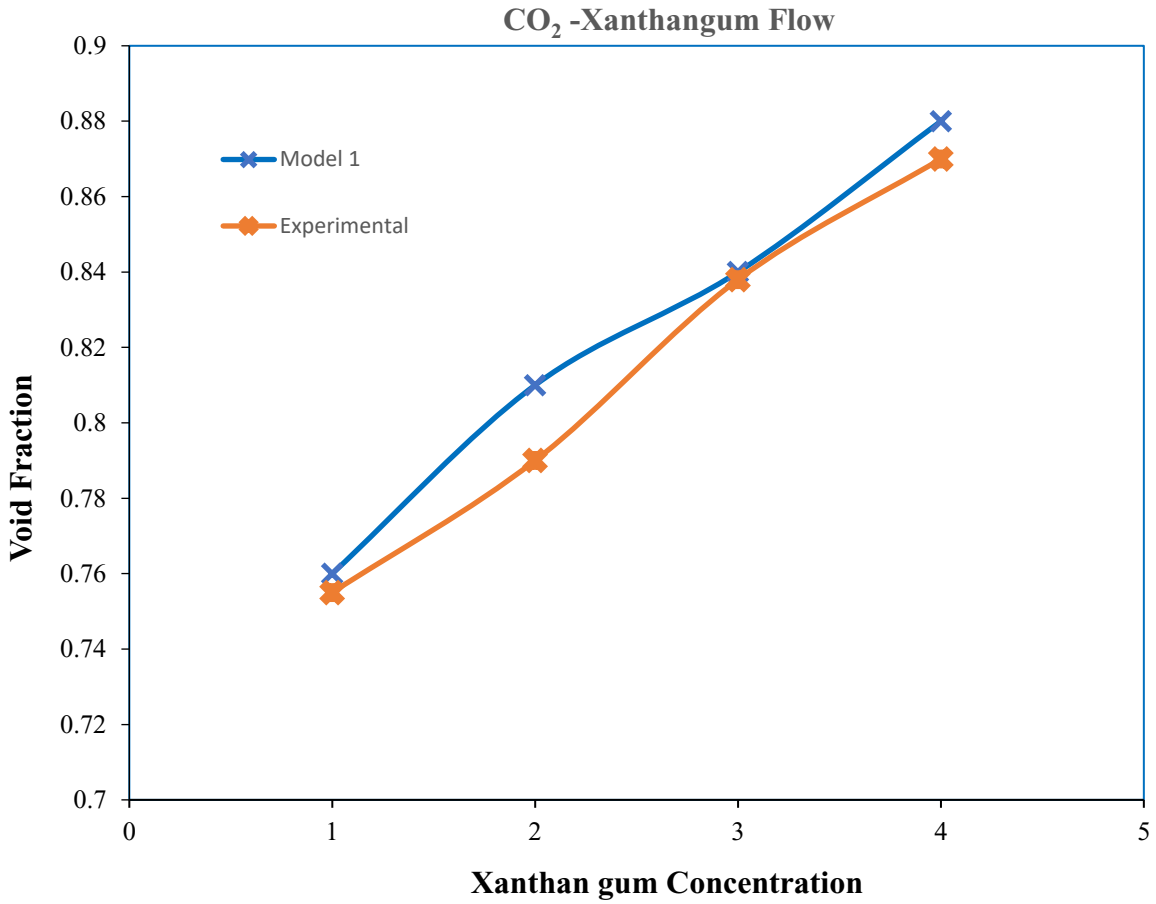

Fig. (6. 17) Experimental and Predicted Void Fraction Equation (6.9)

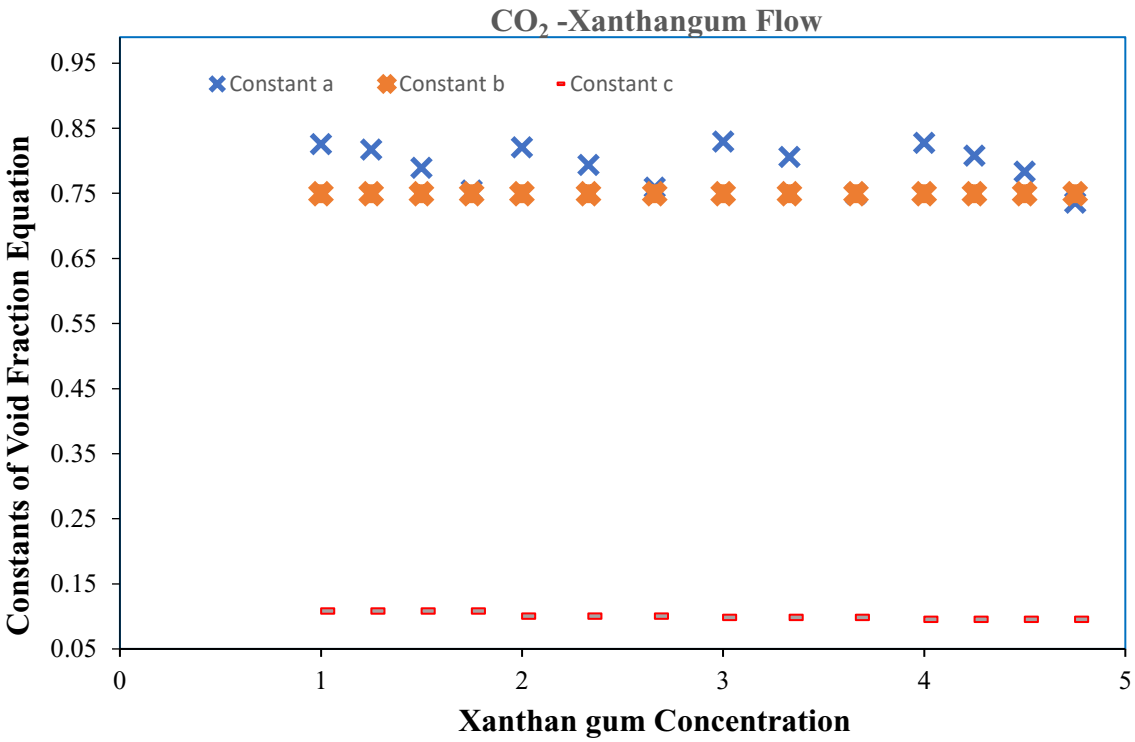

Fig. (6. 18) Void Fraction General Equation Constants

Table 6. **1** – Values of Constants Suggested by Various Correlations

Model	K	a	b	c
Homogeneous	1	1	1	0
Lockhart & Martinelli	0.28	0.64	0.36	0.07
Baroczy	1	0.74	0.65	0.13
Turner & Wallis	1	0.72	0.40	0.08
Developed Model	1	0.79	0.75	0.10

As a result and based on the resulted constants, we can develop another void fraction model related to non-Newtonian fluids as follows ;

$$\boldsymbol{\varepsilon} = \left[1 + \left(\frac{1-x}{x}\right)^{0.79} \left(\frac{\rho_g}{\rho_L}\right)^{0.75} \left(\frac{\mu_L}{\mu_g}\right)^{0.10}\right]^{-1} \tag{6.10}$$

Equation (6.10) is the scend model created to predict the void fraction of gas non-Newtonian flow based on the general equation. The comparison between the two models and the experimental results is illustrated in Figure (6.19).

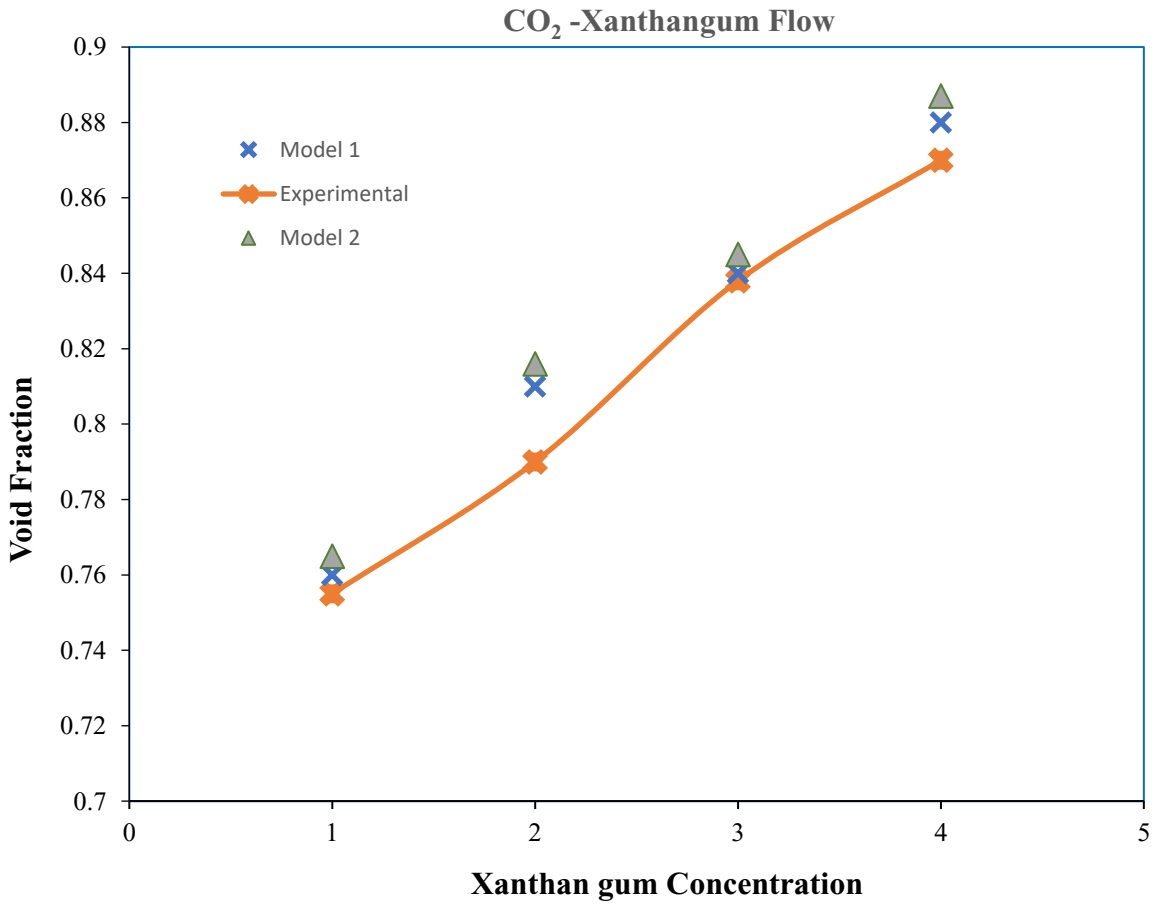

Fig. (6. 19) Experimental and Predicted Void Fraction by Developed Models

As seen in Figure (6.19), the two models can estimate the void fraction of the gas-non-Newtonian flow system with high accuracy. As a result, the two models are good for void fraction estimations for the gas non-Newtonian flow. However, using the other available

correlations unrelated to the gas non-Newtonian flow can result in a significant percentage error, as shown in Figure (6.20).

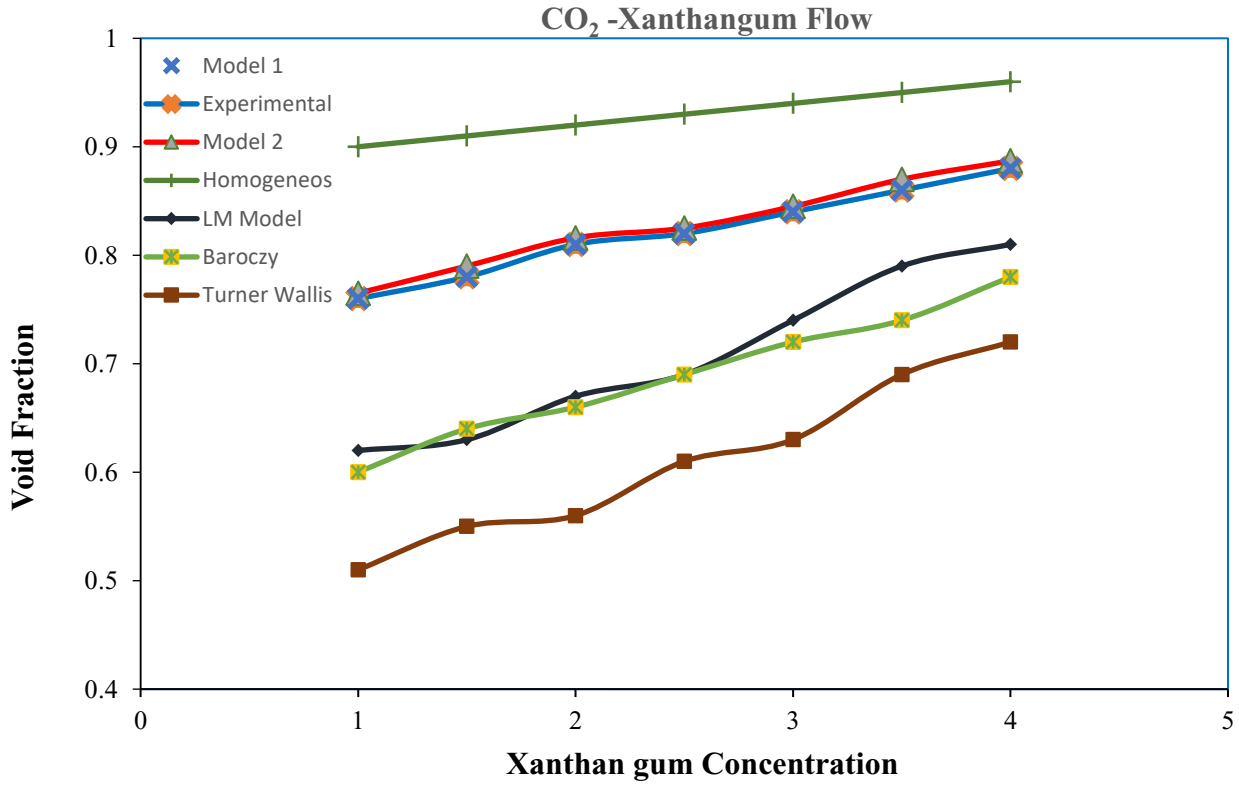

Fig. (6. 20) Comparison of Experimental, Developed, and Other Void Fraction Models

Figure (6.20) clearly indicates that using other correlations that do not govern non-Newtonian fluids to estimate voids can result in a huge mistake. Figure (6.21) shows the error percentage for applying other models for void fraction estimation compared with the percentage error of developed models. Using empirical models derived from Newtonian flow systems for non-Newtonian systems results in a high percentage error.

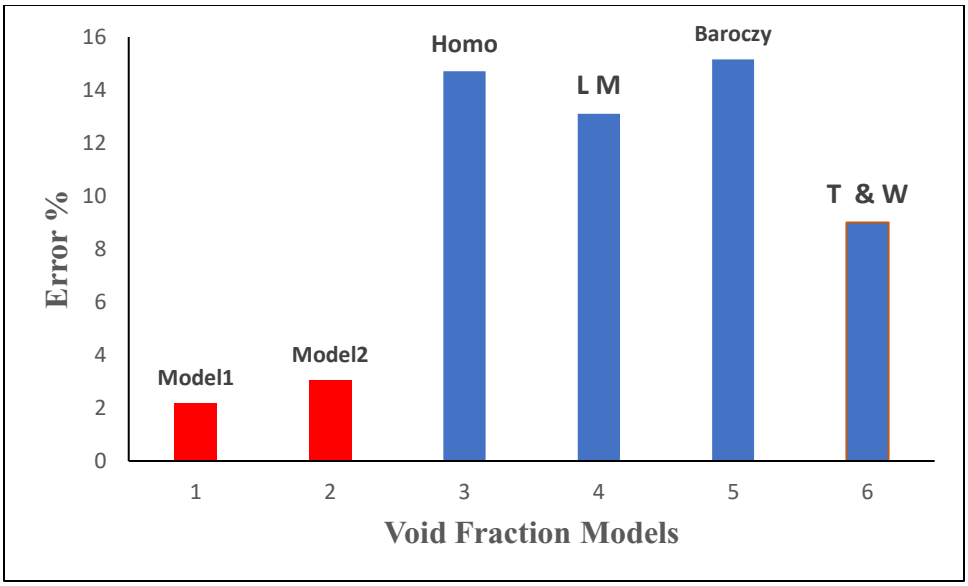

Fig. (6. 21) Comparison of Percentage Error Developed and Other Void Fraction Models

The other correlations' definitions, pros, and cons are :

The homogeneous model is the simplest method to calculate void fraction in a two-phase flow. This way, assuming no slip condition exists between gas and liquid, the two phases travel at the same velocity. Therefore, this model doesn't give a good prediction. This model suits air-water flow in triangular channels with hydraulic diameters between 1.0 and 1.5 mm[42].

Lockhart-Martinelli correlation developed a model to predict pressure drop based on the assumption that the two phases are flowing as a single phase and the two-phase pressure drop can be calculated using the equations used to calculate the pressure drop to a single phase. Therefore, the two-phase pressure drop depends on the friction multiplicator for the liquid or vapor phases separately. The multiplicator parameter for each phase is exactly the inverse of the void fraction. As a result, the Lockhart-Martinelli correlation is the method to calculate pressure drop based on the void fraction.

Baroczy estimated the void fraction for the air-water system for many tube diameters. The results of this method showed good accuracy for Newtonian gas flow but not for non-Newtonian flow.

6.8 Conclusion

Knowledge of void fraction in two-phase flows is crucial for determining pressure drop and heat transfer and designing flow process equipment. Research in void fraction modeling and evaluations started over 60 years ago, but no standard method for modeling void fractions can be used for all boundary conditions. Most available correlations and models are obtained based on empirical relations for a narrow range of data. The simplest experimental way to measure the void fraction is by suddenly shutting off valves and measuring the relative volume of liquid and vapour.

Nearly all experimental void fraction models have been simulated with air/water mixtures, making extending data to a more general model difficult. Therefore, conducting experiments with different Newtonian and non-Newtonian fluids will greatly enhance understanding of the void fraction mechanism.

In this work, the void fraction for the experimented non-Newtonian multiphase flow is experimentally evaluated by the quick valve shut-off technique. Results were plotted against the flow parameters to determine each flow variable's effect and develop a void fraction prediction correlation, and the results proved that:

- The velocities of gas and liquid highly impact the void fraction of the flow. While the increasing velocity of gas raises the void fraction, the increased velocity of liquid reduces the void fraction.

- Fluids with high density are heavier, require more energy to move, and shear less easily. Increasing liquid density will reduce the quantities of liquid transferred in tubes per unit of time. As a result, the amount of gas will rise.
- The gas void fraction decreases with the increase in liquid viscosity. Because an increased liquid viscosity causes an increase in the thickness of the liquid film, which separates gas bubbles from the channel wall, the effective cross-section gas flow decreases. The effect of the viscosity of gas is negligible because it is so small compared with liquid viscosity.
- The experimental model of estimating void fraction for gas-non-Newtonian flow was developed based on the parameters equations and the percentage effect of each parameter on the void fraction value. This model predicts the void fraction with a small error percentage.
- The experimental model has been used to determine the general void fraction equation constants related to gas-non-Newtonian flow. As a result, we conclude with two models to estimate the void fraction for the gas-non-Newtonian flow with high accuracy.
- Experiment with other non-Newtonian fluids that exhibit rheolog

Chapter 7
Summary, Conclusion, and Recommendations

7.1 Summary

Recently, more research has focused on understanding the two-phase flow phenomena in gas and liquid flow. Understanding rheological information and techniques for predicting pressure drop is crucial in estimating proper pump flow rates and avoiding any difficulty facing a regular oil production operation.

In the case of highly viscous materials, the impact of injecting gas into the liquid might be significant, as minor differences in the pressure drop prediction could result in significant reductions in the power consumption of the system pumping and liquid distribution. Gas injection decreases shear stresses at the wall, besides reducing the wetted area of the pipe surface. In another way, understanding Pressure drop behavior for the flow can significantly help in industrial process design.

Non-Newtonian systems are not governed by the Newtonian law of viscosity. Still, minimum experimental work has been dedicated to studying non-Newtonian flow behavior.
This present work has conducted an experimental setup to understand the fundamental physics of non-Newtonian two-phase (gas/ liquid) flow through pipes. In the experiments, four concentrations of Xanthan Gum were used as the non-Newtonian liquid, and both Air and carbon dioxide were used as gases. The flow rate and pressure of liquid and gas are changed by using a pump placed ahead of the mixing point. Pressure values are recorded by pressure sensors fixed at specific points along the pipe loop, and many experimental data points have been collected.

The Experimental data analysis went through four categories. The first step was applying rheology tests on our non-Newtonian fluid to define the fluid behavior and estimate the fluid properties. The second part studied the effect of flow conditions and fluid properties on pressure drop. The third part compared the experimental pressure drop with the estimated pressure drop by well-known correlations. Pressure drop is one of the most challenging concerns related to industrial process design. Multiphase flow process design depends on a better understanding of multiphase flow regimes. Research has been done on gas/Newtonian liquid flow in horizontal and vertical pipes in the past few decades. Still, only a few research studies have been carried out to identify gas/non-Newtonian flow regimes. [82].

Research in void fraction modelling and evaluations started more than 60 years ago, but no standard method of modeling void fractions is suitable for all boundary conditions. Most available correlations and models are obtained based on empirical relations for a narrow range of data. The simplest experimental way to measure the void fraction is by suddenly shutting off valves and measuring the relative volume of liquid and vapour [83].

Developing a new void fraction model for gas-non-Newtonian flow is the 4th objective of the present work. The void fraction is considered one of the most important flow parameters used to describe two-phase flows in tubes. Void fraction is an important process variable for the volume and mass calculation required to transport gas-liquid mixture in pipelines, storage in tanks, metering, and custody transfer. Furthermore, it is important to determine other flow parameters such as two-phase density and viscosity or the average velocities of gas and liquid mixture. In addition, it plays a significant role in estimating and modeling two-phase pressure drop and flow pattern transitions. The created void fraction model is used to determine constants of general form posted by Butterworth[2]. Both developed void fraction models give a good

estimation for the void fraction with about 3% percent errors compared with our experimental results and other available literature experimental results.

7.2 Conclusion

This work built an experimental setup to investigate gas/non-Newtonian two-phase flow in pipes. Four concentrations of Xanthan gum have been used for air/Xanthan gum and CO_2/Xanthan gum flow in a pipe system. Rheology properties of all concentrations of Xanthan gum are obtained by rotary viscometer and high-speed mixer. Many models have been approved to describe the rheological behavior of non-Newtonian fluids based on the relationship between shear rate and shear stress. The results showed that our mixtures follow the Herschel-Bulkley model.

The effect of flow conditions and the fluid properties on the pressure drop is analyzed. The experimental pressure drop compared with the pressure drop was estimated by commonly used models, and the results show that the average error for the Xu et al. model is acceptable compared to other models.

The overall conclusion based on the experimental results and data analysis are:

- The higher the velocity and viscosity of the fluid (liquid or gas), the higher the pressure drop, which is proved by Bernoulli's Principle and Darcy equation.
- Results show that the mixture density significantly affects pressure drop with about 50% more than the mixture velocity, which gives up to 40% of the total effect. The effect of the friction factor is about 1%, and the remaining percentage is for tube diameter and gravity forces.

- The results show that the Xu et al. model exhibits an appropriate average error compared to experimental and other used models. The average error of the model is about 10% based on experimental results.
- The experimental void fraction results were plotted against the flow parameters to determine each flow variable's effect and to develop a correlation with a void fraction prediction.
- The experimental model of estimating void fraction for gas-nonNewtonian flow has been developed with high accuracy, about 3% error.
- The experimental model has been used to determine the general void fraction equation constants related to gas-non-Newtonian flow. As a result, we conclude with two models to estimate void fraction for the gas-non-Newtonian flow with high accuracy.

7.3 Recommendations

Multi-phase flow research, especially for fluids following non-Newtonian behavior, is a very interesting research area. It has essential applications in the oil and gas industry and for gas and liquid transportation. The experimental setup of the gas-liquid flow used in this thesis can conduct different types of multi-phase flow investigations. Based on fluids properties and flow loop operating conditions, the following recommendations for future work are considered:

- The experimental setup in this work is conducted with only one tube diameter size. However, experiments with different tube diameter sizes will clearly indicate the effect of the diameter on pressure drop and void fraction.

- Since the flow regime analysis is fundamental in gas-liquid flow, it is highly recommended for future work to modify the flow loop to help in flow regime investigations.
- Xanthan gum is the non-newtonian liquid used in the experiments, which follows the Herschel-Bulkley model. Experiment with other liquids that follow the other rheology models will extend models to cover all non-Newtonian behaviors.
- Most of the gas and liquid flow tested in this work were under turbulent flow conditions. Studying laminar flow requires minor modifications to the loop.
- The highest concentration tested in the experimental setup was four g/L. The loop can be used for higher than four g/L since the concentration affects many flow conditions.

References

[1] J. Y. Xu, “Investigation on average void fraction for air/non-Newtonian power-law fluids two-phase flow in downward inclined pipes,” *Exp. Therm. Fluid Sci.*, vol. 34, no. 8, pp. 1484–1487, 2010, doi: 10.1016/j.expthermflusci.2010.07.012.

[2] D. BUTTERWORTH, “A COMPARISON OF SOME VOID-FRACTION RELATIONSHIPS FOR CO-CURRENT GAS-LIQUID FLOW,” *Int. J. Multiph. Flow*, vol. Vol. 1, pp. 845–850, 1975.

[3] R. P. Chhabra and J. F. Richardson, “Non-Newtonian fl uid behaviour,” in *Non-Newtonian flow and applied rheology : engineering applications*, 2008, pp. 1–55.

[4] J. R. A. Pearson and P. M. J. Tardy, “Models for flow of non-Newtonian and complex fluids through porous media,” *J. Nonnewton. Fluid Mech.*, vol. 102, no. 2, pp. 447–473, 2002, doi: 10.1016/S0377-0257(01)00191-4.

[5] F. Ben Rajeb *et al.*, “Experimental comparison of Newtonian and non-Newtonian multiphase flow in horizontal pipes,” *Am. Soc. Mech. Eng. Fluids Eng. Div. FEDSM*, vol. 2, pp. 1–8, 2020, doi: 10.1115/FEDSM2020-20236.

[6] A. J. Ghajar and S. M. Bhagwat, *Frontiers and Progress in Multiphase Flow I*. 2014.

[7] F. Ben Rajeb, M. A. Rahman, Y. Zhang, S. Imtiaz, A. Aborig, and M. Odan, “Pressure loss of water–co2 two-phase flow under different operating conditions,” *WIT Trans. Eng. Sci.*, vol. 120, no. July, pp. 263–273, 2018, doi: 10.2495/AFM180271.

[8] S. Al-lababidi, A. Addali, H. Yeung, D. Mba, and F. Khan, “Gas void fraction measurement in two-phase gas/liquid slug flow using acoustic emission technology,” *J. Vib. Acoust. Trans. ASME*, vol. 131, no. 6, pp. 0645011–0645017, 2009, doi: 10.1115/1.4000463.

[9] F. Ben Rajeb, S. Imtiaz, Y. Zhang, A. Aborig, M. M. Awad, and M. A. Rahman, “Void Fraction, Pressure Drop, and Flow Pattern Behavior for Two-Phase Non-Newtonian Slug Flow,” Jun. 2021, doi: 10.1115/OMAE2021-62513.

[10] N. Mackintosh and Z. Atakan, “Flow Assurance leading concern among producers,” *Offshore*. 2000.

[11] R. M. S. M. Schulkes, T. Rinde, and O. H. Utvik, “Pipe flow with radial inflow: Experimental and modeling work,” *J. Fluids Eng. Trans. ASME*, vol. 121, no. 1, pp. 106–111, 1999, doi: 10.1115/1.2821989.

[12] H. Asheim, J. Kolnes, and P. Oudeman, “A flow resistance correlation for completed wellbore,” *J. Pet. Sci. Eng.*, vol. 8, no. 2, pp. 97–104, 1992, doi: 10.1016/0920-4105(92)90048-6.

[13] J. yu Xu, M. chen Gao, and J. Zhang, “Pressure drop models for gas/non-newtonian power-law fluids flow in horizontal pipes,” *Chem. Eng. Technol.*, vol. 37, no. 4, pp. 717–722, 2014, doi: 10.1002/ceat.201300615.

[14] F. Ben Rajeb, M. Odan, S. Imtiaz, Y. Zhang, M. M. Awad, and M. A. Rahman,

"Experimental investigation of pressure drop of gas/non-Newtonian flow in horizontal pipes," *Proc. Int. Conf. Offshore Mech. Arct. Eng. - OMAE*, vol. 11, 2020, doi: 10.1115/OMAE2020-18704.

[15] A. A. Zahid, S. R. ur Rehman, S. Rushd, A. Hasan, and M. A. Rahman, "Experimental investigation of multiphase flow behavior in drilling annuli using high speed visualization technique," *Front. Energy*, vol. 14, no. 3, pp. 635–643, 2020, doi: 10.1007/s11708-018-0582-y.

[16] D. Harrison and F. Particles, "A Flow," vol. 22, no. 1, pp. 47–55, 1976.

[17] I. Belgacem, Y. Salhi, E. K. Si-Ahmed, J. Legrand, and J. M. Rosant, "Experimental investigation of slug pattern in a horizontal two-phase flow," *WIT Trans. Eng. Sci.*, vol. 79, no. March 2015, pp. 423–434, 2013, doi: 10.2495/MPF130351.

[18] K. Wang, J. Ye, and B. Bai, "Profile of huge wave in gas–liquid churn flow," *Chem. Eng. Sci.*, vol. 163, pp. 137–144, 2017, doi: 10.1016/j.ces.2017.01.041.

[19] M. Morshed, M. S. Khan, M. A. Rahman, and S. Imtiaz, "Flow regime, slug frequency and wavelet analysis of air/Newtonian and air/non-Newtonian two-phase flow," *Appl. Sci.*, vol. 10, no. 9, 2020, doi: 10.3390/app10093272.

[20] M. Parsi *et al.*, "Experimental investigation of interfacial structures within churn flow using a dual wire-mesh sensor," *Int. J. Multiph. Flow*, vol. 73, pp. 155–170, 2015, doi: 10.1016/j.ijmultiphaseflow.2015.03.019.

[21] J. yu Xu, Y. xiang Wu, Z. hong Shi, L. yun Lao, and D. hui Li, "Studies on two-phase co-current air/non-Newtonian shear-thinning fluid flows in inclined smooth pipes," *Int. J. Multiph. Flow*, vol. 33, no. 9, pp. 948–969, 2007, doi: 10.1016/j.ijmultiphaseflow.2007.03.008.

[22] R. I. Issa and M. H. W. Kempf, "Simulation of slug flow in horizontal and nearly horizontal pipes with the two-fluid model," *Int. J. Multiph. Flow*, vol. 29, no. 1, pp. 69–95, 2003, doi: 10.1016/S0301-9322(02)00127-1.

[23] E. S. Kordyban and T. Ranov, "Mechanism of Slug Formation in Horizontal Two-Phase Flow," *J. Basic Eng.*, vol. 92, no. 4, pp. 857–864, Dec. 1970, doi: 10.1115/1.3425157.

[24] Y. Taitel and A. E. Dukler, "A model for predicting flow regime transitions in horizontal and near horizontal gas-liquid flow," *AIChE J.*, vol. 22, no. 1, pp. 47–55, 1976, doi: 10.1002/aic.690220105.

[25] O. J. Nydal, S. Pintus, and P. Andreussi, "Statistical characterization of slug flow in horizontal pipes," *Int. J. Multiph. Flow*, vol. 18, no. 3, pp. 439–453, 1992, doi: https://doi.org/10.1016/0301-9322(92)90027-E.

[26] Rizaldy and S. J. Zarrouk, "Pressure Drop in Large Diameter Geothermal Two-Phase Pipelines," *Proc. 38th New Zeal. Geotherm. Work.*, no. November, 2016.

[27] G. H. Abdul-Majeed, "Liquid holdup in horizontal two-phase gas-liquid flow," *J. Pet. Sci.*

Eng., vol. 15, no. 2–4, pp. 271–280, 1996, doi: 10.1016/0920-4105(95)00069-0.

[28] H. T. Molina, "Two Phase Flow. Lockhart-Martinelli calculation method," *LinkedIn*, 2021.

[29] A. B. Metzner, "No TitNon-Newtonian Technology: Fluid Mechanics, Mixing, and Heat Transfer. In Advances in Chemical Engineeringle," *Adv. Chem. Eng.*, vol. Volume 1, no. C, pp. 77–153, pp. 77–153, 1956.

[30] N. Singhal, S. N. Shah, and S. Jain, "Friction pressure correlations for newtonian and non-newtonian fluids in concentric annuli," *SPE Prod. Oper. Symp. Proc.*, pp. 451–464, 2005, doi: 10.2118/94280-ms.

[31] K. Wang, F. Jiang, B. Bai, T. N. Wong, F. Duan, and M. Skote, "Pressure drop, void fraction and wave behavior in two-phase non-Newtonian churn flow," *Chem. Eng. Sci.*, vol. 174, pp. 82–92, 2017, doi: 10.1016/j.ces.2017.08.031.

[32] M. A. Abd El-Moniem and A. H. El-Banbi, "Development of an expert system for selection of multiphase flow correlations," *J. Pet. Explor. Prod. Technol.*, vol. 8, no. 4, pp. 1473–1485, 2018, doi: 10.1007/s13202-018-0442-7.

[33] M. Khasanov, R. Khabibullin, V. Krasnov, A. Pashali, and V. Guk, "A simple mechanistic model for void-fraction and pressure-gradient prediction in vertical and inclined gas/liquid flow," *SPE Prod. Oper.*, vol. 24, no. 1, pp. 165–170, 2009, doi: 10.2118/108506-pa.

[34] P. G. (1952). Poettman, F.H., & Carpenter, "The Multiphase Flow of Gas, Oil, and Water Through Vertical Flow Strings with Application to the Design of Gas-lift Installations. Drilling and Production Practice.," 1952.

[35] K. E. Hagedorn, A.R. and Brown, "Experimental Study of Pressure Gradients Occurring during Continuous Two-Phase Flow in Small-Diameter Vertical Conduits," *J. Pet. Technol.*, pp. 17, 475–484, 1965.

[36] R. P. C. M. Dziubinski, *Int. J. Eng. Fluid Mech*. 1989.

[37] H. Li, T. N. Wong, M. Skote, and F. Duan, "A simple model for predicting the pressure drop and film thickness of non-Newtonian annular flows in horizontal pipes," *Chem. Eng. Sci.*, vol. 102, pp. 121–128, 2013, doi: 10.1016/j.ces.2013.07.046.

[38] H. Li, T. N. Wong, M. Skote, and F. Duan, "Non-Newtonian two-phase stratified flow with curved interface through horizontal and inclined pipes," *Int. J. Heat Mass Transf.*, vol. 74, pp. 113–120, 2014, doi: 10.1016/j.ijheatmasstransfer.2014.02.052.

[39] M. F. Qureshi, M. Ali, M. A. Rahman, I. Hassan, G. Rasul, and R. Hassan, "Experimental investigation of multi-phase flow in an annulus using electric resistance tomography," *Soc. Pet. Eng. - SPE Kuwait Oil Gas Show Conf. 2019, KOGS 2019*, no. September 2018, pp. 1947–1956, 2019, doi: 10.2118/198011-ms.

[40] M. K. Nicholson, K. Aziz, and G. A. Gregory, "Intermittent two phase flow in horizontal pipes: Predictive models," *Can. J. Chem. Eng.*, vol. 56, no. 6, pp. 653–663, 1978, doi:

10.1002/cjce.5450560601.

[41] M. A. Woldesemayat and A. J. Ghajar, “Comparison of void fraction correlations for different flow patterns in horizontal and upward inclined pipes,” *Int. J. Multiph. Flow*, vol. 33, no. 4, pp. 347–370, 2007, doi: 10.1016/j.ijmultiphaseflow.2006.09.004.

[42] J. Winkler, J. Killion, S. Garimella, and B. M. Fronk, “Void fractions for condensing refrigerant flow in small channels: Part i literature review,” *Int. J. Refrig.*, vol. 35, no. 2, pp. 219–245, 2012, doi: 10.1016/j.ijrefrig.2011.09.013.

[43] M. Pietrzak and M. Płaczek, “Void fraction predictive methods in two-phase flow across a small diameter channel,” *Int. J. Multiph. Flow*, vol. 121, p. 103115, 2019, doi: 10.1016/j.ijmultiphaseflow.2019.103115.

[44] H. S. Isbin, H. A. Rodriguez, H. C. Larson, and B. D. Pattie, “Void fractions in two-phase flow,” *AIChE J.*, vol. 5, no. 4, pp. 427–432, 1959, doi: 10.1002/aic.690050406.

[45] Á. R. Gardenghi, E. D. S. Filho, D. G. Chagas, G. Scagnolatto, R. M. Oliveira, and C. B. Tibiriçá, “Overview of void fraction measurement techniques, databases and correlations for two-phase flow in small diameter channels,” *Fluids*, vol. 5, no. 4, 2020, doi: 10.3390/fluids5040216.

[46] B. Chexal, J. Horowitz, and G. S. Lellouche, “An assessment of eight void fraction models,” *Nucl. Eng. Des.*, vol. 126, no. 1, pp. 71–88, 1991, doi: 10.1016/0029-5493(91)90206-W.

[47] W. G. Sim, N. W. Mureithi, and M. J. Pettigrew, “Parametric study of two-phase flow by integral analysis based on power law distribution,” *J. Mech. Sci. Technol.*, vol. 24, no. 7, pp. 1379–1387, 2010, doi: 10.1007/s12206-010-0419-z.

[48] A. L. K.A. Triplett, S.M. Ghiaasiaan *, S.I. Abdel-Khalik and B. N. McCord, “No TitleGas±liquid two-phase ¯ow in microchannels Part II: void fraction and pressure drop,” *Int. J. Multiph. Flow*, vol. 25, p. 395±410, 1999.

[49] B. Chexal, G. Lellouche, J. Horowitz, and J. Healzer, “A void fraction correlation for generalized applications,” *Prog. Nucl. Energy*, vol. 27, no. 4, pp. 255–295, 1992, doi: 10.1016/0149-1970(92)90007-P.

[50] D. A. Yashar, M. J. Wilson, H. R. Kopke, D. M. Graham, J. C. Chato, and T. A. Newell, “An investigation of refrigerant void fraction in horizontal, microfin tubes,” *ASHRAE Trans.*, vol. 107 PART 2, pp. 173–188, 2001.

[51] D. A. Yashar, M. J. Wilson, H. R. Kopke, D. M. Graham, J. C. Chato, and T. A. Newell, “An Investigation of Refrigerant Void Fraction in Horizontal , Microfin Tubes Amana Refrigeration , Inc . Carrier Corporation Caterpillar , Inc . Chrysler Corporation Copeland Corporation Delphi Harrison Thermal Systems Frigidaire Company General Electric ,” vol. 61801, no. 217, 1999.

[52] S. Koyama, J. Lee, and R. Yonemoto, “An investigation on void fraction of vapor-liquid

two-phase flow for smooth and microfin tubes with R134a at adiabatic condition," *Int. J. Multiph. Flow*, vol. 30, no. 3, pp. 291–310, 2004, doi: 10.1016/j.ijmultiphaseflow.2003.10.009.

[53] F. Resources, J. A. Donnegan, S. T. Trimble, K. Kusto, O. Kuegler, and B. A. Hiserote, "DEEPWATER HORIZON MARINE CASUAlTY INVESTIGATION REPORT," *Int. J. Mar. Coast. Law*, vol. 31, no. 4, pp. 732–758, 2016, [Online]. Available: https://www.register-iri.com/wp-content/uploads/Republic_of_the_Marshall_Islands_DEEPWATER_HORIZON_Marine_Casualty_Investigation_Report-Low_Resolution.pdf%0Ahttp://booksandjournals.brillonline.com/content/journals/10.1163/15718085-12341413.

[54] G. Zhou *et al.*, "Pressure-Difference Method for Gas-Kick Detection in Risers," *SPE J.*, vol. 26, no. 5, pp. 2479–2497, 2021, doi: 10.2118/205362-PA.

[55] B. M. Abbagoni and H. Yeung, "Non-invasive classification of gas-liquid two-phase horizontal flow regimes using an ultrasonic Doppler sensor and a neural network," *Meas. Sci. Technol.*, vol. 27, no. 8, 2016, doi: 10.1088/0957-0233/27/8/084002.

[56] C. C. Cormos, "Evaluation of energy integration aspects for IGCC-based hydrogen and electricity co-production with carbon capture and storage," *Int. J. Hydrogen Energy*, vol. 35, no. 14, pp. 7485–7497, 2010, doi: 10.1016/j.ijhydene.2010.04.160.

[57] D. Herath, F. Khan, S. Rathnayaka, and M. A. Rahman, "Probabilistic estimation of hydrate formation," *J. Pet. Sci. Eng.*, vol. 135, pp. 32–38, 2015, doi: 10.1016/j.petrol.2015.08.007.

[58] E. de Visser *et al.*, "Dynamis CO2 quality recommendations," *Int. J. Greenh. Gas Control*, vol. 2, no. 4, pp. 478–484, 2008, doi: 10.1016/j.ijggc.2008.04.006.

[59] "No Tithttps://www.versaperm.com/applications/Permeability%20and%20Supercritical%20carbon%20dioxide%20CO2.phple." .

[60] M. Ahmad and S. Gersen, "Water solubility in CO2 mixtures: Experimental and modelling investigation," *Energy Procedia*, vol. 63, pp. 2402–2411, 2014, doi: 10.1016/j.egypro.2014.11.263.

[61] H. O. Nordhagen, S. Kragset, T. Berstad, A. Morin, C. Dørum, and S. T. Munkejord, "A new coupled fluid-structure modeling methodology for running ductile fracture," *Comput. Struct.*, vol. 94–95, pp. 13–21, 2012, doi: 10.1016/j.compstruc.2012.01.004.

[62] E. Aursand *et al.*, "CO2 pipeline integrity: A coupled fluid-structure model using a reference equation of state for CO2," *Energy Procedia*, vol. 37, no. 1876, pp. 3113–3122, 2013, doi: 10.1016/j.egypro.2013.06.197.

[63] Z. Qiao, Z. Wang, C. Zhang, S. Yuan, Y. Zhu, and J. Wang, "PVAm–PIP/PS composite membrane with high performance for CO_2/N_2 separation," *AIChE J.*, vol. 59, no. 4, pp.

215–228, 2012, doi: 10.1002/aic.

[64] M. Farzaneh-Gord, M. Khatib, M. Deymi-Dashtebayaz, and M. Shahmardan, “Producing electrical power in addition of heat in natural gas pressure drop stations by ICE,” *Energy Explor. Exploit.*, vol. 30, no. 4, pp. 567–588, 2012, doi: 10.1260/0144-5987.30.4.567.

[65] M. Farzaneh-Gord, H. R. Rahbari, M. Bajelan, and L. Pilehvari, “Investigation of hydrate formation in natural gas flow through underground transmission pipeline,” *J. Nat. Gas Sci. Eng.*, vol. 15, pp. 27–37, 2013, doi: 10.1016/j.jngse.2013.09.001.

[66] B. Tohidi, R. Anderson, M. Ben Clennell, R. W. Burgass, and A. B. Biderkab, “Visual observation of gas-hydrate formation and dissociation in synthetic porous media by means of glass micromodels,” *Geology*, vol. 29, no. 9, pp. 867–870, 2001, doi: 10.1130/0091-7613(2001)029<0867:VOOGHF>2.0.CO;2.

[67] A. Gupta, T. J. Kneafsey, G. J. Moridis, Y. Seol, M. B. Kowalsky, and E. D. Sloan, “Composite thermal conductivity in a large heterogeneous porous methane hydrate sample,” *J. Phys. Chem. B*, vol. 110, no. 33, pp. 16384–16392, 2006, doi: 10.1021/jp0619639.

[68] R. W. Henning, A. J. Schnitz, V. Thieu, and Y. Halpern, “Neutron diffraction studies of CO2 clathrate hydrate: formation from deuterated ice,” *J. Phys. Chem. A*, vol. 104, no. 21, pp. 5066–5071, 2000, doi: 10.1021/jp0001642.

[69] “https://www.hollandairpumps.com/product/h220-wwwaa-fws-wf-mwf/.” .

[70] “https://www.emerson.com/en-ca/catalog/rosemount-8711-en-ca?fetchFacets=true#facet:&partsFacet:&modelsFacet:&facetLimit:&searchTerm:&partsSearchTerm:&modelsSearchTerm:&productBeginIndex:0&partsBeginIndex:0&modelsBeginIndex:0&orderBy:&partsOrderBy:&modelsOr.” .

[71] “No Titlehttp://www.omega.com/pptst/PX603.html.,” 2016. http://www.omega.com/pptst/PX603.html.

[72] “No Titlhttps://www.omega.ca/en/pressure-measurement/pressure-transducers/p/PX603-PX613-PX605-PX615e.” .

[73] “No https://www.omega.ca/en/temperature-measurement/temperature-probes/probes-with-lead-wires/p/TC-NPTTitle.” .

[74] “No Thttps://www.megaspeedusa.com/pc-connected/ms55k-sc/itle.” .

[75] Schlumberger, *Rheological Models*. 2022.

[76] I. Færgestad, “The Defining Series: Rheology,” 2016, [Online]. Available: www.slb.com/defining.

[77] T. Hemphil, A. Pilehvari, and W. Campos, “Yield-power law model more accurately predicts mud rheology,” *Oil Gas J.*, vol. 91, no. 34, pp. 45–50, 1993.

[78] “Flow assurance,” pp. 221–222, 2007, doi: 10.1039/9781847550460-00221.

[79] D. Samanta, A. De Lozar, and B. Hof, “Experimental investigation of laminar turbulent intermittency in pipe flow,” *J. Fluid Mech.*, vol. 681, pp. 193–204, 2011, doi: 10.1017/jfm.2011.189.

[80] Hydraulic Institute, *Engineering Data Book, 2nd ed*. 1991.

[81] M. A. Rahman, K. F. Adane, and R. S. Sanders, “An improved method for applying the lockhart-martinelli correlation to three-phase gas-liquid-solid horizontal pipeline flows,” *Can. J. Chem. Eng.*, vol. 91, no. 8, pp. 1372–1382, 2013, doi: 10.1002/cjce.21843.

[82] T. Fu, L. Wei, C. Zhu, and Y. Ma, “Flow patterns of liquid-liquid two-phase flow in non-Newtonian fluids in rectangular microchannels,” *Chem. Eng. Process. Process Intensif.*, vol. 91, pp. 114–120, 2015, doi: 10.1016/j.cep.2015.03.020.

[83] P. K. Gkotsis, S. P. Evgenidis, and T. D. Karapantsios, “Influence of Newtonian and non-Newtonian fluid behaviour on void fraction and bubble size for a gas-liquid flow of sub-millimeter bubbles at low void fractions,” *Exp. Therm. Fluid Sci.*, vol. 109, no. August, p. 109912, 2019, doi: 10.1016/j.expthermflusci.2019.109912.